[redacted]

MARTIN MARIETTA ENERGY SYSTEMS LIBRARIES
3 4456 0360696 1

CENTRAL RESEARCH LIBRARY
DOCUMENT COLLECTION

AEC RESEARCH AND DEVELOPMENT REPORT

ORNL-1677
Progress
Ha

DECLASSIFIED

CLASSIFICATION CHANGED TO:
BY AUTHORITY OF: E. J. Murphy 6-17-59
BY: P. C. Hansen 8-31-59

LABORATORY RECORDS 1954

SOLID STATE DIVISION
SEMIANNUAL PROGRESS REPORT
FOR PERIOD ENDING FEBRUARY 28, 1954

CENTRAL RESEARCH LIBRARY
DOCUMENT COLLECTION

LIBRARY LOAN COPY

DO NOT TRANSFER TO ANOTHER PERSON

If you wish someone else to see this document, send in name with document and the library will arrange a loan.

OAK RIDGE NATIONAL LABORATORY
OPERATED BY
CARBIDE AND CARBON CHEMICALS COMPANY
A DIVISION OF UNION CARBIDE AND CARBON CORPORATION

UCC

POST OFFICE BOX P
OAK RIDGE, TENNESSEE

[redacted]

[redacted]

[redacted]

ORNL-1677

This document consists of 90 pages.
Copy 4 of 157 copies. Series A.

Contract No. W-7405-eng-26

SOLID STATE DIVISION

SEMIANNUAL PROGRESS REPORT

For Period Ending February 28, 1954

D. S. Billington, Director

Edited by
J. T. Howe

DATE ISSUED

MAY 19 1954

OAK RIDGE NATIONAL LABORATORY
Operated by
CARBIDE AND CARBON CHEMICALS COMPANY
A Division of Union Carbide and Carbon Corporation
Post Office Box P
Oak Ridge, Tennessee

[redacted]

MARTIN MARIETTA ENERGY SYSTEMS LIBRARIES

3 4456 0360696 1

[redacted]

INTERNAL DISTRIBUTION

1. C. E. Center
2. Biology Library
3. Health Physics Library
4-5. Central Research Library
6. Reactor Experimental Engineering Library
7-11. Laboratory Records Department
12. Laboratory Records, ORNL R.C.
13. C. E. Larson
14. L. B. Emlet (K-25)
15. J. P. Murray (Y-12)
16. A. M. Weinberg
17. E. H. Taylor
18. E. J. Murphy
19. E. D. Shipley
20. D. S. Billington
21. F. C. VonderLage
22. W. H. Jordan
23. J. A. Swartout
24. S. C. Lind
25. F. L. Culler
26. A. H. Snell
27. A. Hollaender
28. M. T. Kelley
29. G. W. Clewett
30. K. Z. Morgan
31. T. A. Lincoln
32. A. S. Householder
33. C. S. Harrill
34. C. E. Winters
35. D. W. Cardwell
36. E. M. King
37. C. P. Keim
38. L. K. Jetter
39. E. J. Boyle
40. W. D. Manly
41. C. D. Susano
42. B. S. Borie
43. R. J. Gray
44. J. H. Frye, Jr.
45. E. E. Stansbury
46. G. P. Smith
47. J. E. Cunningham
48. E. C. Miller
49. A. F. Cohen
50. J. O. Betterton, Jr.
51. R. B. Oliver
52. T. H. Blewitt
53. J. H. Crawford, Jr.
54. W. E. Brundage
55. O. Sisman
56. G. W. Keilholtz
57. J. T. Howe
58. R. H. Kernohan
59. S. E. Dismuke
60. J. C. Wilson
61. W. J. Sturm
62. M. T. Robinson
63. J. W. Cleland
64. K. Lark-Horovitz (consultant)
65. M. C. Wittels
66. R. A. Weeks
67. W. W. Parkinson
68. C. D. Bopp
69. C. D. Baumann
70. J. B. Trice
71. J. G. Morgan
72. G. E. Klein
73. R. G. Berggren
74. D. K. Holmes
75. D. K. Stevens
76. A. J. Miller
77. R. S. Livingston
78. R. J. Jones
79. D. D. Cowen
80. P. M. Reyling
81. G. C. Williams
82. D. Binder
83. M. J. Feldman
84. C. C. Webster
85. J. M. Warde
86. W. O. Harms
87. W. R. Willis
88. F. Seitz (consultant)
89. E. P. Wigner (consultant)
90. R. L. Sproull (consultant)
91. R. W. Johnson
92. P. M. Uthe

[redacted]

[redacted]

EXTERNAL DISTRIBUTION

93-100. Argonne National Laboratory
101-103. Atomic Energy Commission, Washington
104-107. Brookhaven National Laboratory
108-111. Carbide and Carbon Chemicals Company (Y-12 Plant)
112-114. Knolls Atomic Power Laboratory
115-116. General Electric Company, Richland
117. Hanford Operations Office
118-121. Los Alamos Scientific Laboratory
122-123. New York Operations Office
124. Patent Branch, Washington
125-139. Technical Information Service, Oak Ridge
140-141. University of California Radiation Laboratory, Berkeley
142-143. University of California Radiation Laboratory, Livermore
144. Massachusetts Institute of Technology (Kaufmann)
145. Battelle Memorial Institute
146-148. North American Aviation, Inc.
149. Westinghouse Electric Corporation
150. Savannah River Operations Office, Augusta
151-154. Phillips Petroleum Company
155. Materials Laboratory (WADC) 1 copy – Helen Akerd
156. Directorate of Research (WADC) 1 copy – Helen Akerd
157. National Advisory Committee for Aeronautics, Cleveland (Solid State Division, Lewis Flight Propulsion Laboratory)

[redacted]

[redacted]

Reports previously issued in this series are:

ORNL-1025	Period Ending January 31, 1951
ORNL-1095	Period Ending April 30, 1951
ORNL-1128	Period Ending July 21, 1951
ORNL-1214	Period Ending October 31, 1951
ORNL-1261	Period Ending January 31, 1952
ORNL-1301	Period Ending May 10, 1952
ORNL-1359	Period Ending August 10, 1952
ORNL-1429	Period Ending November 10, 1952
ORNL-1506	Period Ending February 10, 1953
ORNL-1606	Period Ending August 31, 1953

[redacted]

[redacted]

CONTENTS

PART I

SUMMARY 3

RADIATION METALLURGY 7
- Creep Under Irradiation 7
- Phillips Petroleum Company MTR Specimens 8
- Bonded-Wire Strain Gages 8
- Impact Tests 9
- Fatigue Tests 9
- Hot Metallography 9
- Surface-Film Preservation of HRE Samples 12
- Redesign and Extension of the Remote Metallographic Facilities 12

NUCLEAR MEASUREMENTS 14
- MTR Neutron-Flux–Radiation-Damage Measurement Project 14

ENGINEERING PROPERTIES 17
- LITR Fluoride-Fuel Loop 17
- LITR Sodium Stress-Corrosion Loop 18
- ORNL Graphite Reactor Sodium-Inconel Loop 19

FUSED SALTS 20
- Radiation Damage in Fused-Salt Fuels 20
- Temperature Control in the MTR Static-Corrosion Tests 22
- Thermal-Neutron Flux Traverses in the LITR 27
- Thermal-Neutron Flux Measurements in the MTR 27
- Sampling Irradiated Capsules Containing Uranium-Bearing Fuels 27
- Petrographic Examination of Irradiated Fluorides 28
- Design Calculations for Miniature Circulating Loop 29
- Miniature Sump Pump 30
- Miniature Check-Valve Pump 30

PART II

SUMMARY 37

SOLID STATE REACTIONS 41
- Effective Masses and Carrier Degeneracy from the Diamagnetic Behavior of Germanium 41
- Radiation Effects in Ionic Crystals 44
- Magnetic Susceptibility of Germanium 44
- Magnetic Susceptibility of Silicon and Diamond 47
- Rectifier Bombardment 47
- Electrical Effects in Irradiated Barriers 50
- Radiation Damage in SiO_2 Structures 54
- Annealing of Neutron-Irradiated Diamond 54

ENGINEERING PROPERTIES 55
- Dynamic Properties of Irradiated Elastomers 55

[redacted]

[redacted]

CRYSTAL PHYSICS. 60
Effect of Deformation on the Superconducting Properties of Aluminum 60
Radiation Ordering in Cu_3Au. 61
Radiation Effects in Copper Single Crystals 64
Structural Defects in Copper and the Electrical Resistivity Minimum 64

SPECIAL PROJECTS. 66
Neutron Irradiation of LiF Crystals 66
Thermal and Electrical Conductivities of Ductile Irons and Gray Cast Irons 67
Thermal Conductivity of Dielectrics at Low Temperatures. 68
Thermal and Electrical Conductivities of Aluminum Bronzes 70
Small-Angle X-Ray Scattering 70
Effect of Radiation on the Dielectric Constant and Attenuation of Two Coaxial Cables at Radio Frequencies. 71
Dielectric Constant and Loss Tangent of Irradiated Plastics at Microwave Frequencies 77
Paramagnetic Resonance in Irradiated Solids 82

[redacted]

[redacted]

PUBLICATIONS

Publications of the Solid State Division during the past six months were:

M. J. Feldman, "The Metallography of Highly Radioactive Materials," *Metal Progr.* **64**, No. 5, 97 (1953).

O. Sisman, *LITR Fluoride Fuel Test Loop*, ORNL CF-53-9-180 (Sept. 25, 1953).

W. E. Brundage, W. W. Parkinson, and O. Sisman, *Questionnaire for LITR Fluoride Fuel Loop Experiment*, ORNL CF-53-12-140 (Dec. 17, 1953).

W. E. Brundage and W. W. Parkinson, *The Radiation Induced Corrosion of Beryllium Oxide in Sodium at 1500°F*, ORNL CF-53-12-42 (Dec. 3, 1953).

C. D. Bopp and O. Sisman, *Radiation Stability of Plastics and Elastomers*, ORNL-1373 (Feb. 1, 1954).

T. H. Blewitt, "Deformation of Copper Single Crystals at 300°K and 78°K," *Phys. Rev.* **91**, 1115 (1953).

M. C. Wittels and F. A. Sherrill, "Radiation Damage in SiO_2 Structures," *Phys. Rev.* **93**, 1117 (1954).

P. M. Uthe, *Thermal Column Flux*, ORNL CF-53-11-5 (Nov. 3, 1953).

P. M. Uthe, *Perturbation of Thermal Neutron Flux Caused by Gold Foils in a Water Medium*, ORNL CF-53-11-177 (Nov. 24, 1953).

D. Binder and W. J. Sturm, "On the Equivalence of X-Ray Lattice Parameter and Density Changes in Neutron Irradiated LiF," *Bull. Am. Phys. Soc.* **29**, No. 1, 23 (1954).

D. K. Stevens and J. H. Crawford, Jr., "The Magnetic Susceptibility of Germanium," *Phys. Rev.* **92**, 1065 (1953).

J. B. Trice, F. J. Muckenthaler, F. W. Smith, and E. B. Johnson, *Two Neutron Energy Measurements in the Bulk Shielding Facility Using Radioactivants*, ORNL CF-53-5-139 (Oct. 29, 1953).

D. K. Stevens, *Magnetic Susceptibility of Annealed and Fast-Neutron Bombarded Germanium*, ORNL-1599 (Feb. 17, 1954).

G. T. Murray and W. E. Taylor, "Effect of Neutron Irradiation on a Supersaturated Solid Solution of Beryllium in Copper," *Acta Metallurgica* **2**, No. 1, 52 (1954).

W. J. Sturm and R. J. Jones, *Application of Thermocouples to Target Temperature Measurement in the Internal Beam of a Cyclotron*, ORNL-1540 (Nov. 9, 1953).

C. M. Nelson, G. E. Boyd, and W. T. Smith, Jr., "Magnetochemistry of Technetium and Rhenium," *J. Am. Chem. Soc.* **76**, 348-352 (1954).

Publications in press at the close of the period were:

Radiation Damage Conference March 23-24, 1953, ORNL CF-53-3-276.

J. W. Cleland, J. H. Crawford, Jr., "Radiation Effects in Indium Antimonide" (to be published in *Phys. Rev.*).

[redacted]

[redacted]

Part I

SECRET PROJECTS

[redacted]

SOLID STATE DIVISION SEMIANNUAL PROGRESS REPORT

SUMMARY

RADIATION METALLURGY

Creep Under Irradiation. Creep tests in the ORNL Graphite Reactor and in the LITR indicate that Inconel is not seriously affected by irradiation at the ANP temperatures and stresses. Apparatus is being developed to extend the experiments to the higher fluxes of the MTR.

Some specimens are now being irradiated for creep testing after withdrawal from the reactor to determine whether a transient increase in creep occurs during annealing of irradiated materials.

A stress-corrosion apparatus is being built to determine whether increased attack on Inconel occurs when a specimen in contact with an ANP fuel is stressed at high temperature in the presence of radiation. An Inconel tube will contain the fuel and will be surrounded by sodium or some other heat-transfer agent. The tube will be subjected to a bending stress during irradiation so that a transverse section will represent a range of stresses from compression to tensile. Metallographic examination will be made across a transverse section.

Grain growth under irradiation at lower temperatures than are required to cause growth without irradiation is also being investigated because of observations noted on some of the Inconel static-corrosion capsules. Aluminum is being used for preliminary observations.

Phillips Petroleum Company MTR Specimens. Tensile specimens of beryllium, 2S aluminum, and 356 aluminum alloy that had been exposed to 1×10^{21} fast neutrons/cm^2 were received from Phillips Petroleum Company. Density and hardness have been determined; hardness values were increased over values previously measured for specimens subjected to 3.5×10^{20} neutrons/cm^2 but the density changed little, if any. Modified grips are being made so that tensile tests can be run when the tensile machine is delivered.

Bonded-Wire Strain Gages. The search for a high-temperature, bonded-wire strain gage that will withstand irradiation has continued. Gages are being developed by the Cornell Aeronautical Laboratory. Strain measurements were made on several types of commercial bonded gages and strain-gage wires before they were placed in the LITR. The tests are still in progress but changes have been noted in all cases except unbonded Advance wire. It is believed that a wire of high-chromium, aluminum-iron alloy might exhibit the properties desired; a source is being sought.

Impact Tests. A procedure has been developed for economically machining large numbers of radiation impact specimens of carbon steels and pressure-vessel steels. Short tool life still makes the machining of stainless steels uneconomical. Specimens of heat-treated SAE 4340 steel and a tool steel irradiated in a Hanford fuel channel are now ready for impact testing. Other steels are being irradiated in the LITR, and types 301 and 446 stainless steel are in a beam hole of the MTR.

One of the impact machines has been modified and is now being tested. If the modifications prove to be satisfactory they will be added to the remotely controlled machine.

Fatigue Tests. Trial tests indicate that satisfactory subsize fatigue specimens can be developed for rotating-beam and sheet-bending fatigue machines. The machines are being modified for remote operation.

Hot Metallography. Metallographic examination of fused-salt capsules that had been irradiated in the MTR and in the LITR has given a reasonable check on the results obtained in examinations of capsules previously. Examination has also begun of the capsules along the longitudinal axes to determine the cause of a few variations from the average.

Fuel sandwiches are being inspected for the Pratt and Whitney Aircraft Division of United Aircraft Corporation. Radiation effects on the density, bonding, hardness, etc. of the core and cladding are under study. It has been found that irradiation increases the hardness of both the core and the cladding.

Surface-Film Preservation of HRE Samples. HRE metals in contact with the liquid or vapor phases of the fuel solution develop a film. A study is being made to determine the composition and thickness of the film. Since the film is quite thin it must be backed up by a supporting medium. Supporting mediums tried thus far have been a hard polyvinyl plastic and electrolytic plates of copper and iron. The plastic is too thin to prevent edge rounding. If the film is electrically nonconductive the plated metals may not make intimate contact with the film and will give erroneous data on the actual film thickness; there is also some question as to the effect the plating bath may have on the film. Copper plating appears to be the best method of the three, but developmental work will continue on all three methods.

Redesign and Extension of the Remote Metallographic Facilities. Much of the existing metallographic equipment is undergoing modification and design changes to enlarge the range and size of materials that can be processed. The facilities are being enlarged so as to separate optical, chemical, and mechanical operations and to permit workers to perform the various operations without obstructing those working on another phase.

NUCLEAR MEASUREMENTS

MTR Neutron-Flux–Radiation-Damage Measurement Project. A probe-type fission chamber has been developed to measure the fast-neutron flux pattern in the HB-3 facility of the MTR. A number of different threshold-energy-type fissionable materials will cover an energy range of several Mev.

Since it was necessary that the probe leads be more than 15 ft long, the capacitance between the probe and the preamplifier was large enough to severely distort the signal. The capacitance was reduced from 430 to 180 $\mu\mu f$ by using 10-mil wire instead of 25-mil copper wire as the center conductor of the signal lead and by increasing the inside diameter of the fused-quartz insulators in the probe.

The probe was calibrated in the ORNL thermal column by comparing the probe response to a gold-foil flux measurement.

The water-cooled plug for the HB-3 facility and the probe with its auxiliary equipment have been shipped to Idaho.

ENGINEERING PROPERTIES

LITR Fluoride-Fuel Loop. Fabrication of parts for three fluoride-fuel loops to operate in the LITR is about 50% complete. A spiral-fin heat exchanger was substituted for the parallel-flow exchanger after tests proved the latter to be inadequate. A prototype pressure-transmitter cell (for the venturi flowmeter) has been tested with a fluoride fuel under simulated operating conditions. At the end of a month there was no evidence of attack on the diaphragm.

A sump-type pump was tested with water and some modifications were made. It is now being installed in a fluoride testing system.

Excessive leakage was experienced along the longitudinal vane in the water jacket. It was necessary to split the outer tube open and to weld the separator vane along its entire length to the inner and outer walls of the jacket.

The withdrawal shield is complete and the shield for the pump and tube section outside the reactor is nearly complete.

The instrumentation is complete and will be used for bench-testing the loop.

Design of the special inspection and handling tools needed for postirradiation inspection is about 80% complete.

LITR Sodium Stress-Corrosion Loop. A radiochemical analysis of the sodium that was run in the LITR stress-corrosion loop showed that Ag^{110} made up about 80% of the long-lived activity and that Na^{22} made up the remainder. Spectrographic analysis showed about 20 ppm each of silver and palladium; both probably dissolved from the nickel-palladium braze joints.

The Widmannstätten-like structure found in the irradiated specimen was not present in the control specimen.

ORNL Graphite Reactor Sodium-Inconel Loop. After a heater of the sodium-Inconel loop failed during operation in the ORNL Graphite Reactor, the loop was removed and permitted to decay. The heaters were then replaced and in-pile operation was continued with automatic controls. After 17 hr of operation a leak developed. Even though the sodium was highly radioactive and the temperature was 1500°F, the loop was handled without overexposure of personnel and without danger to personnel or the reactor. Examination of the loop for cause of failure will conclude this work in the Graphite Reactor.

FUSED SALTS

Radiation Damage in Fused-Salt Fuels. The study of the effects of radiation on the chemical stability and corrosion properties of ANP fused-salt fuels in Inconel capsules at 1500°F has indicated that, for 600-hr tests, a capsule irradiated in the LITR (2×10^{13} neutrons/cm^2·sec) will show predominating intergranular corrosion to a depth of about 4 mils compared with about 1 mil of subsurface void type of corrosion for the control sample. Sufficient tests must be made to obtain statistical averages since capsules occasionally deviate markedly from the normal depth of corrosion.

If the reactor flux is increased, the corrosion rate increases also. A depth of 4 to 5 mils was experienced in 350 hr at the MTR flux of 2.4×10^{14} neutrons/cm^2·sec.

Addition of U^{235} to the salt necessitates higher power dissipation to maintain the capsule at 1500°F but does not seem to affect the corrosion rate.

Temperature Control in the MTR Static-Corrosion Tests. Temperature control for the MTR static corrosion tests is accomplished by means of thermocouples placed on the capsule surface. The difference in temperature between the capsule-salt interface and the outer surface of the capsule was calculated, and the control temperature was chosen to allow for the difference.

The amount of heat withdrawn by the thermocouple acting as a cooling fin was calculated from the results of this experiment.

A test-section mockup, with added thermocouples and provisions for use of an optical pyrometer, was constructed and was operated under simulated conditions of the A-38 facility at the MTR. The part the thermocouples play in the role of cooling fins was determined.

Another experiment duplicated conditions in the fuel column of the MTR except that the conditions of this test were more severe than those normally experienced in the reactor.

It was concluded that, for the worst thermocouple, the error would be no greater than 250°F for the hottest portion of the inside surface of the capsule, or a temperature of 1750°F for a thermocouple reading of 1500°F. A true temperature of 1850°F would set the reactor back; this has never happened.

Thermal-Neutron Flux Traverses in the LITR. Thermal-neutron flux traverses were made in positions C-46 and C-48 of the LITR at a reactor power of 3 megawatts for two positions of the No. 2 shim rod. A plot of the results is given in Fig. 26.

Thermal-Neutron Flux Measurements in the MTR. The MTR loading was changed from a 3 × 9, north slab pattern to a 5 × 6 pattern. The thermal-neutron flux in position A-38 was determined for a reactor power of 30 megawatts by irradiating cobalt foils for 1 hr each at the beginning of two fuel cycles. The thermal-neutron flux is calculated to be $1.92\ (\pm 0.16) \times 10^{14}$ neutrons/cm^2·sec, which is about 19% lower than it was with the former loading.

Sampling Irradiated Capsules Containing Uranium-Bearing Fuel. The method of taking salt samples in the molten state is subject to error because the molten salt may not be homogeneous throughout. A method of sampling by drilling out the center of the solidified salt with successively larger drills yielded samples from which the distribution of the components within the capsule could be determined, but the fine dust created a contamination hazard. Plexiglas boxes fitted with vacuum cleaners were built to enclose the equipment and catch the radioactive dust.

Petrographic Examination of Irradiated Fluorides. Irradiated and unirradiated salt samples were examined with the shielded petrographic microscope. A few of the irradiated salts showed the presence of ZrO_2 and/or UO_2; oxides were not found in salts irradiated in other capsules nor in the unirradiated salts. It was concluded that the oxides resulted from leaks in the capsules and that reactor irradiation has no detectable effect on the composition of the salts inspected.

Samples of fuel No. 41 were exposed to the ORNL Co^{60} source for a total of 4.7×10^8 r, and samples of fuel No. 30 were exposed to the MTR source for a total of 5.1×10^9 r. No oxides were observed.

Design Calculations of Miniature Circulating Loop. A miniature circulating loop is being designed. The fluoride-fuel flow will be turbulent, the fission-power generation will be up to 1000 watts/cc, and the temperature difference between hot and cold legs will be 100°C. The loop is to operate in position C-48 of the LITR, with the lowest point of the loop in the maximum flux. It was assumed that the circulating liquid would be fuel No. 44, which would generate 540 watts/cc, but one calculation was made for fuel No. 41, which would generate 1100 watts/cc. The effects

of variations in air-flow velocity, fuel-flow velocity, loop dimensions, and loop position on the fuel temperature distribution were studied. Thus far it has not been possible to obtain loop dimensions that meet all the design requirements simultaneously.

Miniature Sump Pump. A totally enclosed, molten-salt, pump-and-motor unit was designed to operate above position C-48 of the LITR. The pump has a centrifugal-type impeller and requires a $\frac{1}{15}$-hp motor.

Miniature Check-Valve Pump. Another miniature pump has been developed for miniature in-pile corrosion loops. The pump is made up of a rectifier unit that contains four check valves, a surge tank, and a solenoid-driven piston to supply power. Piston pressure is transmitted to the salt by means of helium.

RADIATION METALLURGY

CREEP UNDER IRRADIATION

W. W. Davis J. C. Zukas J. C. Wilson

The bulk of the effort of the Radiation Metallurgy Section has been concentrated on the development of an in-pile stress-corrosion apparatus for testing metals under stress at elevated temperatures in contact with fissioning fused-salt fuels of interest to the ANP program. The creep work has been limited to redesigning and testing of the in-pile creep apparatus for more reliable operation with either of two new extensometers that will replace the microformers formerly used.

At the neutron fluxes of the LITR and the ORNL Graphite Reactor, the creep behavior of Inconel is not seriously affected by neutron bombardment[1] over a range of stresses and temperatures applicable to presently conceived aircraft reactor designs. Apparatus for testing in the higher flux of the MTR is nearing completion; the apparatus used in the past for cantilever tests is being modified to give a constant moment over the full gage length and to provide for use of an extensometer other than a microformer. The high incidence of microformer failures has caused their use to be discontinued; the outcome of bench tests now in progress will determine whether the Bourdon-tube extensometer or a newly developed thermal expansion (bimetal) unit will be used. High-purity nickel will be used for the in-pile tests to eliminate the numerous possible metallurgical instabilities attendant upon the use of Inconel and stainless steel. A large number of annealing treatments, followed by metallurgical examination, have been carried out on the nickel to determine the effects of time and temperature on oxidation and grain growth. In addition, a number of specimens are being irradiated for creep testing after withdrawal from the reactor in an attempt to determine whether a transient increase in creep occurs during annealing of bombarded materials. Such behavior is believed to have been observed at the time of reactor shutdowns following periods of irradiation during in-pile tests on Inconel.

Intergranular separations in Inconel fuel-test capsules have occasionally been observed during metallographic examination of metal irradiated in the MTR (cf. "Radiation Damage in Fused-Salt Fuels," this report); the appearance of this phenomenon suggests that it might be cracking caused by thermal stresses alone or in combination with chemical attack. If the attack is chemical alone, the presence of a tensile stress should lead to an increase in attack or a weakening of the metal. Furthermore, stress-induced acceleration of attack on Inconel in static (and unirradiated) fused-salt systems has been observed during stress-to-rupture tests in the Metallurgy Division.[2] In order to determine the importance of these phenomena to reactor systems, an in-pile stress-corrosion apparatus has been built and is undergoing heat-transfer tests. To reveal the function of stress in the corrosion, the test specimen is tubular and is stressed in bending. This arrangement should considerably reduce the number of tests required because post-irradiation metallographic examination across a single transverse section will permit simultaneous observation, in the same test specimen, of the corrosive effects of the fused salt (and, incidentally, of the sodium used as a heat-transfer agent) on regions subjected to a continuous range of stresses from tensile to compressive, as well as regions of zero stress along the neutral axis of the tubular beam.

In the apparatus under test the tubular specimen contains the salt, and an annulus of molten sodium surrounds the specimen to conduct the fission heat to an outer Inconel container that is water cooled at its periphery to serve as a heat sink. The column of sodium is cooled at its upper end to minimize vaporization. Initially, no provision is being made for strain measurements during the test, but the design is readily adaptable to such measurements should they be desired in the future. Assembly details and brazing and welding methods are being tested and the heat flow pattern is being determined. Heat-transfer agents, other than sodium, are being corrosion tested in the hope that a material can be found which will not require, as does sodium, loading and welding in a dry box. The presence of sodium on one side of the test specimens and fused salt on the other has the

[1] W. W. Davis, J. C. Wilson, and J. C. Zukas, *Solid State Semiann. Prog. Rep. Aug. 31, 1953*, ORNL-1606, p 8.

[2] R. B. Oliver, D. A. Douglas, Jr., and J. W. Woods, *Met. Semiann. Prog. Rep. April 10, 1953*, ORNL-1551, Figs. 43 and 44.

advantage, however, of duplicating the arrangement in the ARE.

Recrystallization and grain growth of half-hard type 2S aluminum have been observed[3] during irradiation in a Hanford reactor at a temperature several hundred degrees below that at which such events usually occur. This observation is of particular interest because grain growth of annealed Inconel in static corrosion capsules has occasionally taken place during MTR irradiation, and it has been suggested that radiation, rather than the simple metallurgical interpretation of overheating, may have been responsible. Although radiation-induced grain growth in well-annealed Inconel appears to be unlikely, its occurrence would indicate radiation changes in the nature of one of the grain-growth restraining phases at the grain boundaries rather than a bulk radiation effect. Inconel specimens subjected to 500 hr of irradiation in the LITR at 1500°F showed no grain growth when they were examined after irradiation. Specimens of 98% cold-reduced type 2S aluminum are now being irradiated at 436°F, a temperature at which no recrystallization is observed after 24 hr on the bench; at 482°F, however, recrystallization occurs after only 4 hr in bench tests. Aluminum was chosen for the first tests because of the lower irradiation temperature required and because the phenomenon has already been observed in the metal.

PHILLIPS PETROLEUM COMPANY MTR SPECIMENS

R. W. Hall[4] J. C. Wilson

A second set of tensile specimens has been received from the Phillips Petroleum Company; the irradiation was 1×10^{21} fast neutrons/cm^2 compared with a dose of 3.5×10^{20} neutrons/cm^2 for the first set.[5] Density measurements have been completed and hardness values have been measured for the beryllium and for types 2S and 356 aluminum alloys. The hardness values of all specimens were higher with the longer irradiation than they were for the shorter irradiation. No significant density changes were noted. The grip mountings for the tensile machine have been modified to permit flexible couplings to be inserted in series with both the upper and lower specimen grips; a pneumatic arrangement is provided so that the lower grip may be axially supported until the specimens are under load. Upon delivery of the tensile machine, the tensile tests will be performed.

BONDED-WIRE STRAIN GAGES

R. G. Berggren J. C. Wilson

Work on in-pile behavior of strain-gage wires and insulation has been described in conjunction with assistance rendered to the Cornell Aeronautical Laboratory[6,7] in developing a high-temperature, bonded-wire strain gage. Pending the final irradiation tests on some of the materials supplied by the Cornell Aeronautical Laboratory, some preliminary tests were started on commercial strain gages and strain-gage wires. Instrumentation and Controls Division and Homogeneous Reactor Project personnel are particularly interested in obtaining radiation-resistant gages for engineering use. Both paper- and bakelite-bonded gages are now being irradiated in the LITR. The gages were mounted on a thin strip and dead-weight loaded; strain measurements were made before irradiation so that the post-irradiation values might be compared. In addition, Karma[8] wire in three conditions of heat treatment and a specimen of constantan are being irradiated in the unbonded condition. The test is still in progress, but substantial changes have been noted in all cases except the unbonded Advance wire. The change in the Karma wire was predicted on the basis of its similarity in composition and structure to Evanohm wire that had been tested previously.[6] It is believed that both Karma and Evanohm changed resistance because of the effect of neutrons on the kinetics of the order-disorder transformation in these alloys. A source for a high-chromium, aluminum-iron alloy is being sought because this material is believed to possess the highly desirable qualities of high resistivity, low temperature coefficient of resistivity, and a stable structure with respect to neutron irradiation that

[3] S. Goldsmith, *Interim Report Production Test No. 105-510-E Determination of Pile Irradiation Effects on Corrosion of 2-S Aluminum*, HW-27531 (June 1, 1953).

[4] On loan from NACA, Cleveland.

[5] R. W. Hall and J. C. Wilson, *Solid State Semiann. Prog. Rep. Aug. 31, 1953*, ORNL-1606, p 19.

[6] R. G. Berggren and J. C. Wilson, *Solid State Quar. Prog. Rep. Nov. 10, 1952*, ORNL-1429, p 10.

[7] R. G. Berggren and J. C. Wilson, *Solid State Quar. Prog. Rep. Feb. 10, 1953*, ORNL-1506, p 9.

[8] Composition: 73% Ni, 20% Cr, and small amounts of iron and aluminum; manufactured by Driver-Harris Co., Harrison, N. J.

would make it suitable for use as a strain-gage wire.

IMPACT TESTS

R. G. Berggren J. C. Wilson

Considerable time and effort have been expended in developing shop procedures for machining economically large numbers of impact specimens in the recently developed geometry.[9] A procedure for machining such specimens of carbon steels and pressure-vessel steels has been developed. When notching stainless steels, tool life was prohibitively short, and satisfactory machining procedures are still to be developed.

Several steels have been, or are being, irradiated but have not been tested at this date. Specimens of type SAE 4340 steel and a tool steel (1.0% C, 1.2% Mn, 0.35% Si, 0.5% Cr, 0.5% W) that had been quenched and then tempered at various temperatures have been irradiated in a Hanford fuel channel and are now ready for impact testing. Specimens of type SA-212B firebox steel have been irradiated in a beam hole of the LITR. Irradiations now in progress include types SAE 1040 carbon steel, both hot-rolled and spheroidized, SA-212B hot-rolled, high-purity iron, and 301 stainless steel, in a beam hole of the LITR, and types 301 and 446 stainless steel in a beam hole of the MTR.

A pendulum stop, required to prevent occasional damage to the impact machine, has been built and is being tested on a second machine prior to installation on the remotely controlled machine. Revision of the second impact machine for subsize specimens and temperature control has been postponed until experience with the first machine has indicated the most desirable design modifications.

Assistance has also been rendered the Metallurgy Division in impact testing of titanium and Zircaloy specimens.

FATIGUE TESTS

R. G. Berggren

Trial runs have been made of subsize fatigue specimens in the Moore rotating-beam fatigue machine, and results indicate that a satisfactory subsize specimen can be developed. During the trial runs several of the specimens failed in an unusual manner and resulted in some damage to the machine. Repairs have been completed and trial runs with subsize specimens will be resumed.

Design has been started on modification of both the rotating-beam and the sheet-bending fatigue machines to adapt them for remote operation.

HOT METALLOGRAPHY

A. E. Richt E. Schwartz M. J. Feldman

Examination of irradiated static-corrosion capsules for the Fused Salt Section of this Division has continued. Eleven additional MTR-irradiated capsules and two LITR-irradiated capsules have been metallographically examined. The corrosion data obtained from these eleven experiments correlate well, with one or two exceptions, with the data obtained on earlier examinations. To assist in ascertaining the cause of the variation in datc obtained from a few of the capsules inspected, longitudinal examination of the specimens has begun. Where variations in structure have been noted, they have been along the longitudinal axis of the specimen. Figure 1 shows the variation found in three areas of a 1-in., longitudinally sectioned capsule.

Inspection of solid-type fuel sandwiches for the Pratt and Whitney Aircraft Division of United Aircraft Corporation is being carried on. Work has been completed on two experiments of a proposed 11-experiment project, and three more are in process at the present time. Irradiation-bomb pressure determinations, density measurements, bonding tests, and metallography and hardness measurements have been made on the fuel plates to date. The bonding test on the first two runs consisted of subjecting the samples to a bend radius just below the maximum to which this type of sample could be subjected in the unirradiated condition and not cause cracking of the core. Further bond (or bend) tests will be done on the basis of calculated thermal bending expected under operating conditions. Figure 2*a* is a photograph of a sample as irradiated, and Fig. 2*b* is a matching irradiated sample which had been bent about a $\frac{1}{8}$-in. radius to a 105-deg included angle. Hardness of the claddings was 109 to 124 DPH before irradiation and 171 to 194 DPH after irradiation; hardness of the cores was 231 to 233 DPH before irradiation and 479 to 481 DPH after irradiation. (Hardness numbers are for 136-deg diamond with *k* kg load on clad + 2-kg load on core.)

[9] R. G. Berggren, N. E. Hinkle, and J. C. Wilson, *Solid State Semiann. Prog. Rep. Aug. 31, 1953*, ORNL-1606, p 10.

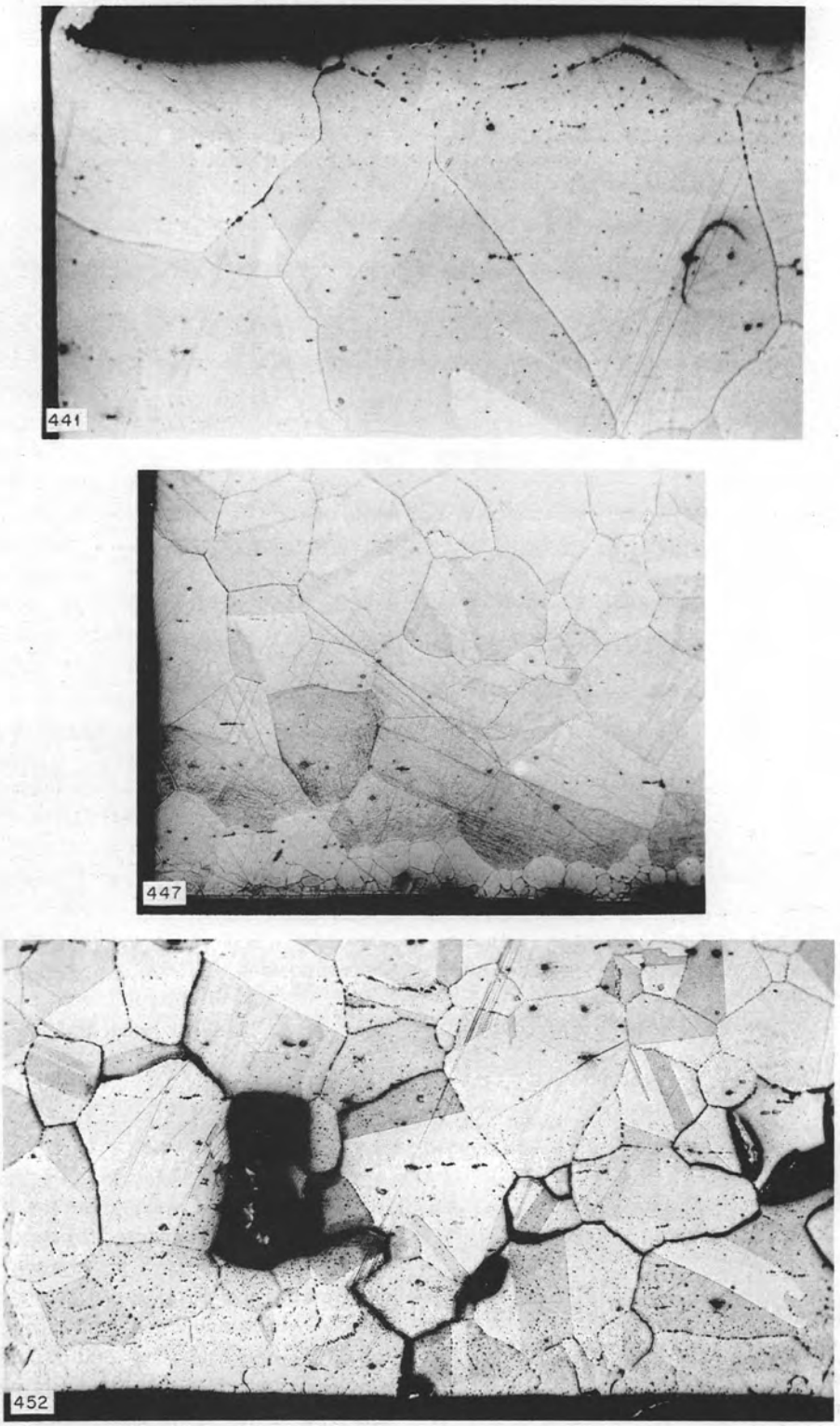

Fig. 1. Variations Found in Three Areas of a 1-in., Longitudinally Sectioned Capsule. 100X. Reduced 27%.

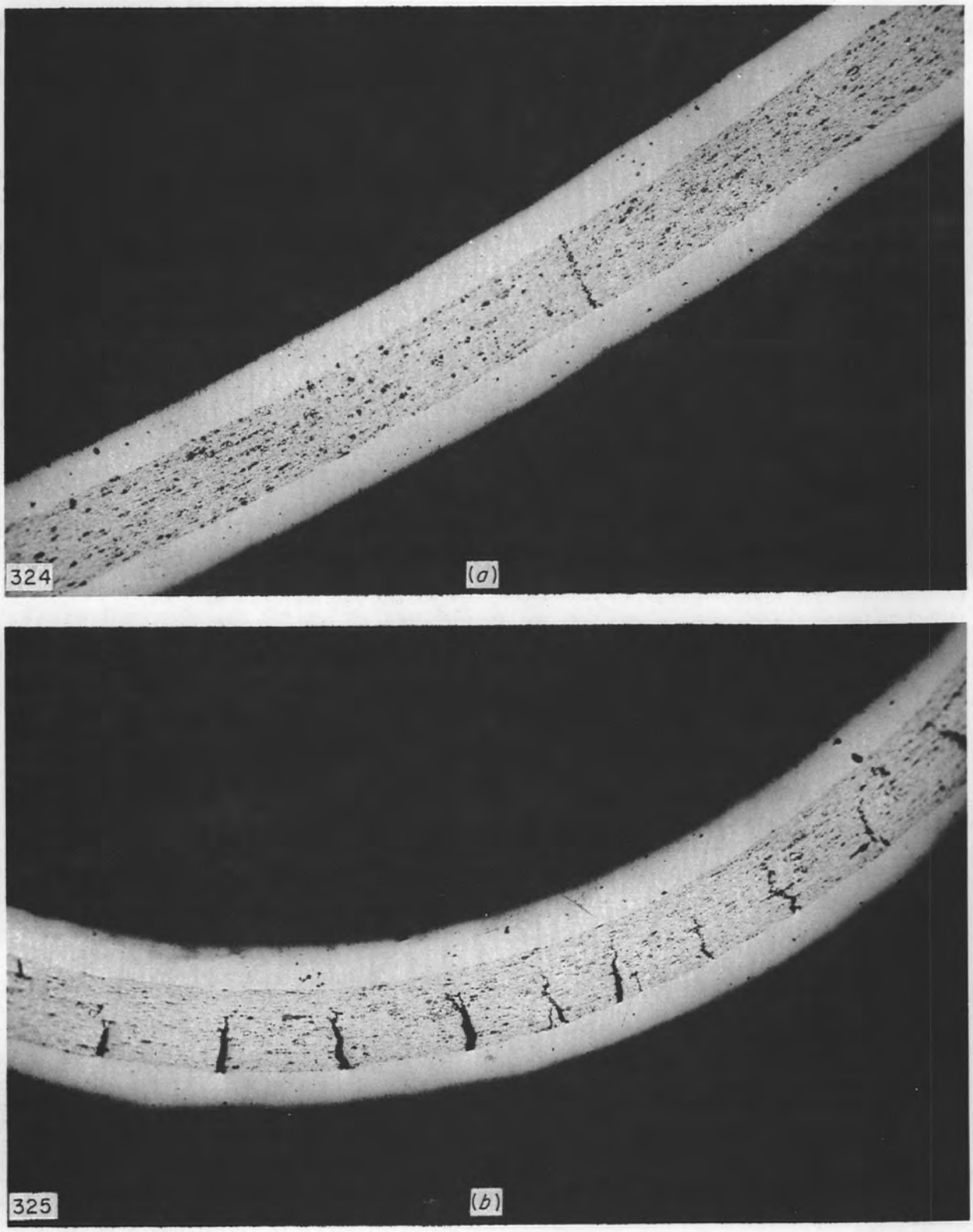

Fig. 2. Effect of Bending on the Bond in a Fuel Plate. (*a*) Fuel plate before bending; (*b*) fuel plate after bending. 60X.

SURFACE-FILM PRESERVATION OF HRE SAMPLES

A. E. Richt

Among the major interests in the HRE experiments is the determination of composition and thickness of the films formed upon the metallic surface by contact with the liquid and vapor phases of the fuel solution. To determine the thickness of these films by metallographical means, it is necessary to back up the surface film to prevent rounding of the specimen edge during the polishing operations because the films are quite thin. Figure 3 is a photomicrograph of an irradiated bomb to which no protective plate had been applied. Three methods of applying backing were tried.

The first method consisted of coating the specimens with a hard polyvinyl plastic (designated VMCH) by dipping the samples in a solution of the plastic and either heating to 350°F for 1 hr or pulling a vacuum of about 5 mm Hg over the sample to polymerize the plastic. Difficulty was encountered in obtaining a sufficient thickness of coating to prevent edge rounding; also, the light-reflecting power of the plastic is very poor and it is difficult to determine the border line between the film and plastic. This process does have the advantage that the solution wets the specimen walls extremely well and thus assures intimate contact between the plastic and the film.

The other two methods involved electrolytically plating the samples with copper or iron. The real problem in these methods is in the possibility that the film is electrically nonconductive (as some think it is), which might prevent the plated surface from being in intimate contact with the film and might give an erroneous impression of the actual film thickness. There is also some question as to the effect of the plating baths upon the surface film. The iron plating is done from a ferrous chloride bath which is maintained at 185°F. Temperature control and current density are quite critical during the plating process. Also, the plate itself is somewhat inhomogeneous in nature, as is shown in Fig. 4. These factors tend to make adaptation to hot-cell operation complex and unreliable. The copper plating is done from a cupric sulfate bath at room temperature. Temperature and current density are not critical and a uniform plate is obtained. Figure 5 shows a copper plate deposited on a relatively clean surface, while Fig. 6 is a section of the capsule showing the location of the surface film as fixed by the copper plate.

At the present time, copper plating of the specimens seems to be the most practicable method, but further investigation is to be made, since the other two methods offer some definite advantages.

Fig. 3. Corrosion Interface of HRE Capsule, Showing Interface Film. 400X. Reduced 30%.

REDESIGN AND EXTENSION OF THE REMOTE METALLOGRAPHIC FACILITIES

M. J. Feldman

In an attempt to keep pace with the increased need for metallographic examination of irradiated experiments, a redesign and extension program has been initiated. This program will encompass re-

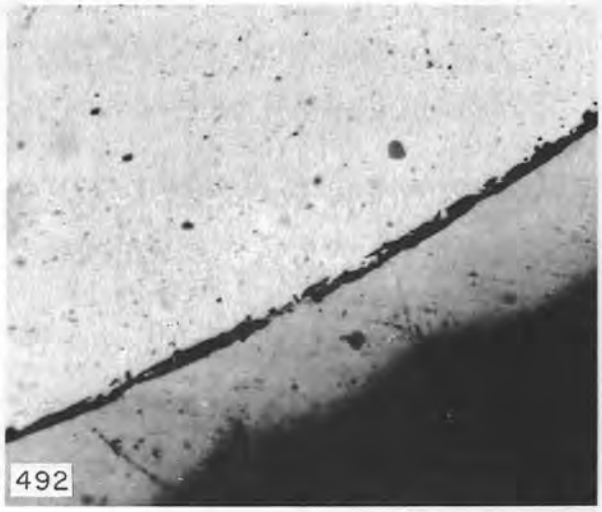

Fig. 4. HRE Capsule, Showing Surface Film and Iron Backing Plate. 250X.

design of existing equipment (which has been used for pilot-plant operation), addition of equipment to increase production, and an extension of the existing cell to isolate the optical, chemical, and mechanical components of the process. The redesign and extension program will serve two major purposes: it will separate the operations so that adequate personnel will be able to keep pace with the demands for hot metallographic work, and it will enlarge the range and size of materials that can be processed. Design work is now in progress and equipment orders are being placed. Improvements will be installed as completed, with a final completion date estimated for early 1955.

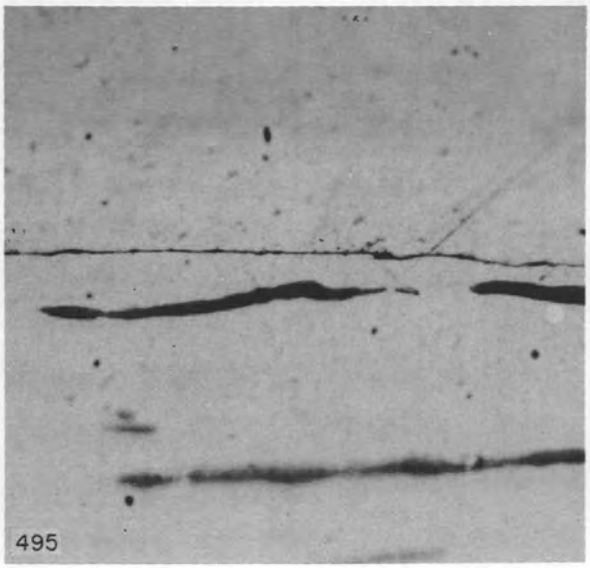

Fig. 5. HRE Capsule, Showing Copper Plated on a Relatively Clean Surface. 1800X. Reduced 14%.

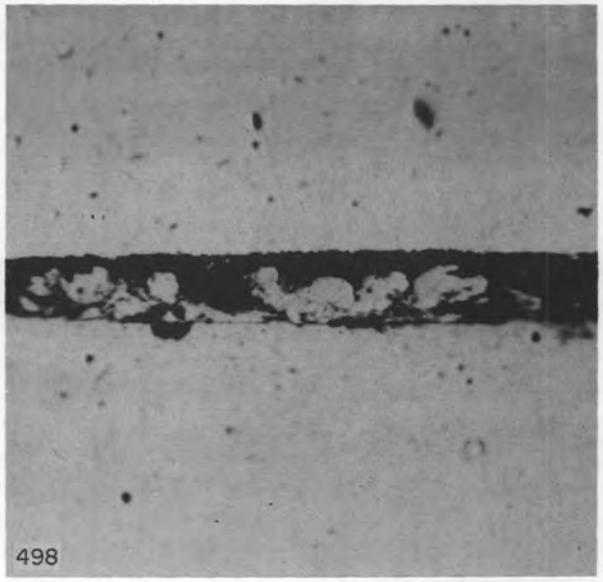

Fig. 6. HRE Capsule, Showing Surface Film and Copper Backing Plate. 1800X. Reduced 13%.

NUCLEAR MEASUREMENTS

MTR NEUTRON-FLUX–RADIATION-DAMAGE MEASUREMENT PROJECT

J. B. Trice P. M. Uthe

The project for the measurement of radiation damage resulting from MTR neutron flux is being undertaken in two stages. The first stage is an experimental evaluation of fast-neutron flux patterns in facility HB-3 of the MTR by means of a probe-type fission chamber utilizing several different threshold-energy-type fissionable materials to span an energy interval of several Mev. The second stage, similar in principle, uses threshold- and resonance-energy activations of various elements that span a larger energy interval and extend the energy range in order to broaden and support the results from the fission probes. Both experimental phases will include radiation-damage studies, and an attempt will be made to correlate neutron spectra with observed damage. A comprehensive description of the experiment has been presented.[1,2]

Fission-Probe Phase

Figure 7 shows the fission probe and some of its accompanying electronic equipment. The probe electrode assembly is shown schematically in Fig. 8. The plates which hold the fissioning material are easily detached in order that the entire series of fissionable elements may be used sequentially in one probe.

The major problems encountered during the developmental stage of the probe were the needs for (1) a minimized capacitance of the 15-ft probe leads so that an acceptable plateau width could be obtained, (2) a probe construction to maintain high performance characteristics for 50 to 100 hr in flux fields above 10^{10} fast neutrons/cm^2·sec and in the accompanying high-intensity gamma fields found in MTR-type reactors, and (3) an accurate determination of the probe counting efficiency for each of the fissionable threshold materials to be used in the probe.

The first problem, the reduction of probe-lead capacitance, was solved by varying both the geometry and materials of the probe signal-lead system. A minimum distance in the reactor beam hole of 16 ft between the chamber and its preamplifier implied such a large capacitance (430 $\mu\mu f$) between the probe and the preamplifier that the signal from the probe was severely distorted by the time it reached the preamplifier. It was recognized that the absence of a pulse-height plateau was the result of this large capacitance. The capacitance was

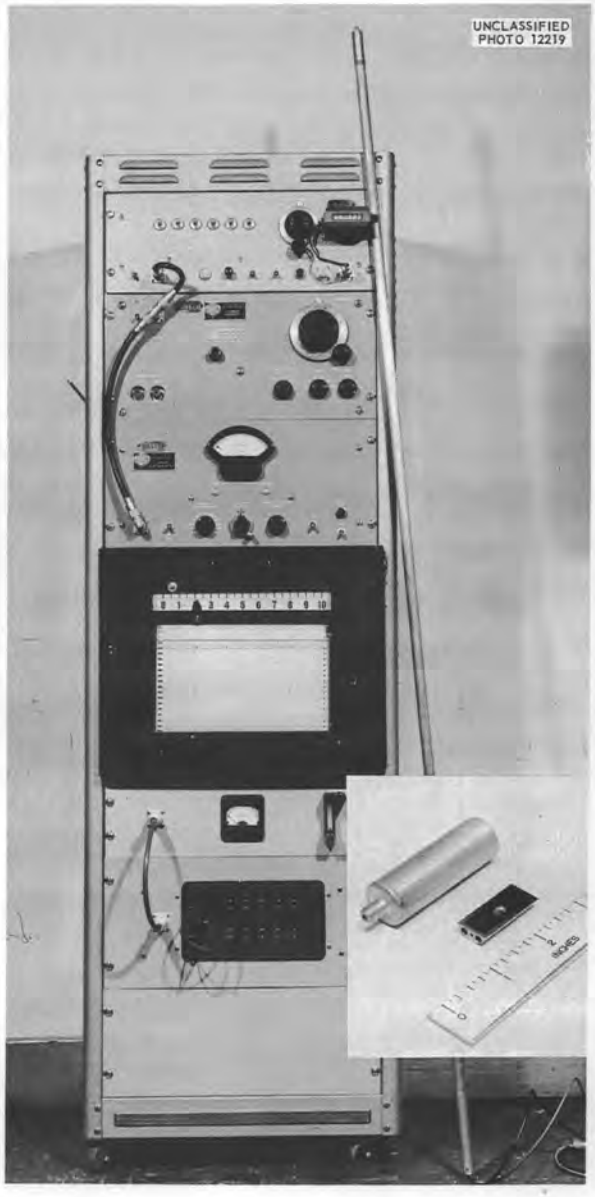

Fig. 7. Fission Probe and Controls.

[1] J. B. Trice, F. W. Smith, and F. J. Muckenthaler, *Solid State Quar. Prog. Rep. Feb. 10, 1953*, ORNL-1506, p 11.

[2] J. B. Trice and P. M. Uthe, *Solid State Semiann. Prog. Rep. Aug. 31, 1953*, ORNL-1606, p 23.

reduced to 180 $\mu\mu f$ for 21 ft by using 10-mil nickel wire instead of 25-mil copper wire as the center conductor for the signal lead and by increasing the inside diameter of the fused-quartz insulators in the probe. Figure 9 shows the pulse-height plateau which was obtained with a potential difference of 360 volts across the probe plates. Operation of the probe for 50 hr in a field of 10^{11} fast neutrons/cm^2·sec together with the accompanying gamma field ($\sim 10^{12}$ gammas/cm^2·sec) proved that the probe has good radiation stability. Breakdown did occur at intensities of the order of 10^{12} fast neutrons/cm^2·sec but was probably caused by the accompanying gamma rays and not by the neutrons. A convenient feature of the probe is that it can easily be handled after a day or so out of a neutron field of 10^{12} thermal neutrons/cm^2·sec.

The probe was calibrated in the ORNL thermal column, which provides a satisfactory plane source of thermal neutrons in water. The ratio of thermal to fast neutrons in this facility is approximately 10^6. Calibration consisted of a comparison between the probe response and a gold-foil flux measurement along a vertical traverse through the water. Use of the probe efficiency as measured with U^{235} and gold for other fissionable materials to be used in the probe seems to be justified because the *calculated* chamber response for a known thermal flux agreed closely with the *measured* chamber response. The results from the vertical-traverse calibration are shown in Table 1 in which the flux measured with the probe using a response determined by calculation (from amount of fissionable material plus electrode geometry) is compared with the flux measured by a gold foil exposed to the same thermal flux as the probe electrode plates. Only after comparative measurements were made between a foil placed on the external surface of the probe and a foil placed between the electrodes was it assumed that the gold foil mounted on the side of the probe

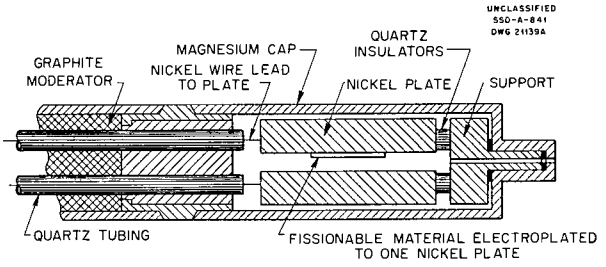

Fig. 8. Cross Section of Fission Chamber.

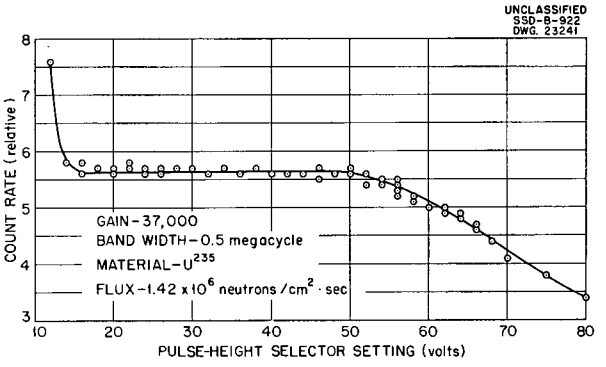

Fig. 9. Typical Pulse-Height Plateau Curve.

TABLE 1. CALIBRATION DATA FOR FISSION CHAMBER

THERMAL-NEUTRON FLUX (as indicated by chamber)	THERMAL-NEUTRON FLUX (as indicated by foil)	DIFFERENCE (%)
2.64×10^7	2.77×10^7	4.5
2.73×10^7	2.81×10^7	2.7
1.81×10^7	1.82×10^7	0.2
2.62×10^7	2.78×10^7	6.0
2.87×10^7	2.94×10^7	2.2
2.55×10^7	2.54×10^7	0.6
5.62×10^6	5.46×10^6	2.9
6.64×10^6	6.83×10^6	2.8

Standard deviation is 1.8%

was exposed to the same flux as the probe electrodes. The two responses were identical within the limits of experimental accuracy (99%). Detection efficiency of the probe as determined by these measurements is 98 ±1.8%.

A major uncertainty in the use of gold to measure thermal-neutron flux in water was in the so-called "perturbation factor" which is a measure of the change in flux caused by the presence of the foil. This factor was determined by a comparison in the ORNL thermal column of the gold with the known perturbation of indium in water. The gold result was then compared with a gold-flux measurement in the ORNL Graphite Reactor in which the perturbation effect is quite well known. Here, the thermal-neutron flux is given by $\phi = 3.29\ A$, where A is the saturated activity in counts per second for a beta counting rate in a certain beta counter (Physics Division's counter "Bob") and 3.29 is an experimentally determined number which includes counter geometry, gold nuclear and geometrical properties, self-absorption of both neutrons during irradiation and betas during counting, and the perturbation factor for a graphite medium.

The flux equation for water is $\phi = 3.29(A)a$, where a is the ratio of perturbation effects in graphite and water. Flux traverses made in the thermal column with gold were compared with indium measurements which were used as the standard of measurement for a water medium. The flux ϕ, calculated by using indium, and A, the saturated activity for gold, were substituted into the equation

$$a_{Au} = \frac{(0.0753)A_{In}}{(3.29)A_{Au}}$$

to obtain $a_{Au} = 1.011$. Since experimental errors of 5% are expected for these measurements, it was decided that the 1% variation indicated by a_{Au} was meaningless; hence a_{Au} was called unity. The vertical flux traverse in the ORNL thermal column is shown in Fig. 10.

The water-cooled plug designed for insertion into hole HB-3 of the MTR was tested, and the plug and the probe with its auxiliary equipment have been shipped to Idaho.

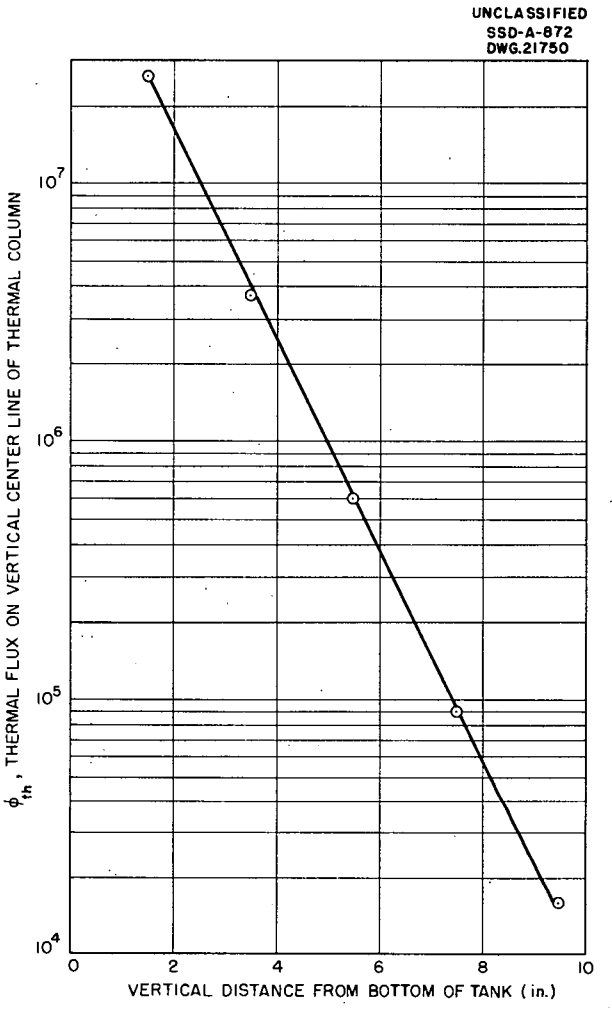

Fig. 10. Thermal Flux in Thermal Column as a Function of Vertical Position.

ENGINEERING PROPERTIES

LITR FLUORIDE-FUEL LOOP

W. E. Brundage
C. D. Baumann
F. M. Blacksher
C. Ellis
M. T. Morgan
A. S. Olson
W. W. Parkinson
O. Sisman

The circulating-fuel experiment for the study of the stability and corrosion characteristics of molten fluoride fuels under reactor irradiation has been described in earlier reports.[1] Figure 11 is a drawing of the LITR fluoride-fuel loop which consists essentially of a specimen section for irradiation, an air-fuel heat exchanger, a venturi flowmeter, and a pump (not shown in the drawing). The design values for the loop are:

Temperature of irradiated end	1500°F
Temperature at pump	1400°F
Fission heat generation, maximum density	1000 to 2000 watts/cc
Total fission heat generation	10,000 to 15,000 watts
Linear flow in irradiated section (0.225-in. ID)	10 fps

The fuel system will be all Inconel, and the composition of the fuel will be $NaF\text{-}ZrF_4\text{-}UF_4$ (62.5-12.5-25 mole %).

Fabrication of parts for three loops is about 50% complete. The effort is being concentrated on finishing and testing parts for a single loop that is about 80% complete. The specimen section, X in Fig. 11, has been finished and parts for a second assembly are made. The assembly of the parallel-flow heat exchanger, L in Fig. 11, proved to be difficult, and heat-transfer tests indicated that the operation of the exchanger was inadequate. A spiral-fin-type exchanger has been built and tests have shown that it is capable of removing the fission heat generated in the fuel.

Parts for three venturi flowmeters, K in Fig. 11, have been fabricated and a prototype pressure-transmitter cell has been tested under simulated operating conditions. It was filled with a fluoride-fuel mixture and pressure cycled for one month. At the end of this time the diaphragm was sectioned and examined microscopically. The only evidence of corrosion was local surface discoloration and there was no indication of incipient failure. To complete the loop proper, only the bending and attachment of the connecting tubing remains to be done, provided current tests of the heat exchanger and the pump are satisfactory.

Parts for three sump-type pumps, including one for test purposes only, have been completed. The test pump was modified after tests with water and is being installed in a fluoride testing system. A second pump is being tested with water and should be ready for incorporation into the first fuel loop in a few days.

The water jackets, A in Fig. 11, for the three loops have been assembled, but excessive leakage was found around the longitudinal vanes separating the incoming and outgoing water channels. It was found necessary to split the outer tube and to weld the separator vane along its entire length to both the inner and outer walls of the jacket. This modification has been completed on only one of the jackets.

Shielding for personnel protection is required around both the pump and the short length of fuel tube between the reactor shield and the pump. Paraffin blocks for neutron shielding have been made up, and sheet-metal shells are ready to be filled with lead to form the gamma shields. These gamma shields are designed in sections to facilitate removal of the pump from the rest of the loop after the fuel has become radioactive. The pump shield will provide 6 in. of lead that will be augmented by 4 in. of stacked lead bricks and 12 in. of paraffin, and the tube shield between pump and reactor face is comparable in thickness. The withdrawal shield, into which the loop and water jacket will be withdrawn after removal of the pump, has been completed. This shield is a 15-ft horizontal cylinder with an 8½-in. central hole and 5-in. lead walls.

The instrument panel has been finished and is installed in Building 3550 for bench-testing the loop. This panel contains all the instruments for measurement and control of the loop, with the exception of pressure regulators and valves in the water and gas lines for the loop. These additional valves and controls are on hand and installation in the LITR Building has begun. Because of the heater power requirement it was necessary

[1] W. E. Brundage *et al.*, *Solid State Semiann. Prog. Rep. Aug. 31, 1953*, ORNL-1606, p 29.

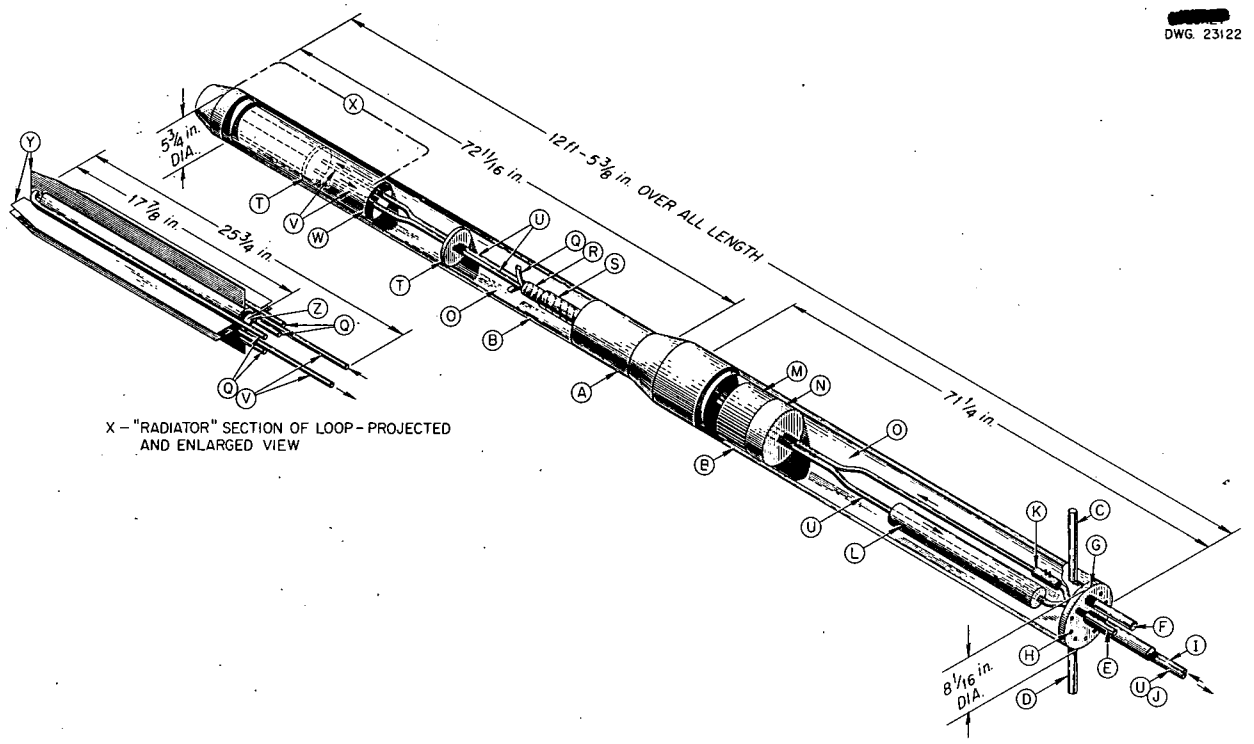

A – LINER, WATER JACKET
B – WATER FLOW THROUGH ANNULAR SPACE
C – COOLING WATER OUT
D – COOLING WATER IN
E – AIR INLET
F – AIR OUTLET
AIR-TO-FUEL HEAT EXCHANGER
G – FACE PLATE
H – PORTS FOR THERMOCOUPLE, HEATER, AND VENTURI LEADS
I – FUEL TUBES TO PUMP
J – FUEL TUBE JACKET (HELIUM FILLED)
K – VENTURI METER
L – AIR-TO-FUEL HEAT EXCHANGER
M – GRAPHITE
N – STEEL
RADIATION SHIELDING
O – HELIUM-FILLED SPACE
Q – CALROD HEATERS (OVER ENTIRE LENGTH OF LOOP)
R – STAINLESS STEEL SHEET WRAPPING
S – HIGH-TEMPERATURE WRAPPED INSULATION
T – B_4C-Fe DISKS (NEUTRON SHIELDING)
U – FUEL TUBING (0.404 in. ID, 0.500 in. OD)
V – FUEL TUBING (0.225 in. ID, 0.275 in. OD)
W – STAINLESS STEEL COVER
X – IRRADIATED SECTION OF LOOP
Y – RADIATOR FINS
Z – INTERNAL HEATER, NICHROME V HELIX

Fig. 11. LITR Fluoride Fuel Loop Assembly.

to increase the electrical power available at the LITR; this has been completed.

The disassembly of the fuel loop after operation in the reactor will require additional tools and a special door in the Solid State Division hot cells. The design of the door is complete and the necessary tools have been ordered. Design work to modify the tools for remote operation is 80% complete.

[2]W. W. Parkinson *et al.*, *Solid State Semiann. Prog. Rep. Aug. 31, 1953*, ORNL-1606, p 31.

LITR SODIUM STRESS-CORROSION LOOP

W. W. Parkinson

At the time of the last report,[2] work on the LITR sodium stress-corrosion loop was completed except for analysis of the sodium for the long-lived activity and the heat treatment of a control sample of Inconel to duplicate the conditions to which the irradiated specimen was exposed. A radiochemical analysis of the sodium from the loop by the Analytical Chemistry Division indicated that Ag^{110} made up about 80% of the long-lived activity, with

Na^{22} constituting the remainder. An earlier spectrographic analysis showed silver present to the extent of about 20 ppm in the sodium and about the same concentration of palladium. Both these contaminants were presumed to have dissolved out of the nickel-palladium braze used to attach the stressed specimen to the Inconel loop tubing. A short-lived radioactivity in the sodium had been identified[2] earlier as Pd^{103} (13-day half life).

The heat treatment of an Inconel control specimen by the Radiation Metallurgy Section failed to yield a precipitate with the characteristics distribution[2] found in the irradiated and stressed specimen. Therefore the origin of the Widmannstätten-like structure is still not clear.

ORNL GRAPHITE REACTOR SODIUM-INCONEL LOOP

W. E. Brundage M. T. Morgan

After a heater failure during in-pile operation of the Graphite Reactor sodium-Inconel loop,[3] new heaters were attached and the controls were modified to permit operation without attendance of an operator. The loop operated for only 17 hr before a leak was indicated by loss of vacuum in the jacket around the loop, radioactivity in the off-gas system, and erratic flow. The loop was allowed to cool and was then removed from the reactor. Examination of the loop tubing for the cause of the leak and a metallographic examination will conclude this work in the Graphite Reactor. Since this was an extension of the earlier experiment in which the heaters burned out, this early failure is not too serious. It is perhaps more significant that a rather large leak of highly radioactive sodium at 1500°F was handled without overexposure to personnel or without any danger to personnel or reactor. Any additional studies will be made in a higher flux.

---

[3] C. D. Baumann *et al.*, *Solid State Quar. Prog. Rep. Feb. 10, 1953*, ORNL-1506, p 13.

FUSED SALTS

RADIATION DAMAGE IN FUSED-SALT FUELS

G. W. Keilholtz
J. G. Morgan
H. E. Robertson
C. C. Webster
M. T. Robinson
W. R. Willis
W. E. Browning
M. F. Osborne

ANP fused-salt fuels are being irradiated in the LITR and in the MTR. They are being studied chiefly for chemical stability and corrosion properties. Present results indicate that within a 600-hr period under high flux conditions the salts have retained their original melting points, and chemical analysis is used to check the uranium concentration if a burnup correction is made.[1] Corrosion of the Inconel container is about 1 mil in control samples and about 4 mils in irradiated samples. Intergranular corrosion in the presence of high-purity fuels has been noted in irradiated capsules but not in the unirradiated controls. The subsurface void type of attack is noted in both irradiated and unirradiated tests.

To date, tests have been made in capsules such as those shown in Fig. 12. The capsules have an inside diameter of 100 mils and a 50-mil Inconel wall and are operated so that the salt-Inconel interface is 815°C (1500°F).

Figure 13 illustrates the installation used in the MTR. The temperature is maintained at 1500°F by a variable airflow over the capsule. External heating of the capsule is unnecessary in the MTR.

The principal salt under study has been a composition of 50-46-4 mole % sodium, zirconium, and uranium fluorides. The capsules are filled in a vacuum-type dry box with a dry helium atmosphere over the salt. Figure 14 shows controls of 100, 300, 520, and 700 hr for this salt with 1 to 2 mils

[1] G. W. Keilholtz *et al.*, *ANP Quar. Prog. Rep. Sept. 10, 1953*, ORNL-1609, p 111.

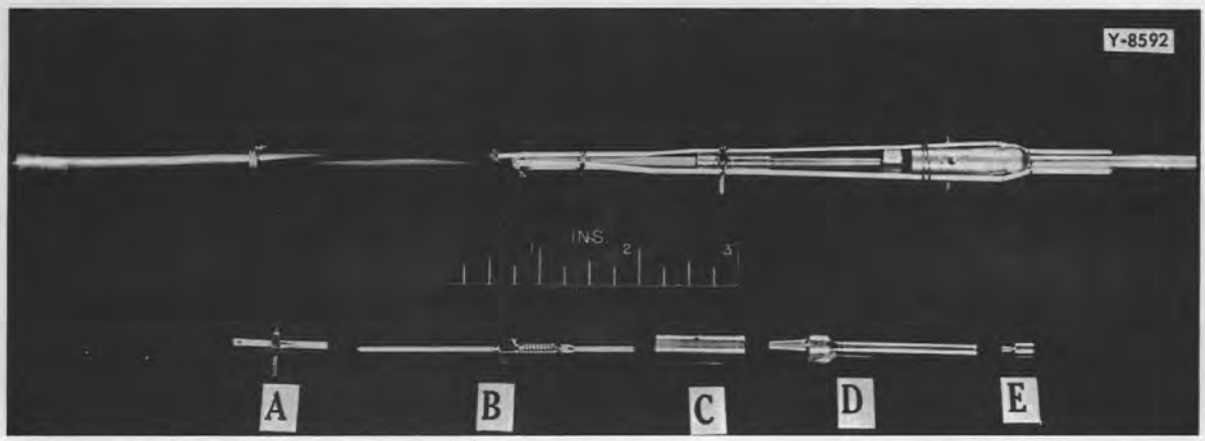

Fig. 12. Corrosion Capsule Assembly and Exploded Parts.

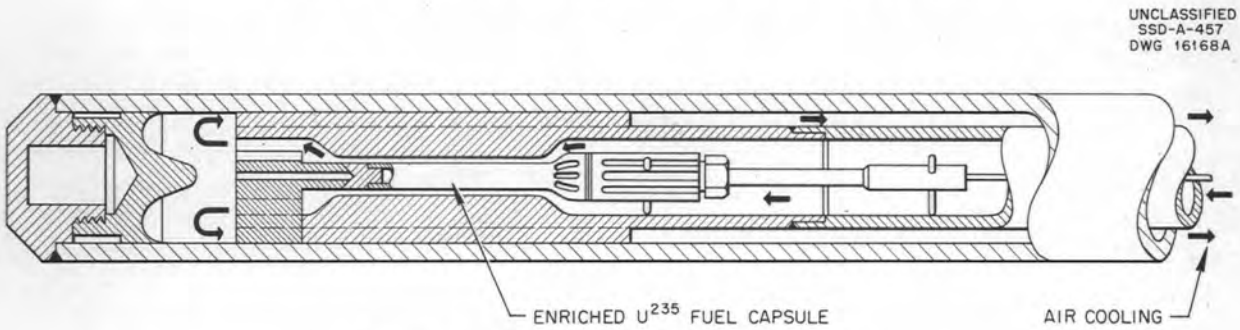

Fig. 13. MTR Air-cooled Capsule Assembly.

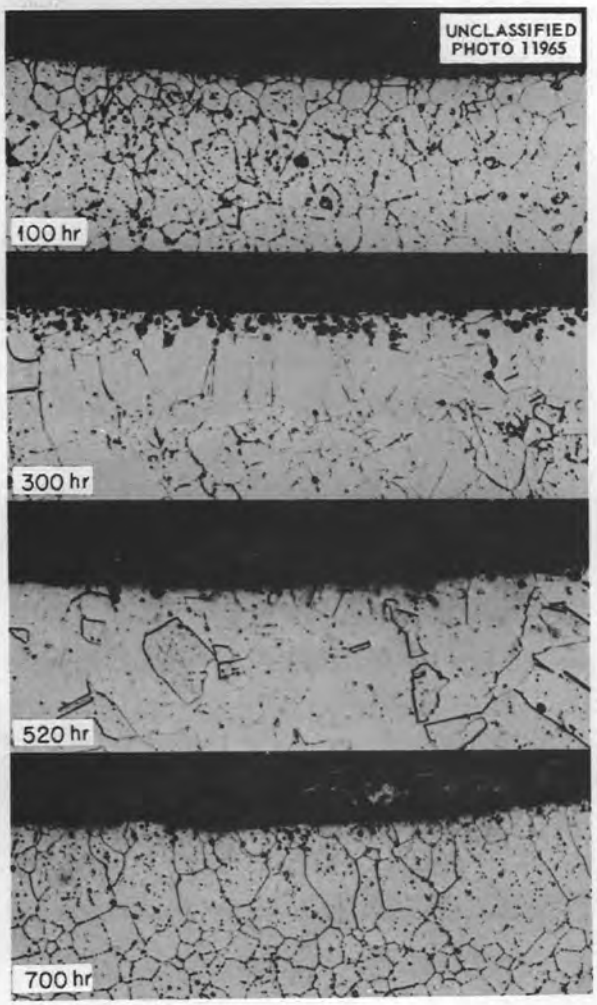

Fig. 14. Inconel Capsule Surfaces After Exposure to Fluoride Fuel at 815°C in the Absence of Irradiation. 250 X.

of maximum corrosion for 300 hr in the absence of radiation.[2]

Figure 15 indicates corrosion with increase in irradiation time: 53, 140, 270, 565, 685, and 810 hr.[2] The salts with 8.05 wt % U^{235} are calculated to generate 210 watts/cc when placed in the LITR at a flux of 2×10^{13} neutrons/cm^2·sec. There is a progressive corrosion of approximately 0.5 mil/100 hr. The 810-hr test, however, shows only 1 mil of corrosion. This should emphasize the need for caution when making general statements based on a limited number of samples. More tests are under way.

Figure 16 is a photomicrograph of the same salt (8.05 wt % U^{235}) exposed in the MTR facility at a flux of 2.4×10^{14} neutrons/cm^2·sec, generating 2500 watts/cc.[3] The corrosion is extended to between 4 and 5 mils in 575 hr and is of the intergranular type.

The fission power generated at 1500°F in three of the fluoride fuels in the MTR and the LITR is given in Table 2. The flux values used for the LITR are the maximum values from Fig. 25. The thermal-neutron flux in facility A-38 of the MTR has been measured[4] by cobalt activation to be 2.4×10^{14} neutrons/cm^2·sec. The power generation values have a probable uncertainty of ±25%. The values for the MTR are for the 3 × 9, north slab-loading pattern used until November 1953.

[2]More detailed information in Remote Metallography Group (RMG) File No. 53-8-130.

[3]More detailed information in RMG File No. 53-8-157.

[4]M. T. Robinson and P. R. Klein, *Solid State Semiann. Prog. Rep. Aug. 31, 1953*, ORNL-1606, p 43.

TABLE 2. FISSION POWER GENERATED AT 1500°F

FUEL NO.	CONCENTRATION OF U^{235} (wt %)	POWER GENERATED (watts/cc)		
		MTR* Position A-38	LITR** Position	
			C-46	C-48
30	8.05	2500	430	330
44	12.4	3900	680	510
41	24.5	8000	1400	1000

*30 megawatts.

**3 megawatts.

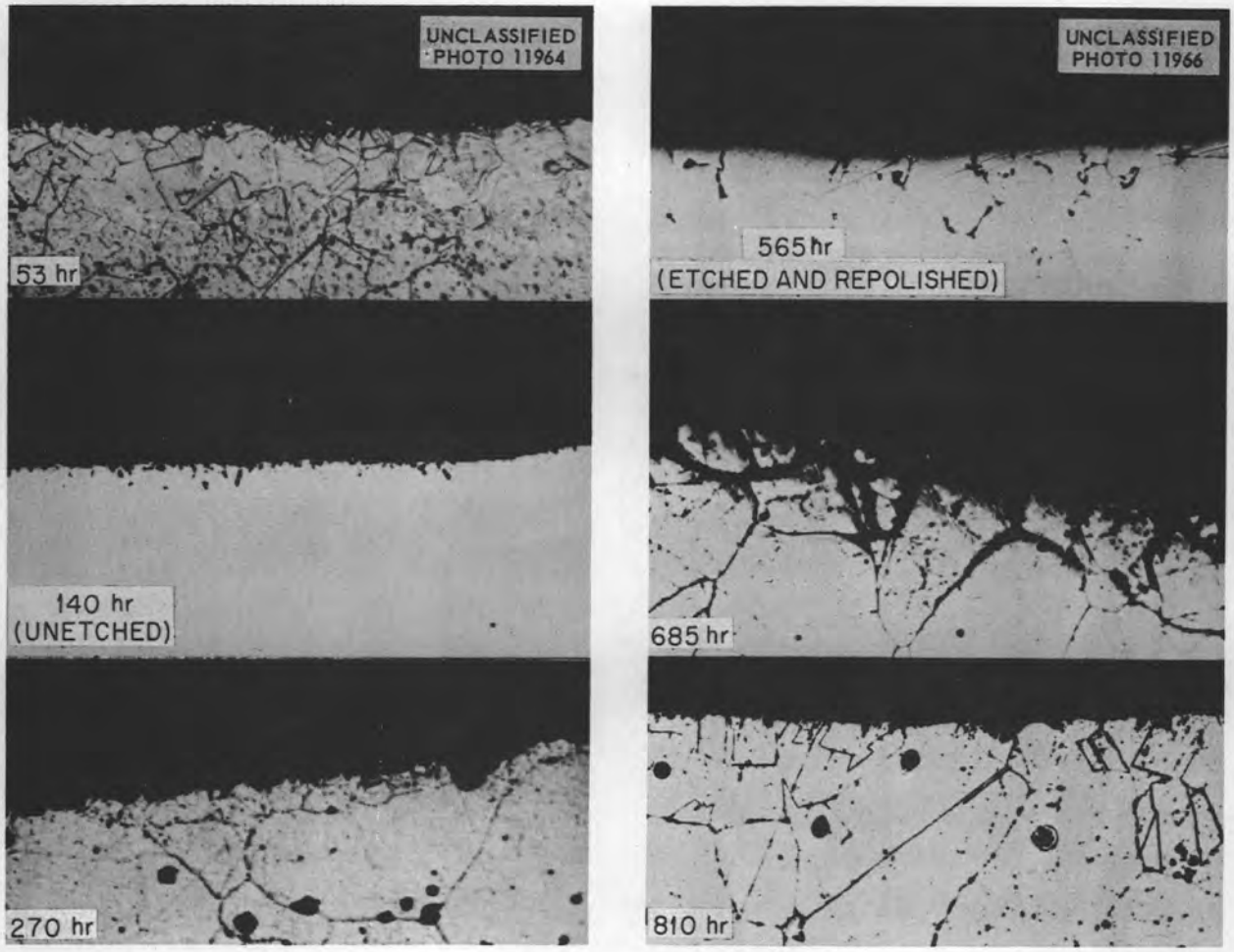

Fig. 15. Corrosion of Inconel After Exposures to Fluoride Fuel at 815°C in the LITR for Various Irradiation Times. 250X.

Figure 17 shows the cross section[3] of a capsule which contained a sodium-zirconium-uranium salt with an increase in uranium to 12.4 wt % U^{235}. The exposure was 419 hr in a flux of 2.4×10^{14} neutrons/cm^2·sec and the power dissipation was calculated to be 3900 watts/cc. The sample shown[5] in Fig. 18 contains still more uranium, 24.5 wt % U^{235}, and was irradiated for 350 hr; the calculated power dissipation was 8000 watts/cc. Figures 16, 17, and 18 exhibit that no unusual changes occur in the corrosion pattern when the power is increased by adding more uranium to the fuel.

The deep intergranular penetration of 13 mils shown in Fig. 19 has been observed on a few capsules.[5] It has occurred at random and is not a function of uranium concentration or of irradiation time in the MTR. This penetration occurs with large-grained Inconel, but it has not been established as a radiation effect.

TEMPERATURE CONTROL IN THE MTR STATIC-CORROSION TESTS

J. G. Morgan W. R. Willis M. F. Osborne

Controlling the temperature in the static-corrosion tests resolves into the problem of using thermocouples to measure the temperature of a surface when it is cooled by air flowing at high velocity.

In analyzing this problem, H. F. Poppendiek[6] has considered the thermocouple as a cooling fin

[5]More detailed information in RMG File No. 53-10-50.

[6]Reactor Experimental Engineering Division.

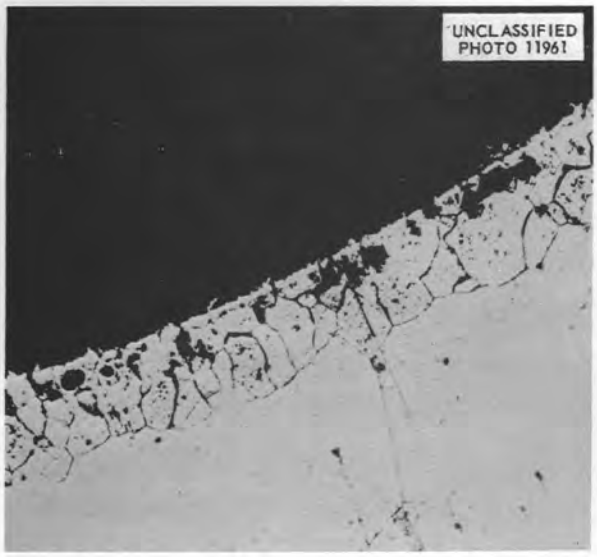

Fig. 16. Inconel Capsule Surface After Irradiation in the MTR for 575 hr at 815°C. 250X.

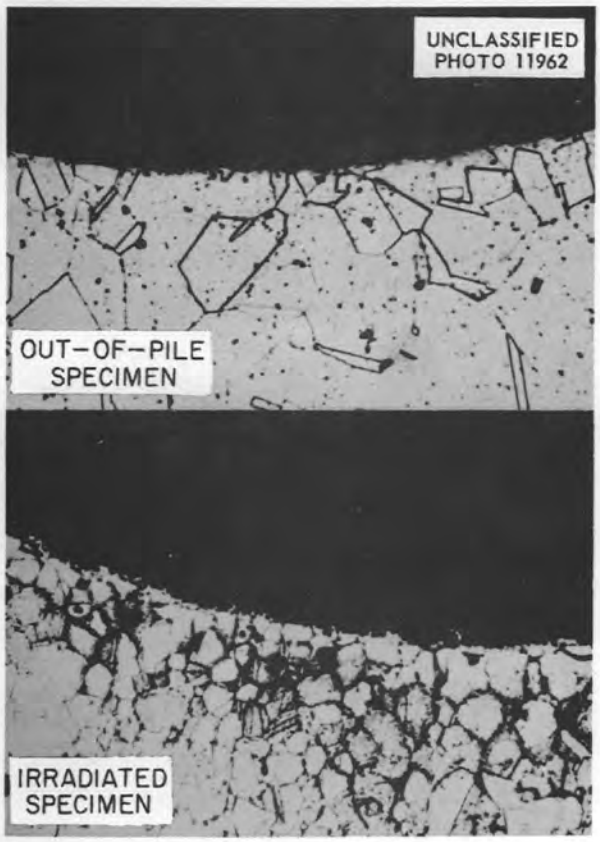

Fig. 17. Comparison of a Control Specimen and a Specimen Irradiated in the MTR for 419 hr at 815°C. 250X.

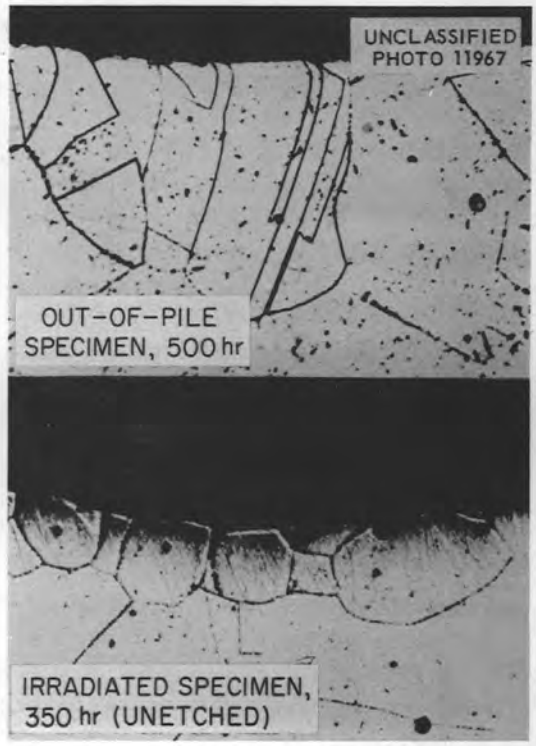

Fig. 18. Comparison of a 500-hr Control Specimen with a Specimen Irradiated in the MTR for 350 hr at 815°C. 250X.

attached to the capsule. On this basis, then, there are three temperatures to be considered, as illustrated in Fig. 20 where the temperature is plotted as a function of distance along the capsule.

The temperature designations are as follows:

T_S = the temperature the capsule surface would be if the thermocouple were not present,

T_D = the temperature the surface assumes because of the cooling action of the thermocouple,

T_C = the indicated temperature of the thermocouple; T_C is lower than T_D because the effective bead of the thermocouple does not lie at the capsule but at some short distance along the thermocouple,

T_P = the surface temperature observed with an optical pyrometer.

In estimating the maximum temperature that was attained in the MTR static-corrosion tests, three points should be considered: (1) the magnitude of $T_S - T_C$, (2) the difference in temperature between the inner and outer surfaces of the capsule, and (3) the possible difference between the peak temperature at any point along the capsule and the temper-

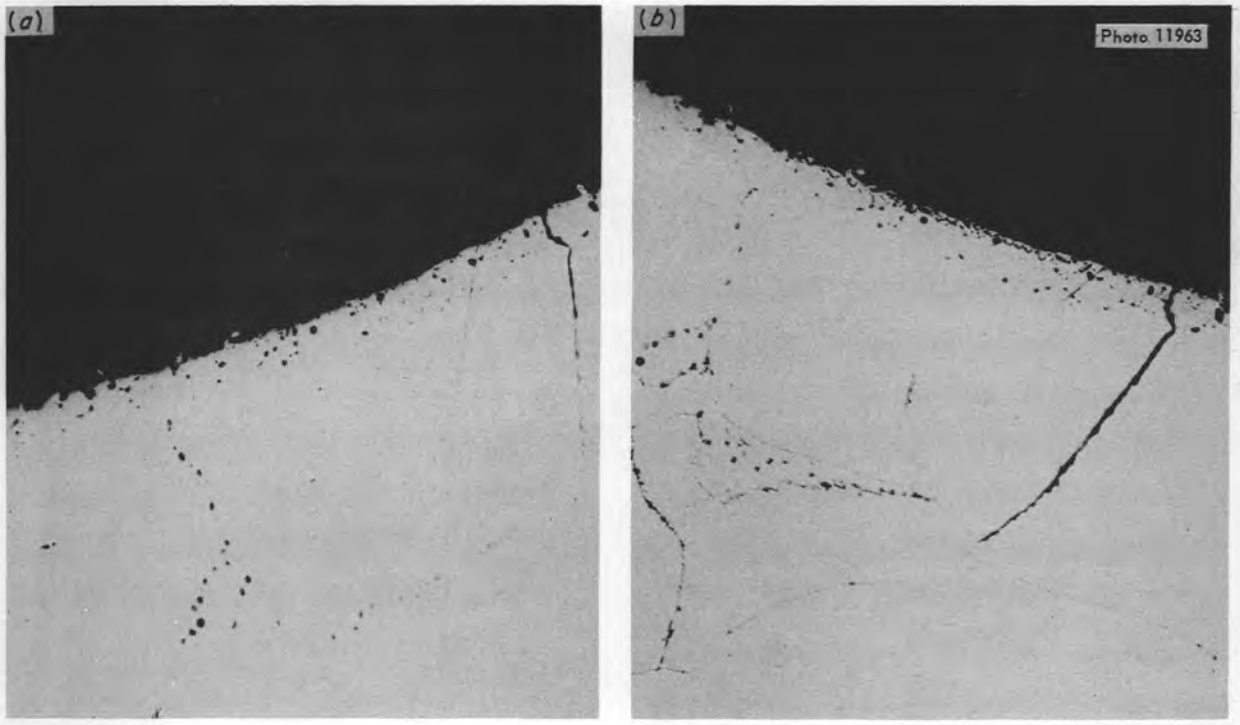

Fig. 19. Inconel Capsule Surface After Irradiation in the MTR for 406 hr at 815°C. (*a*) Unetched, (*b*) etched.

ature of the highest-reading thermocouple. The highest-reading couple controls the cooling air flow and is thus maintained at operating temperature.

The temperature difference in (2) was calculated and the operating temperature was chosen to eliminate this effect. The following experiments were performed to evaluate (1) and (3).

Figure 21 is a cross section of the MTR mockup. All pertinent dimensions needed to evaluate (1) were identical to the actual in-pile tests. Chromel-Alumel thermocouples were spot-welded at 120 deg on the outside surface of the test section. The thermocouple junction was with as small a bead as possible and duplicated MTR capsule assembly technique. An additional thermocouple was inserted into the center of the test section out of the air stream. Surface temperature was observed with an optical pyrometer sighted through the sight glass that surrounded the test section. The test section was heated by resistance heating through electrodes soldered to each end of the section. Air was passed over the heated section, and the volume flow was measured with a standard orifice (Fig. 22). Steady-state measurements were taken

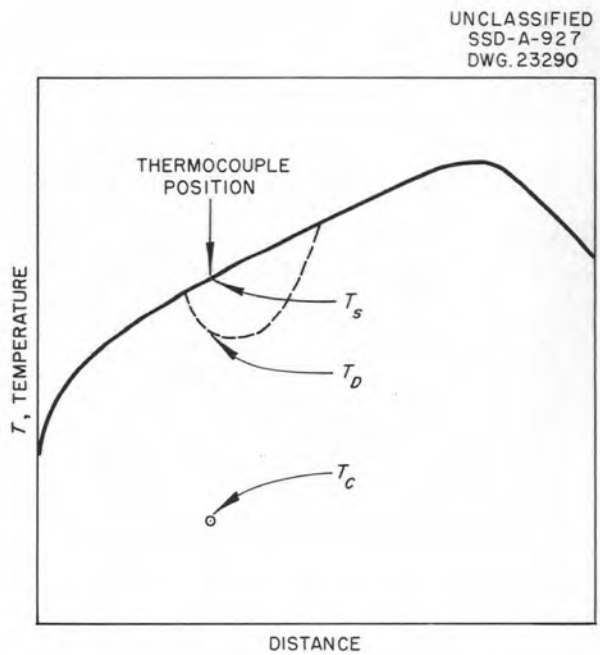

Fig. 20. Qualitative Temperature Distortions Caused by Fin Action of Thermocouple.

at 1500°F with varying air flow and power inputs. Air flows up to maximum MTR operating conditions were obtained; the results are given below:

Air Flow (fps)	$T_P - T_C$ (°F)
77	40
119	52
175	77
220	115

Figure 23 shows a plot of $T_P - T_C$ vs air flow. The optical pyrometer readings have been corrected to true temperature by using a value of 0.9 for the emissivity of oxidized Inconel. Two of the three thermocouples used in this test agreed to within 5 deg; the third one was a poorly constructed couple which would have been rejected if it had been inspected.

The pyrometer temperatures T_P in the above experiment would be somewhere between T_S and T_D. The worst case then would be for the temperature differences to be $T_D - T_C$. A second experiment was performed to measure $T_S - T_C$ and to measure the longitudinal gradient along the capsule.

In the experiment to evaluate (3), the length of the test section was 1 in., the same as that used in the fuel column in MTR capsules. Power generation was about 3200 watts/cc, as compared with 2500 watts/cc in the capsules. The massive electrodes on the test section gave greater end effects than were experienced in the reactor. Thus the conditions are more severe for this test than for the in-pile test.

A single thermocouple, judged beforehand to be a mediocre example of usual construction, was attached as before. The optical pyrometer was used to measure the longitudinal gradient on the side of the section away from the thermocouple. The results are shown in Fig. 24.

If it is assumed that the temperature variations along the test section were more extreme than those in the capsules, a value of $T_S - T_C$ can be obtained that is larger than any to be expected in the reactor. The difference includes all the errors mentioned before, and it is assumed that the peak temperature along the capsule is in the worst position.

The error for the worst thermocouple found would be 250°F, including temperature peaking between thermocouple positions. If the control temperature is taken as 1400°F and 100°F is added for the temperature drop in the Inconel wall, the hottest portion on the inside wall of the capsule would be 1750°F. At an indicated temperature of 1600°F (or 1950°F for the hottest portion) the reactor would be set back; this has never happened.

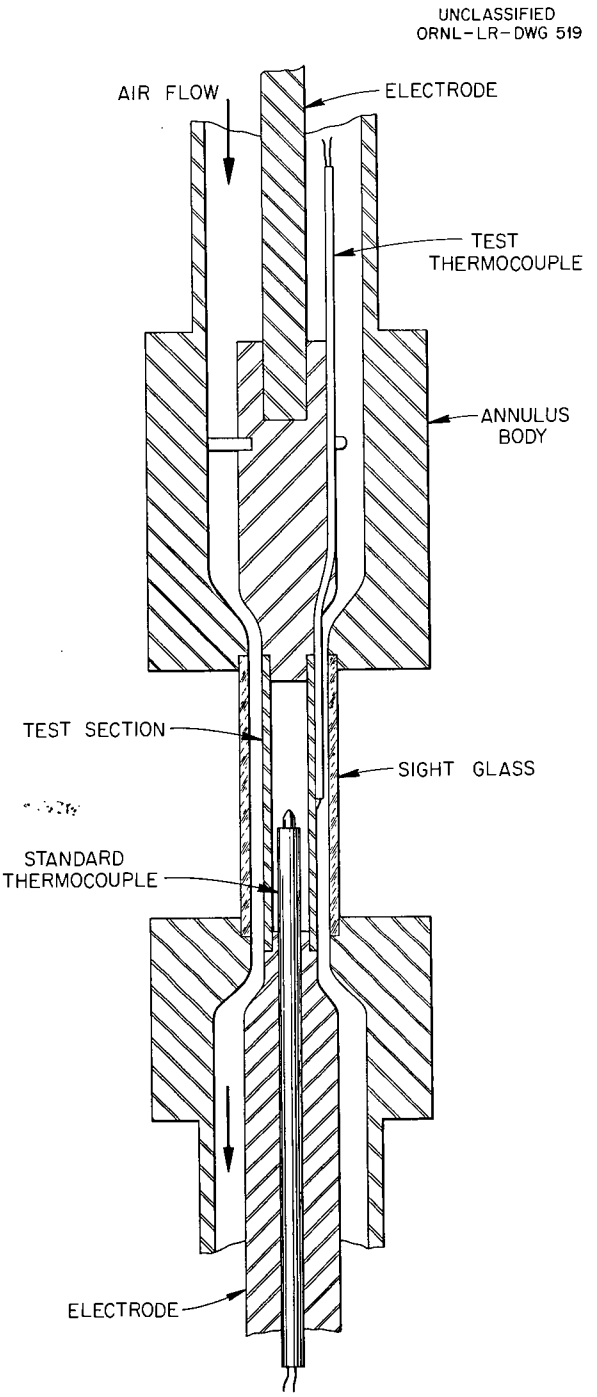

Fig. 21. Thermocouple Test Section.

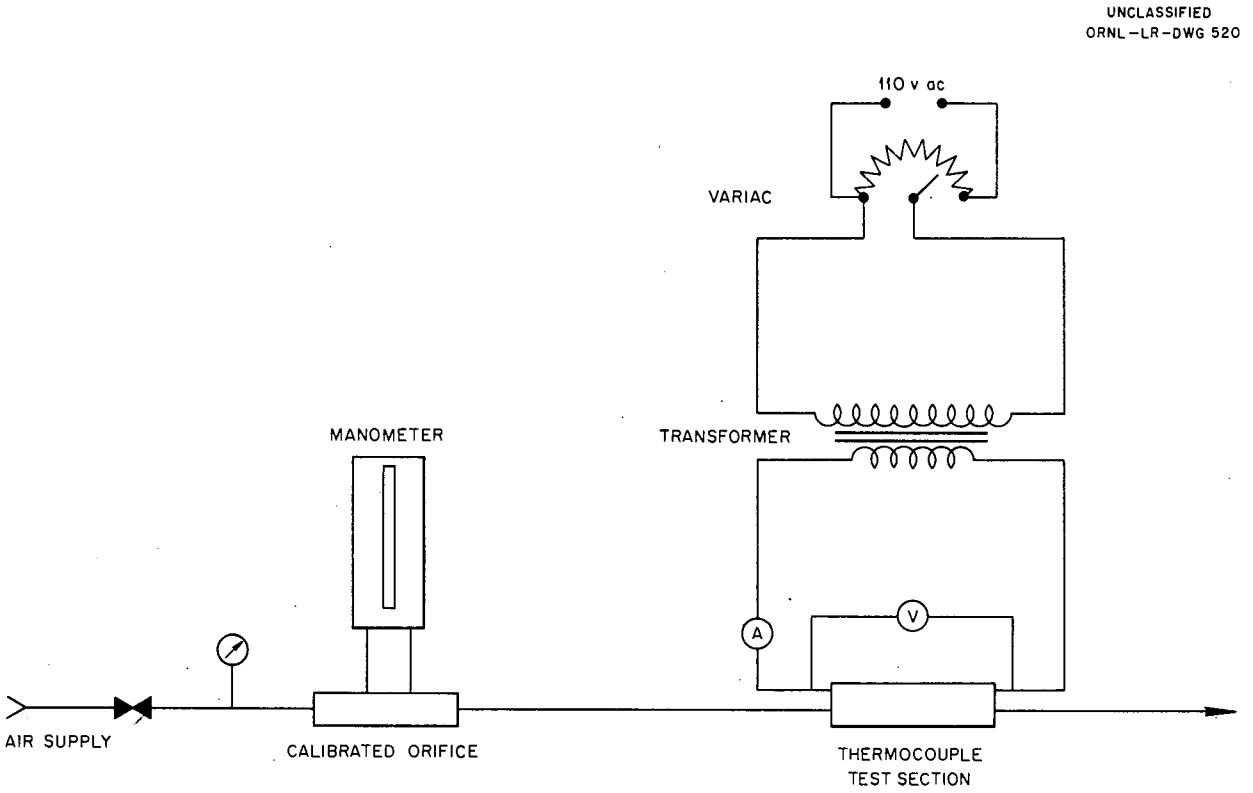

Fig. 22. Schematic Diagram Showing Air and Power Supply to Thermocouple Test.

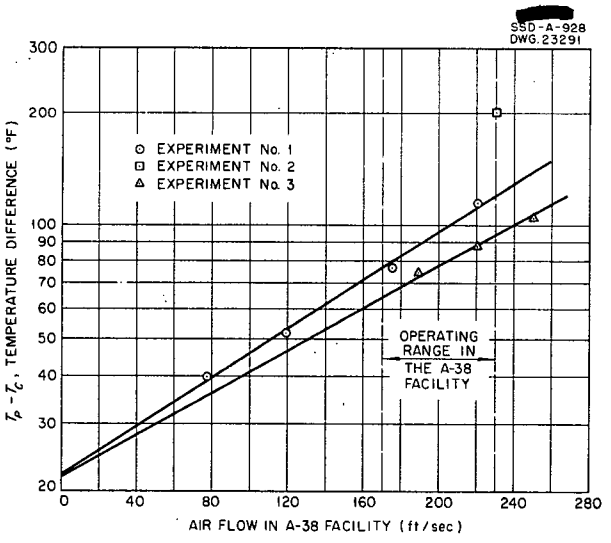

Fig. 23. Thermocouple Correction for Various Air Flows at Simulated Conditions in the A-38 Facility of the MTR.

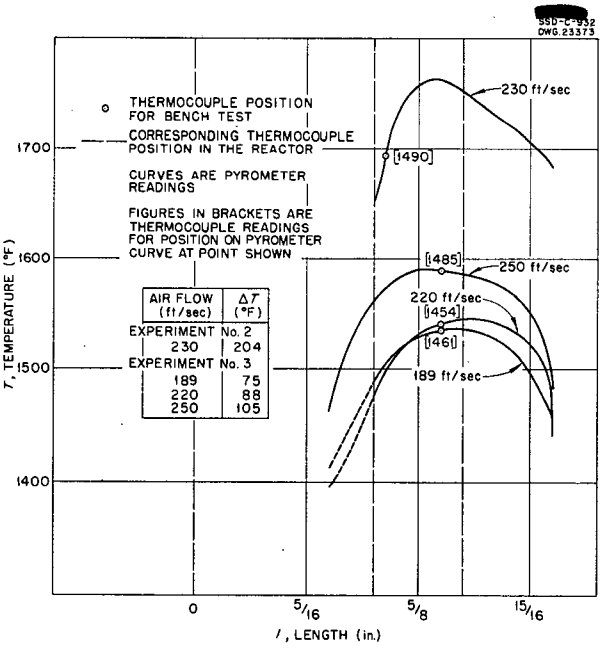

Fig. 24. Temperature Measurements on Fuel Tube at Simulated Conditions in the A-38 Facility of the MTR.

THERMAL-NEUTRON FLUX TRAVERSES IN THE LITR

M. T. Robinson

Thermal-neutron fluxes have been measured in vertical tubes C-46 and C-48 of the LITR at a reactor power of 3 megawatts. A set of four traverses was made in each facility to determine the effect of the No. 2 shim-rod position. Several small cobalt foils were supported at 2-in. intervals in an aluminum rod and irradiated for 1 hr. After the foils were weighed, they were counted in the high-pressure ionization chamber of the Radioisotope Development Department.

The flux pattern obtained is shown in Fig. 25. A detailed plot on a linear scale of the effect of shim-rod position is shown in Fig. 26. The curves obtained at two intermediate shim-rod positions fell between the plotted curves. Since the tubes were filled with air, no peaking in the flux was found above the active lattice as was found by Trice[7] in the BSF.

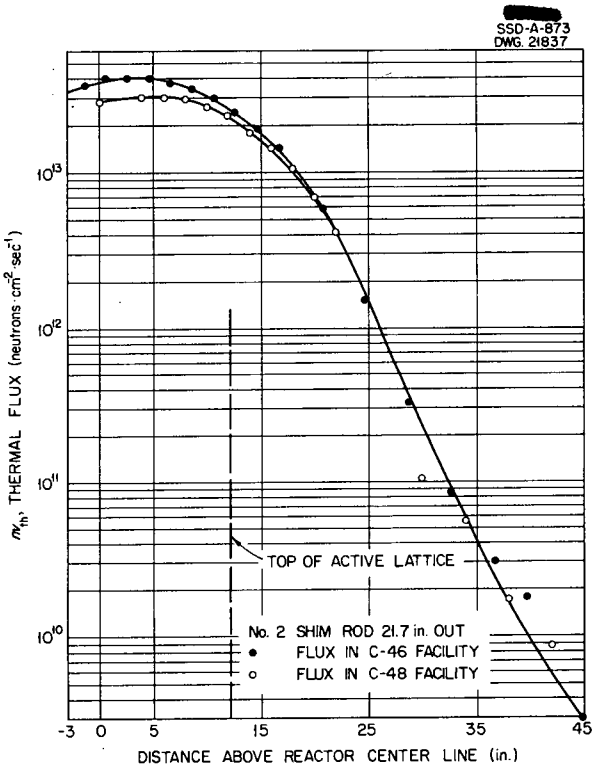

Fig. 25. Thermal-Neutron Flux in the C-46 and C-48 Facilities of the LITR at 3000 kw with No. 2 Shim Rod 21.7 in. Out.

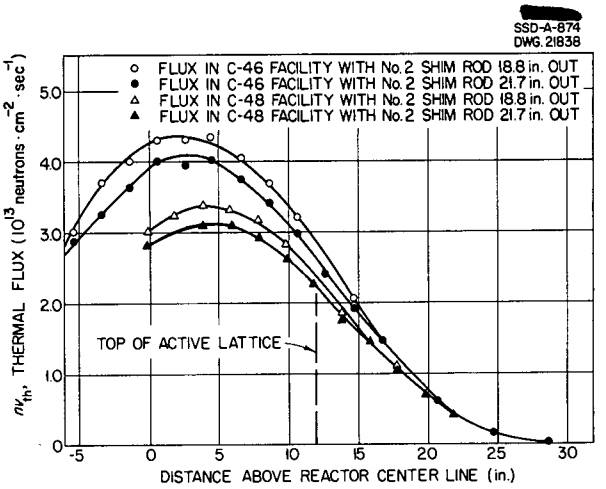

Fig. 26. Thermal-Neutron Flux in the C-46 and C-48 Facilities of the LITR at 3000 kw with No. 2 Shim Rod Out 21.7 and 18.8 in.

THERMAL-NEUTRON FLUX MEASUREMENTS IN THE MTR

M. T. Robinson

The recent decision to change the loading of the MTR from a 3 × 9, north slab pattern to a 5 × 6 pattern required remeasurement of the thermal-neutron flux in position A-38. In each of two tests made at 30-megawatt reactor power near the start of a fuel cycle, a piece of cobalt foil in an aluminum container was irradiated for 1 hr. The foils were returned to Oak Ridge where they were weighed and counted in the high-pressure ionization chamber of the Radioisotope Development Department. The activity obtained was 1.06 (±0.03) rutherfords/mg per hour of exposure. Taking the capture cross section of Co^{59} to be 34.8 (±2.0) barns and the half life of Co^{60} to be 5.10 (±0.15) years,[4] the thermal-neutron flux in A-38 is calculated to be 1.92 (±0.16) × 10^{14} neutrons/cm^2·sec. This result is 19% lower than that found with the old loading.

SAMPLING IRRADIATED CAPSULES CONTAINING URANIUM-BEARING FUELS

C. C. Webster J. G. Morgan

It was realized after much consideration that the sampling technique which involved melting the

[7] J. B. Trice and F. W. Smith, *Solid State Semiann. Prog. Rep. Aug. 31, 1953*, ORNL-1606, p 22.

salt out of the irradiated capsules was uncertain and inadequate because of the nature of the salt in the molten state. A new sampling technique[8] was developed but the fine powder formed created a contamination hazard to equipment and personnel.

It was decided to enclose the equipment where the sampling operation took place and try to contain the radioactive dust. This was done with Plexiglas boxes fitted with doors and connected to household vacuum cleaners. The equipment is painted with strippable paint to facilitate decontamination. Figure 27 shows the enclosure for the lathe and drill press used in the sampling operation. The vacuum cleaner is fitted with a special filter to catch the radioactive material. The Plexiglas boxes are under a slight negative pressure, with all drafts at cracks and openings sucking inward. Any airborne material is drawn into the vacuum line.

This sampling procedure has been used for two months, and the quantity of contamination in the rest of the hot cell can be attributed to other sources. The contamination problem for this type of operation appears to have been solved.

[8] J. G. Morgan *et al.*, *Solid State Semiann. Prog. Rep. Aug. 31, 1953*, ORNL-1606, p 40.

PETROGRAPHIC EXAMINATION OF IRRADIATED FLUORIDES

G. D. White[9] M. T. Robinson

The shielded petrographic microscope has been described in a previous report.[10] This equipment has been used to examine salt samples from 20 capsules, 11 of which had been irradiated in the

[9] Ceramic Laboratory, Metallurgy Division.

[10] M. T. Robinson, *Solid State Semiann. Prog. Rep. Aug. 31, 1953*, ORNL-10606, p 43.

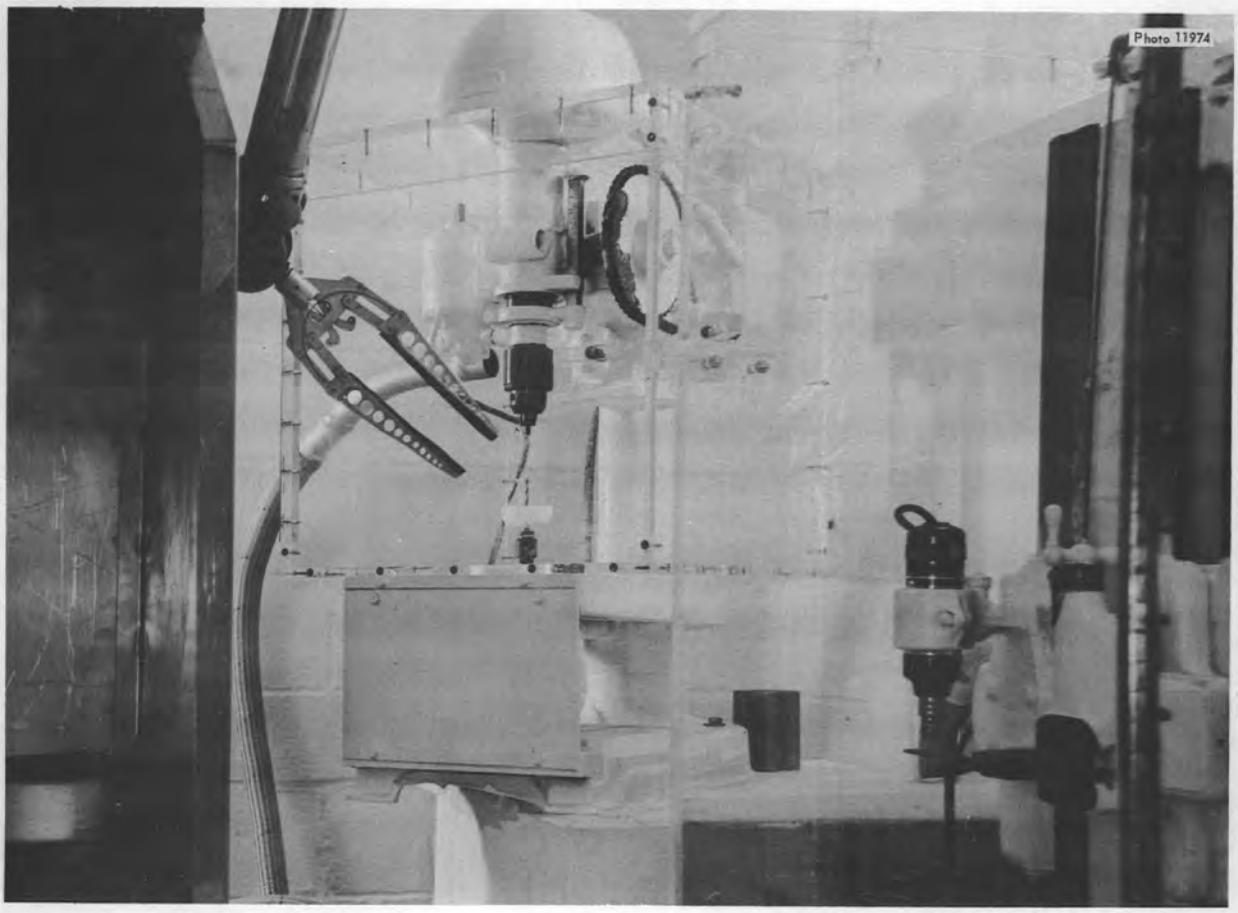

Fig. 27. Enclosed Lathe and Drill Press Used for Sampling Fuel Capsules.

LITR or MTR, as well as a number of miscellaneous salt samples. Slides were prepared rapidly in the open laboratory by sprinkling a small quantity of powdered salt from a lead-shielded container into the immersion oil.

Three different salt compositions have been examined. The capsules had been irradiated for periods ranging up to 492 hr in the MTR. Four irradiated capsules showed the presence of considerable amounts of ZrO_2 and/or UO_2. Oxides were not found in any control samples, in any of the original salts, or in any other irradiated capsules. Attempts to produce oxides at room temperature by the action of H_2O_2 or gamma radiation in the presence of moisture have been entirely unsuccessful. It must therefore be concluded that these four capsules leaked.

In general, both irradiated specimens and controls showed a small amount of reduction ($U^{4+} \longrightarrow U^{3+}$), evidenced by a yellow cast to the crystals in these samples. The refractive index of the solid solution was generally somewhat lower than the normal 1.504, evidence of the presence of low-index impurities or partial vitrification. No evidence was found of segregation of UF_4. It may be firmly concluded that the presence of reactor radiation has no detectable effect on the composition of the fluoride fuels studied.

In spite of burnups of 20% having been reached in some capsules, no phases attributable to fission products have been observed. The elements Rb, Cs, Ba, Sr, I, and Br would certainly be carried into the solid solution, $NaZr(U)F_5$. Other elements are present in quantities far too small to make detection likely. The presence of the alkali, alkaline earth, and halogen elements may cause the lowering of refractive index referred to above.

Two experiments were performed to study the effect of gamma radiation on solid fluorides in the presence of moisture. Two samples of fuel (composition 41: NaF-ZrF_4-UF_4, 63-25-12 mole %) were irradiated by means of the Co^{60} gamma source in the canal of the ORNL Graphite Reactor for a total exposure of 4.7×10^8 r and were exposed to ordinary air throughout their irradiation. In the other experiment, designated as ORNL-502, three samples of fuel (composition 30: NaF-ZrF_4-UF_4, 50-46-4 mole %) were irradiated by means of the fission-product gamma source in the MTR canal for a total exposure of 5.1×10^9 r. Two of the capsules were exposed to air saturated with water vapor at 79°F; the third was a control capsule sealed under dry helium. In no case was any oxide observed. The salts did not differ in appearance from their original condition.

DESIGN CALCULATIONS FOR MINIATURE CIRCULATING LOOP

M. T. Robinson

A series of calculations has been made for use in designing a miniature loop for a vertical tube in the LITR. It was desired to have the fluoride fuel in turbulent flow, the maximum fission-power generation 1000 watts/cc, and the difference in temperature between maximum and minimum fuel temperatures about 100°C.

The model studied consisted of a long Inconel U tube, which contained the salt, surrounded by an annular U tube for passage of cooling air. In most calculations the direction of air flow was opposite to that of fuel flow. In almost every case it was assumed that the loop was to be placed in vertical tube C-48 of the LITR, with its lowest point placed at the maximum flux as recently measured (see Fig. 26). The fuel assumed was composition 44 (NaF-ZrF_4-UF_4, 53.5-40-6.5 mole %), which generates 540 watts/cc at the maximum thermal flux of C-48. In one case, fuel composition 41 (NaF-ZrF_4-UF_4, 63-25-12 mole %), which generates 1100 watts/cc in C-48, was assumed.

The calculations were based on a simple heat balance in which variation of air and fuel physical properties with temperature was neglected, as was thermal conduction along the length of the loop metal. The effects of variation of air-flow velocity, fuel-flow velocity, loop dimensions, and loop position in the reactor on the fuel temperature distribution were studied. About two-thirds of the computations were carried out by R. C. Weaver of the ORNL Mathematics Panel.

Thus far, all the desired design criteria have not been met simultaneously. While it is easily possible to obtain the desired difference of 100°C between maximum and minimum salt temperature at any flow rate, if the dimensions of the loop are suitably chosen, the large quantity of heat involved can be successfully handled only at low fuel velocities (Reynolds' number <1000). At higher flow rates, the temperature differential must be sacrificed in present designs to enable all fission heat to be successfully removed.

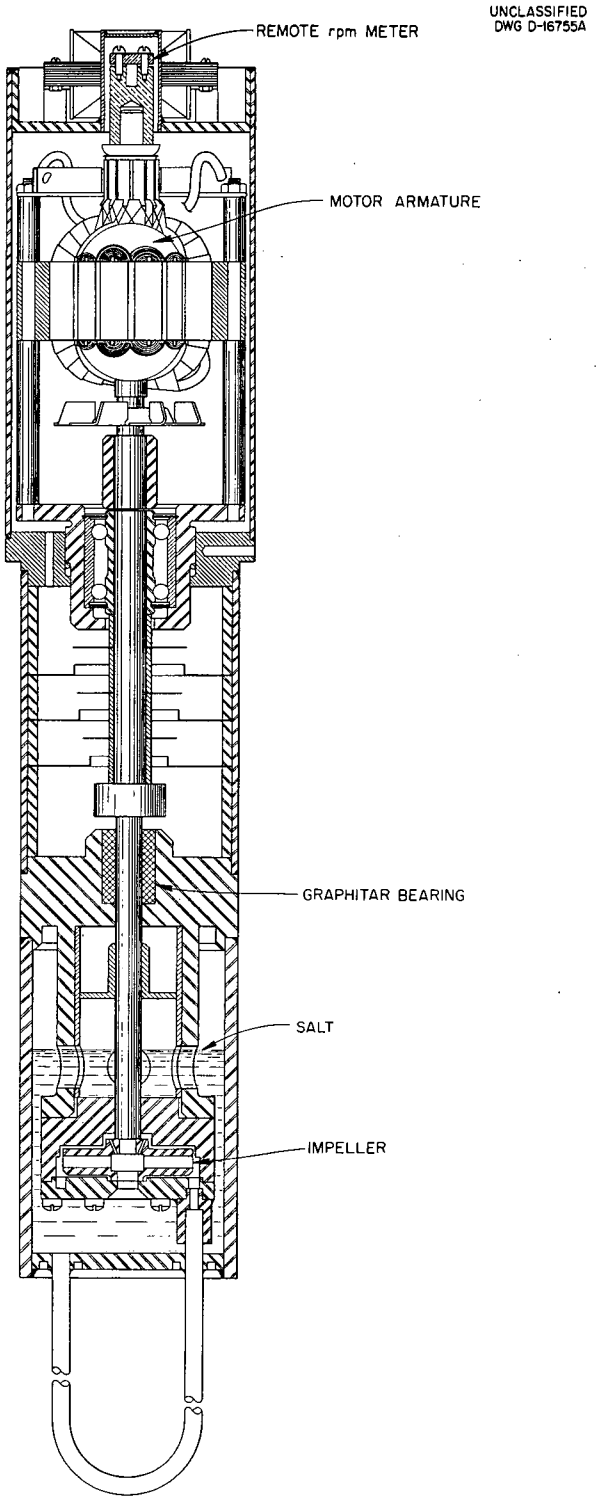

Fig. 28. Cross Section of Miniature Sump Pump.

MINIATURE SUMP PUMP

J. G. Morgan

A totally enclosed, molten-salt, pump-and-motor unit has been designed for use in position C-48 of the LITR. Figure 28 shows a cross-section layout of the unit which will operate vertically directly above the C-48 position and will extend into the grid assembly. The centrifugal-type impeller operates immersed in the molten salt. The impeller shaft is positioned by the lower Graphitar bearing and upper bearing race. The armature of the $\frac{1}{15}$-hp motor is mounted as an integral part of the shaft.

Speed of revolution is measured by a remote rpm indicator consisting of a permanent magnet rotating between ends of an iron C on which is wound a coil. As the magnet rotates, electrical pulses are generated and are counted by a frequency meter.

MINIATURE CHECK-VALVE PUMP

W. R. Willis

Figure 29 shows a cross-section view of a hydraulic rectifier pump developed for miniature in-pile corrosion loops.

The pump consists of the rectifier unit which contains four check valves as shown, surge tanks above the unit, and a solenoid-driven piston to supply power. The piston pressure is transmitted to the salt by means of helium gas. Present designs are expected to be capable of developing a peak pressure differential of about 15 psi.

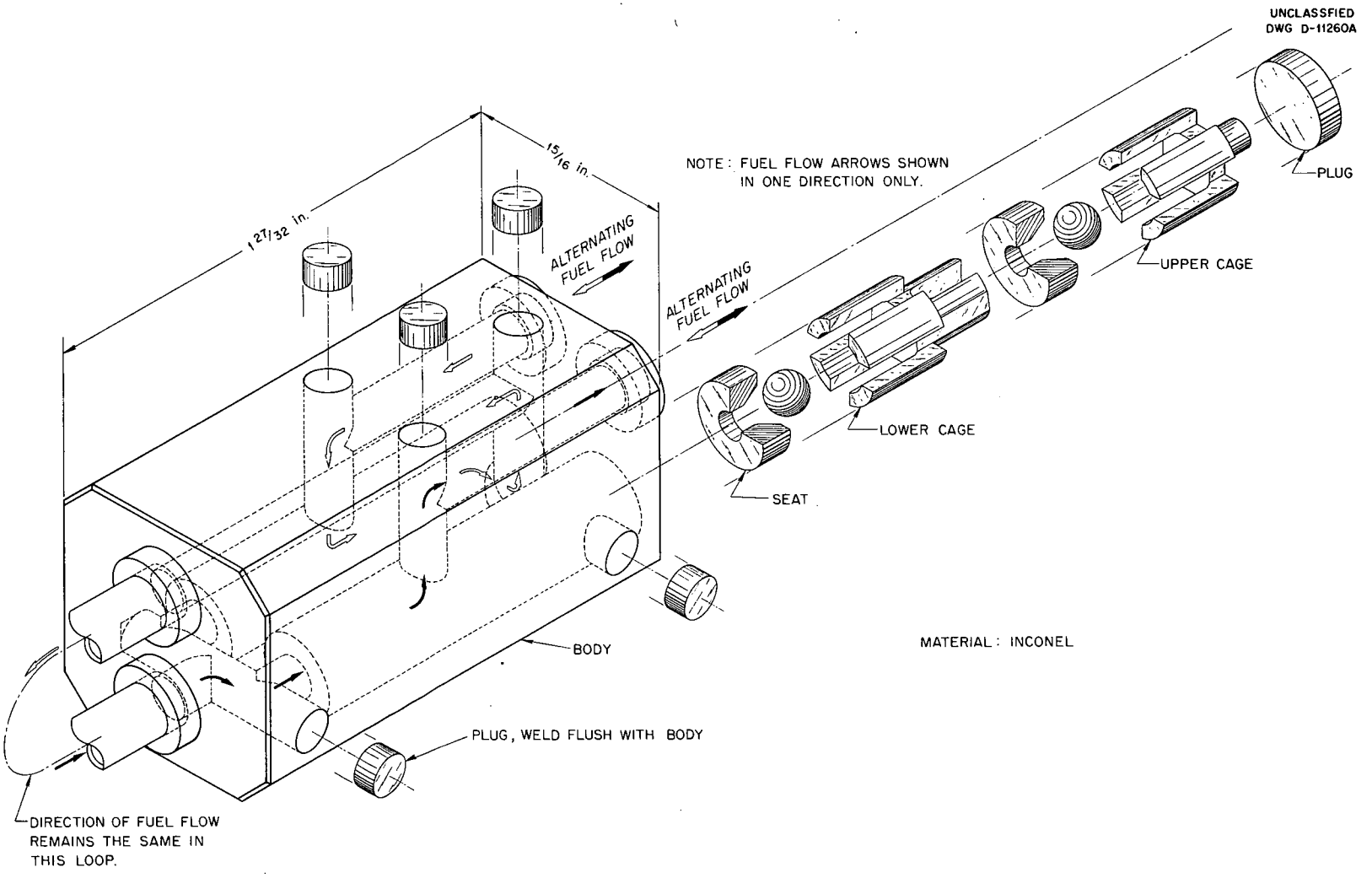

Fig. 29. Cross Section of Hydraulic Rectifier Pump.

Part II

UNCLASSIFIED PROJECTS

CONTENTS

PART II

SUMMARY 37

SOLID STATE REACTIONS 41
Effective Masses and Carrier Degeneracy from the Diamagnetic Behavior of Germanium 41
Radiation Effects in Ionic Crystals 44
Magnetic Susceptibility of Germanium 44
Magnetic Susceptibility of Silicon and Diamond 47
Rectifier Bombardment 47
Electrical Effects in Irradiated Barriers 50
Radiation Damage in SiO_2 Structures 54
Annealing of Neutron-Irradiated Diamond 54

ENGINEERING PROPERTIES 55
Dynamic Properties of Irradiated Elastomers 55

CRYSTAL PHYSICS 60
Effect of Deformation on the Superconducting Properties of Aluminum 60
Radiation Ordering in Cu_3Au 61
Radiation Effects in Copper Single Crystals 64
Structural Defects in Copper and the Electrical Resistivity Minimum 64

SPECIAL PROJECTS 66
Neutron Irradiation of LiF Crystals 66
Thermal and Electrical Conductivities of Ductile Irons and Gray Cast Irons 67
Thermal Conductivity of Dielectrics at Low Temperatures 68
Thermal and Electrical Conductivities of Aluminum Bronzes 70
Small-Angle X-Ray Scattering 70
Effect of Radiation on the Dielectric Constant and Attenuation of Two Coaxial Cables at Radio Frequencies 71
Dielectric Constant and Loss Tangent of Irradiated Plastics at Microwave Frequencies 77
Paramagnetic Resonance in Irradiated Solids 82

SUMMARY

SOLID STATE REACTIONS

Effective Masses and Carrier Degeneracy from the Diamagnetic Behavior of Germanium. In diamond-lattice semiconductors, surfaces of constant energy in momentum or wave-number space are usually assumed to be spherical for calculations; there are experimental indications, however, that these surfaces may actually be of complex shape. Information which might lead to an empirical determination of the curvature of these surfaces may be obtained from diamagnetic- or cyclotron-resonance experiments.

Magnetic-susceptibility measurements of the effective mass of the carriers were made on *n*- and *p*-type germanium and are in good agreement with cyclotron-resonance measurements made by Dresselhaus, Kip, and Kittel. Magnetic-susceptibility measurements have the advantage that a direct check on the assumption of spherical surfaces is possible from one series of measurements. The measurements indicate that either the energy surfaces are not spherical or that some additional effect considerably increases the density of states over that expected. In *n*-type germanium there appears to be a sixfold spatial degeneracy for the lowest energy of the conduction band; this degeneracy would result in an increase in the density of states by a factor of 6. For the top of the valence band, however, if the surfaces are spherical, the density of states would be increased by only a factor of 3. A curve calculated for *n*-type germanium with sixfold spatial degeneracy assumed gave an excellent fit with experimental data. Experimental points for *p*-type germanium conform best to the classical curve for which there is no carrier degeneracy. The actual surfaces seem to be quite complex; this may be caused by the complex nature of the wave functions at the top of the valence band. The possible effects of the two distinct effective masses obtained from the diamagnetic-resonance experiments were not analyzed.

Radiation Effects in Ionic Crystals. Electrical-conductivity measurements were made at temperatures from 25 to 300°C on potassium chloride crystals that had been subjected to 7×10^{14} to 4.5×10^{18} fast neutrons/cm^2 in the ORNL Graphite Reactor. Annealing behavior was very similar to the behavior of crystals that had been exposed to a Co^{60} gamma source.

Studies have begun on the effect of gamma and neutron irradiation on the optical-absorption properties of potassium chloride crystals. Only crude preliminary experiments have been made thus far, and no correlation has been noted with the annealing behavior found in the electrical-conductivity measurements.

Magnetic Susceptibility of Germanium. An *n*-type germanium cube and a thin plate cut from the adjacent section of the same ingot were subjected to successive irradiations in hole 51 of the ORNL Graphite Reactor. The magnetic susceptibility of the cube was measured as a function of temperature prior to each irradiation; the Hall voltage and electrical conductivity were measured for the comparison plate.

The susceptibility curves show that, in the early stages of irradiation, electrons are apparently being removed from the conduction band by radiation-introduced traps; the plate curves indicate that the material has not yet been converted to the intrinsic region. There is some possibility of difference between the plate and the cube because the cube was given an HCl wash to remove surface contamination after each of the first three irradiations; some annealing that did not occur in the plate almost certainly occurred in the cube.

The susceptibility apparatus is being overhauled to increase the precision of measurements, and the cubes and plates will be given a high-temperature anneal to increase their homogeneity.

Magnetic Susceptibility of Silicon and Diamond. The magnetic susceptibilities of an *n*-type polycrystalline cable of fairly high-purity silicon and of a flawless No. 1 color diamond were measured as a function of temperature. The slope of the silicon curve in the high-temperature region is about half that of germanium, whereas the susceptibility of the diamond was found to be essentially independent of temperature at these temperatures. At first inspection there appears to be a correlation between slope and the Debye temperature for these elements, although present theory does not predict temperature dependence of this order.

Rectifier Bombardment. The behavior of bulk germanium for temperature variations and for neutron bombardment is well known. Since the

behavior of a rectifier depends on both the properties of the bulk material and the nature of the rectifying mechanism, it was decided to study the properties of germanium rectifiers as a function of temperature and radiation.

It was found that the activation energy is strongly dependent on the bias voltage and that different mechanisms appear to operate above and below 290°K. At a certain critical value of bias voltage, $dI/d(nvt)$ changes from positive to negative; the critical value may vary for different samples and may be a function of temperature.

Electrical Effects in Irradiated Barriers. The open-circuit output voltages of several Ge-10-A germanium, diffused-*pn*-junction rectifiers were measured as a function of radiation. The voltages were strongly dependent on temperature. The voltage decreased from 125 mv at the beginning of the exposure to zero after a few hours.

If the rectifier were removed from the reactor before the output voltage decreased to zero, there was partial recovery after a few hours; there was no recovery if output voltage had been bombarded to zero output.

A rectifier of lead-brass with a surface area of 234 cm^2, 0.32-cm plate separation, and air between the barriers exhibited an increase in output from 0.20 to 0.27 volt upon irradiation.

Radiation Damage in SiO_2 Structures. Quartz, low cristobalite, low tridymite, and glass are reduced to a common phase (silica glass) by heavy doses of fast-neutron flux. The new phase has a density and an average refractive index near those of tridymite and can apparently be transformed to to alpha quartz in a solid-state reaction. Experimenters have been unsuccessful to date in attempts to transform any of the silica phases into alpha quartz by means of a solid-state transformation without chemical aid.

Annealing of Neutron-Irradiated Diamond. Diamond powder was irradiated for 3×10^{20} neutrons/cm^2 and annealed in 100°C steps for approximately 30 min each up to 1025°C. X-ray density was measured after each anneal. Defects begin to anneal at temperatures slightly higher than bombardment temperatures, but only 70% of the lattice-parameter change was annealed at 1025°C.

ENGINEERING PROPERTIES

Dynamic Properties of Irradiated Elastomers. Studies of the hysteresis losses and of radiation-induced hardening of elastomers are being made by means of dynamic-property measurements. The resonant frequency and the band width were measured when specimens were vibrated as clamped-free bars.

For materials composed entirely of hydrogen and carbon the energy absorbed is roughly proportional to the hydrogen content. If other elements are present, the energy is determined largely by the thermal-neutron absorption cross section of the additional elements. The increase in the dynamic Young's modulus is proportional to the first power of radiation exposure for all formulations based on natural rubber; the increase for formulations based on other polymers is proportional to higher powers of exposure. The dynamic Young's modulus is not a good measure of radiation effects on Thiokol because no change is shown for exposures in which the strength and the compression set are affected. For the other elastomers tested the dynamic Young's modulus was quite sensitive to radiation over long exposures. There is very little statistical variation; so only a few samples need to be tested.

CRYSTAL PHYSICS

Effect of Deformation on the Superconducting Properties of Aluminum. The superconductivity of three aluminum single crystals and of two relatively coarse-grained polycrystals of aluminum was studied. The samples were made from high-purity aluminum. One of the single crystals had only one operative slip system; another had two operative slip systems; the third was not strained. Deformation took place at 77°K. Elongation was about 18% in both the strained specimens; the sample in which only one slip system was operative work hardened more than the one with two operative slip systems. The polycrystalline samples, which have an estimated five operative slip systems, elongated about 20%. The shoulders of all samples were cut off prior to conductivity measurements at 4.2°K. It was found that the deformation of the samples did not affect the superconducting transition temperature or the magnetic-threshold curve within experimental error. It is possible that if aluminum could be deformed at lower temperatures some changes in the superconducting properties might be observed.

Radiation Ordering in Cu_3Au. Irradiation of Cu_3Au and CuAu in a reactor has been found in

some cases to cause a disordering effect and in other cases to increase the rate of ordering. The disordering phenomenon is a result of thermal spikes. The conditions for increased ordering rate and the mechanism by which it occurs are subject to question, however.

There is some evidence that the ordering phenomenon is initimately connected with the production of Frenkel defects and that interstitial atoms or vacant lattice sites increase the diffusion rate.

Data taken at other sites have been interpreted to indicate that radiation ordering is dependent on transmutation which forms impurities of mercury and sometimes zinc and nickel. These impurity atoms presumably act similar to vacant lattice sites or interstitital atoms in the diffusion process. The principal evidence is that radiation ordering is decreased when the sample is bombarded in a neutron converter. It was assumed that the decrease in ordering was caused by the decrease in thermal neutrons. The increase in fast-neutron flux was ignored. If the increase in disordering is caused by transmutation impurities, bombardment with fast electrons of low energy should produce few transmutations compared with those produced by reactor bombardment.

Recently, Cu_3Au was bombarded with 3-Mev electrons at Harwell. A pronounced increase in the rate of ordering was found over a relatively short period. Thus, structural defects must strongly influence the increased ordering rate.

Experiments performed in the ORNL Graphite Reactor indicate that substantial radiation ordering can occur during reactor bombardment even when the number of transmutations is very small. The resistance of Cu_3Au samples was observed to decrease under bombardment before mercury could have been formed in an appreciable quantity. It is thought that the increased fast flux was responsible for the suppression of radiation ordering in the neutron-converter experiment.

Radiation Effects in Copper Single Crystals. Since radiation affects only the residual resistivity of metals, a much better idea of radiation effects can be obtained if resistivity measurements are made at 4.2°K. The resistivity of single-crystal copper was found to increase at a rate proportional to approximately the $\frac{2}{3}$ power of the integrated flux.

Stress-strain measurements of irradiated copper single crystals indicated that the critical shear stress was greatly increased (for equivalent irradiations) over that obtained in the past at 78°K.

Structural Defects in Copper and the Electrical Resistivity Minimum. Studies of the effect of plastic deformation on the residual resistivity of unirradiated copper single crystals at 4.2°K indicate that a substantial portion of the residual resistivity measured in polycrystalline materials probably arises from the interaction of conduction electrons with structural defects, especially grain boundaries, rather than from scattering of conduction electrons by chemical defects, as has been generally assumed.

The resistivity obtained for annealed single crystals was much lower than that reported for polycrystalline metals; it could be increased to the value reported for polycrystalline metal by tensile deformation, and recrystallization of the worked crystals, by annealing in a vacuum, reduced the resistivity very little.

The value of residual resistivity found for copper single crystals is in agreement with data reported by Meissner for single crystals of gold and zinc.

Deformation studies of unirradiated copper single crystals were also extended to 4.2°K. The resistivity of samples deformed at 4.2°K increased with the shear stress at a rate which was proportional to approximately the square of the stress. None of the increase annealed out at 78°K, but approximately half the resistivity change was recovered at 300°K.

SPECIAL PROJECTS

Neutron Irradiation of LiF Crystals. Further calculations have been made of the neutron attenuation in LiF crystals, and density and x-ray measurements of neutron-irradiated LiF crystals have been determined to be equivalent to within 10%. The maximum lattice-parameter increase was 1.6×10^{-3}, which is equivalent to a volume expansion of 5×10^{-3}. The maximum concentration of Schottky defects is only 5×10^{-4}. The major cause of lattice expansion is therefore not Schottky defects.

Thermal and Electrical Conductivity of Ductile Irons and Gray Cast Irons. Where electrical and thermal conductivities are controlled by electrons only, the ratio of thermal to electrical conductivity is a constant. If the conductivities are controlled by electrons only, the thermal conductivity of gray cast iron (based on the properties of ductile iron)

should be about half that of ductile iron. It was found, however, that the thermal conductivity of gray cast iron is actually greater than the thermal conductivity of ductile cast iron in the temperature range from 95 to 250°C and is roughly parallel to that of Armco iron, whereas the thermal conductivity of ductile iron is not strongly temperature dependent in this range.

Thermal Conductivity of Dielectrics at Low Temperatures. Testing of the cryostat for measuring the thermal conductivity of dielectrics at low temperatures has been extended to 1.7°K. Since the surfaces of the resistors used in the apparatus were found to be sensitive to atmospheric conditions and to other contaminants and possibly to past electrical history, the calibration was accomplished while the conductivity of a single crystal of quartz was being measured. The pressure over the pumped liquefied gases was used to determine the temperatures. The same method was used to obtain a second set of measurements on quartz in the helium temperature range. The results of these measurements are in qualitative agreement with those reported in the literature.

Thermal and Electrical Conductivities of Aluminum Bronzes. The thermal conductivities of 94% Cu, 6% Al and 92% Cu, 8% Al were found to be higher than those for pure nickel at temperatures from 130 to 200°C. The measurements will be extended to higher temperatures.

Small-Angle X-Ray Scattering. A small-angle x-ray scattering camera for qualitative studies of cluster formation and growth phenomena in materials as a function of fast-neutron irradiation and temperature history has been constructed. Scattering angles less than $2\theta = 0°20'$ may be measured. The camera has been designed so that it can be easily modified to obtain quantitative data should this become desirable.

Effect of Radiation on the Dielectric Constant and Attenuation of Two Coaxial Cables at Radio Frequencies. Radiation effects on the attenuation and specific dielectric constant were measured on plastic dielectrics in the form of coaxial cable. The dielectric constant for an RG-11/U cable with polyethylene dielectric increased about 1% after a 900-hr exposure in hole B of the ORNL Graphite Reactor; change in attenuation was about 9% total, or about 15% for the irradiated section, since only about 60% of the cable was exposed to radiation. The dielectric constant for another cable with Teflon dielectric increased about 1% for a 700-hr exposure and there was little change in attenuation. All measurements were made at about 4 megacycles.

There was no significant change in dielectric constant and attenuation of the Teflon for reactor-on and reactor-off periods. For the RG-11/U cable there were observable changes in dielectric constant but none in attenuation when the reactor was on and off; these changes followed closely the change in temperature of the average temperature based on temperatures measured of the air at the inlet and exit. The differences were much smaller than the total change observed in dielectric constant for the entire period of irradiation.

Dielectric Constant and Loss Tangent of Irradiated Plastics at Microwave Frequencies. Before-and-after irradiation measurements were made at 1000, 3000, and 8700 megacycles of the dielectric constant and of the loss tangent of Teflon, polyethylene, polystyrene, and bakelite. The samples were irradiated in the water-cooled facility of hole 19 of the ORNL Graphite Reactor. Measurements were made at 1, 3, and 8.7 kmc on samples irradiated for 0.5×10^{18} and 0.9×10^{18} neutrons/cm^2. Gamma effects were not taken into consideration. The dielectric constant changed very little in every case; the maximum increase was 3% in a Teflon sample measured at 3 kmc. The loss tangent also increased most in Teflon at 3 kmc; the increase was 1370%. Loss tangents for the other materials increased from 15% to several hundred per cent except for bakelite in which there was a decrease of 1 to 3%.

Small changes in dielectric constant and large changes in loss tangent indicate that energy losses in the dielectrics at these frequencies are increased by irradiation.

Paramagnetic Resonance in Irradiated Solids. Microwave apparatus has been set up for the investigation of the radiation-induced paramagnetic resonances in simple cubic crystals and in semiconductors. A measurement of an irradiated LiF single crystal checks the results reported in the literature.

SOLID STATE REACTIONS

EFFECTIVE MASSES AND CARRIER DEGENERACY FROM THE DIAMAGNETIC BEHAVIOR OF GERMANIUM

J. H. Crawford, Jr. D. K. Stevens

One of the major theoretical problems in the study of the diamond-lattice semiconductors is the determination of the nature of surfaces of constant energy in momentum or wave-number space. Shockley[1] and Seitz[2] have suggested that instead of being spherical, as is usually assumed for calculations, these surfaces may be of complex shape. There are experimental indications which bear out this view. In particular, the magnetoresistance of germanium[3] cannot be explained by the usual assumption of spherical energy surfaces. Shockley[4] has pointed out that information which might lead to an empirical determination of the curvature of these surfaces may be obtained from diamagnetic- or cyclotron-resonance experiments. Calculations indicate that effective masses of charge carriers, which are a direct function of energy surface curvature, determined from the position of these resonance-absorption peaks would be a function of the orientation of the crystal in the static magnetic field for nonspherical energy surfaces.

Recently, Dresselhaus, Kip, and Kittel[5] have succeeded in measuring cyclotron resonance in both *n*- and *p*-type germanium at 4°K by using high-purity germanium and an exciting frequency of 9050 megacycles/sec. The *n*-type crystal, which gave a single resonance corresponding to $m_e^*/m \cong 0.11$, was examined in only one orientation, (100); *p*-type material, however, was examined in three different orientations: (100), (110), and (111). In the latter case two of the resonance peaks that were observed, one corresponding to $m_h^*/m = 0.04$, were independent of orientation.

The values of the effective mass of the carriers in *n*- and *p*-type germanium determined at this laboratory from magnetic-susceptibility measurements[6] are in reasonable agreement, considering the differences in experimental conditions (much higher temperature and carrier concentration), with those obtained by the cyclotron-resonance experiments. A comparison of the values is given below:

Method	m_e^*/m	m_h^*/m
Cyclotron resonance	0.11	0.33; 0.04
Magnetic susceptibility	0.14	0.25

The *n*-type value given by susceptibility measurements is slightly larger than that obtained from resonance experiments, a fact which may be associated with different experimental conditions since, in the range of temperatures involved in the former case, occupied states extend above the conduction-band edge approximately 0.02 ev as a result of thermal excitation. In the case of *p*-type material, two discrete values of m_h^*/m cannot be observed directly from susceptibility measurements. Only an average, weighted by the relative occupation of the states in question, would be obtained. It is tentatively suggested that this may be the reason that the m_h^*/m value obtained from susceptibility measurements is smaller than the larger of the two observed by Dresselhaus *et al.*[5]

Although both types of measurements are capable of yielding the effective mass appropriate to the orbital motion of a charge carrier in a magnetic field, magnetic-susceptibility results have the advantage that a direct check on the assumption of spherical surfaces is possible from one series of measurements. The generalized equation for carrier susceptibility for $\beta H \ll kT$, neglecting second-order oscillatory terms which are important only at very low temperatures (de Haas–Van Alphen effect), is

$$(1) \quad \chi_c = \frac{\beta^2}{3\rho kT} \frac{C(kT)^{3/2}}{f_s^{3/2}} (3 - f_0) F'_{1/2}(\eta) ,$$

where

$$C = \frac{4\pi(2m)^{3/2}}{h^3},$$

[1] W. Shockley, *Phys. Rev.* 78, 173 (1950).

[2] F. Seitz, *Phys. Rev.* 79, 372 (1950).

[3] G. L. Pearson and H. Suhl, *Phys. Rev.* 83, 768 (1951).

[4] W. Shockley, *Phys. Rev.* 90, 491 (1953).

[5] G. Dresselhaus, A. F. Kip, and C. Kittel, *Phys. Rev.* 92, 827 (1953).

[6] D. K. Stevens, J. H. Crawford, Jr., and J. W. Cleland, *Solid State Semiann. Prog. Rep. Aug. 31, 1953*, ORNL-1606, p 71.

$f_s = m/m_c^*$ averaged over all occupied states in the conduction band,

$f_0 = m/m_c^*$ averaged over K-space under restrictions imposed by the force of the magnetic field acting on the carrier,

$$F'_{1/2}(\eta) = \frac{\partial}{\partial \eta} F_{1/2}(\eta) ,$$

in which

$$F_{1/2}(\eta) = \int_0^\infty \frac{x^{1/2} dx}{1 + e^{x-\eta}} ,$$

$$x = \frac{E}{kT} ,$$

$$\eta = \frac{\zeta}{kT} .$$

$F_{1/2}(\eta)$ may be obtained from the relation

$$n = \frac{C(kT)^{3/2}}{h^3 f_s^{\,3/2}} F_{1/2}(\eta) ,$$

where n is the charge-carrier concentration; $F'_{1/2}(\eta)$ may be obtained from tabulated values of the functions.[7] The two mass-ratio parameters, f_s and f_0, are obtained by averaging over K-space in two completely different ways; f_s is the mass ratio that appears in the expression for the density of quantum states in the conduction or the valence band, while f_0 is the mass ratio that applies to the orbital motion of the charge carrier in the magnetic field. These parameters are equivalent only in the case of spherical energy surfaces. When the number of charge carriers becomes small compared with the the number of quantum states in the band supporting conduction, Eq. 1, which is based on Fermi-Dirac statistics, reduces to the classical equation

$$\chi_c = \frac{\beta^2}{3\rho kT} n(3 - f^2) , \tag{2}$$

where n is the concentration of charge carriers, either electrons or holes as the case may be. In both Eqs. 1 and 2 the mass ratios also refer to the appropriate carrier; n also may be temperature dependent, but in the case of germanium it arises from ionized chemical impurities with a very small ionization energy (<0.005 ev) and can be considered constant over the temperature range of interest. It should be noted that Eq. 2 is independent of f_s.

For energies near the band edge, the density of states is given by

$$g(E) = \frac{4\pi(2m)^{3/2} E^{1/2}}{h^3 f_s^{\,3/2}} , \tag{3}$$

and the number of states in the conduction band (or valence band) available for a given concentration of carriers increases with temperature. Hence, transition from behavior described by Eq. 1 at low temperature to that described by Eq. 2 at higher temperatures in an experimentally realizable temperature range is expected for a certain range of carrier concentrations. Consequently, the assumption of spherical energy surfaces may be checked directly in the following manner: (1) f_0 is obtained in the classical range (high temperatures) from the slope of the χ_c vs $1/T$ curve according to Eq. 2; (2) this value is substituted in Eq. 1 for both f_0 and f_s and the complete χ_c vs $1/T$ curve is calculated. If the energy surfaces are spherical, $f_0 = f_s$, and the calculated curve should coincide with the experimental curve.

Examination of the data reveals that the carrier concentrations n_e and n_h fall within the range for which this analysis can be carried out. The curves calculated from Eq. 1 for an n-type specimen, $n_e = 7.4 \times 10^{17}$ cm^{-3} and $f_0 = 7$, are compared with classical behavior (Eq. 2) and the experimental points in Fig. 30. A similar comparison for p-type germanium ($n_h = 5.0 \times 10^{17}$ cm^{-3} and $f_0 = 4$) is made in Fig. 31. The remaining curve in each figure refers to degenerate quantum states and will be discussed later. It is evident from this comparison that the calculated curve predicts the onset of carrier degeneracy (influence of Fermi-Dirac statistics) at a much higher temperature than is experimentally observed. This observation indicates that $f_0 > f_s$ is the actual case, since the density of states required to fit experimental points must be greater than that employed in the calculation.

In view of this discrepancy between calculation and experiment, it may be concluded that either the energy surfaces are not spherical or that the density of states is increased considerably over that expected from Eq. 3 by some additional effect.

[7] J. McDougall and E. C. Stoner, *Trans. Roy. Soc. (London)* A 237, 67 (1939).

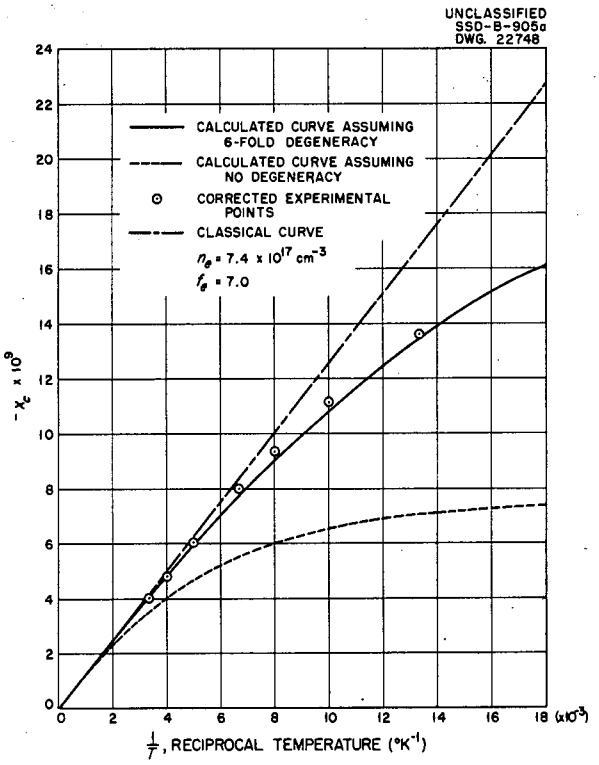

Fig. 30. *n*-Type Germanium Carrier Contribution to Susceptibility vs $1/T$.

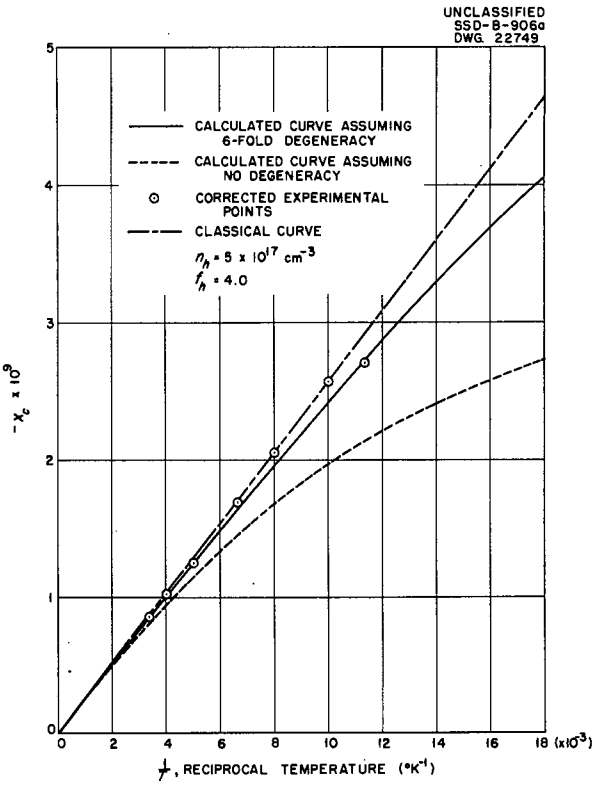

Fig. 31. *p*-Type Germanium Carrier Contribution to Susceptibility vs $1/T$.

Recent calculations of the band scheme of germanium by Herman and Callaway[8] indicate that there is perhaps a spatial degeneracy for the lowest energy of the conduction band. They find that the lowest energy in this case does not lie at the center of the Brillouin zone but rather at an intermediate position in the (100) direction. Since there are six equivalent energy minima in the six equivalent (100) directions, a sixfold spatial degeneracy and a resulting increase in the density of states by a factor of 6 would be expected. For the top of the valence band, however, Herman and Calloway found that the energy maximum occurs at the center of the zone, at which point the wave functions themselves are triply degenerate. In this case, when the surfaces are spherical, the density of states may be increased by a factor of 3.

The remaining curve in Fig. 30 was calculated for the *n*-type sample on the assumption that there is a sixfold spatial degeneracy. The agreement with experiment is remarkably good when experimental error is taken into account. In the case of the *p*-type sample in Fig. 31, the χ_c vs $1/T$ curve calculated with threefold wave-function degeneracy assumed (not shown) falls much lower than the experimental points. In this case even the assumption of sixfold degeneracy falls perceptibly lower than the data. The points appear to conform better with the classical curve for which there is no carrier degeneracy.

On the basis of the foregoing analysis, the following tentative conclusions may be drawn: The effective masses of electrons in *n*-type germanium appear to bear out the theoretical calculations of the band scheme with respect to a sixfold spatial degeneracy of the lowest states in the conduction band if the energy surfaces can be represented by six spheres, centered at each of the energy minima on the (100) directions; the energy surfaces in *p*-type material do not conform to the spherical assumption (even if effects caused by a possible threefold degeneracy of the wave functions are considered) and indicate that perhaps the actual

[8] F. Herman and J. Callaway, *Phys. Rev.* 89, 518 (1953).

surfaces are quite complex in nature, a situation that might arise from the complex nature of the wave functions at the top of the valence band.[1] It should be pointed out, however, that no attempt was made in the analysis of the *p*-type data to consider possible effects, as were obtained from diamagnetic-resonance experiments, which arise from two distinct effective masses.

RADIATION EFFECTS IN IONIC CRYSTALS

C. M. Nelson

The electrical-conductivity studies have been continued on potassium chloride crystals. These crystals were placed in various experimental holes in the ORNL Graphite Reactor so that the total irradiation would vary from about 7×10^{14} to 4.5×10^{18} fast neutrons/cm^2. Nine different bombardments were made with three samples taken from each experiment. Electrical-conductivity measurements were made on these crystals at various temperatures between 25 and 300°C. The results obtained showed very little difference in annealing behavior from that observed with crystals irradiated by gamma rays from a Co^{60} source. The sequence of decrease, increase, decrease, etc. during annealing for the gamma-irradiated crystals has been described in the preceding semiannual report.[9] A difference in annealing behavior at some point might have been expected, since the fast neutrons should cause vacancies in the lattice and thereby alter the electrical conductivity.

Considerable time has been spent during this period in designing a new conductivity apparatus. Preliminary tests on the new model indicate that it has much more adaptable and flexible properties. The new apparatus has a very low heat capacity which enables it to be heated very rapidly to high temperatures and, conversely, to be cooled rapidly where required. Electrical-conductivity measurements can now be made up to and above 600°C. The apparatus is very easily opened and the sample can be easily placed for measurements. The reliability of this apparatus has not been fully tested because of troubles in the vibrating-reed instrument used in the circuit. Several changes have already been made and it is hoped that a complete description can be made in the next report. Appreciation for assistance in the design of this apparatus is expressed to R. L. Sproull of Cornell University. The assistance of J. C. Pigg in overcoming the troubles with the electrometer is gratefully acknowledged.

Studies have been started in the optical-absorption properties observed in gamma- and neutron-irradiated potassium chloride crystals. From the very crude preliminary absorption measurements, no correlation was found between the annealing behavior of the electrical-conductivity property and that of the color centers. Only the *F* center and some of the *V* centers were observed under the conditions of the experiments. Irradiations were made at room temperature or slightly above but the absorption curves were taken at various temperatures in liquid nitrogen. An apparatus which will be used for studying the annealing behavior of the color centers and the electrical conductivity at the same time is in the process of design and construction. The Cary automatic recording spectrophotometer made by Applied Physics Corporation, Pasadena, California has been used for these optical-absorption measurements. These experiments are being made in collaboration with J. A. Ghormley of the Chemistry Division.

MAGNETIC SUSCEPTIBILITY OF GERMANIUM

D. K. Stevens J. W. Cleland
J. H. Crawford, Jr.

An *n*-type germanium cube originally containing approximately 7×10^{17} free current carriers per cubic centimeter has been subjected to successive fast-neutron irradiations in hole 51 of the ORNL Graphite Reactor. Subsequent to each irradiation its susceptibility was measured as a function of temperature, as were the Hall voltage and the electrical conductivity of a simultaneously irradiated companion plate. Since the cube and the plate were single crystals[10] and were cut from adjacent sections of the same ingot, it is assumed that the free current-carrier concentrations calculated from the plate Hall data applied equally well for the cube.

Part of the magnetic data is shown plotted in Fig. 32. It can be seen that in the early stages of the irradiation the shape and the position of the susceptibility curves change in a manner consistent

[9] C. M. Nelson, *Solid State Semiann. Prog. Rep. Aug. 31, 1953*, ORNL-1606, p 80.

[10] L. Roth of the Physics Department of Purdue University prepared the samples.

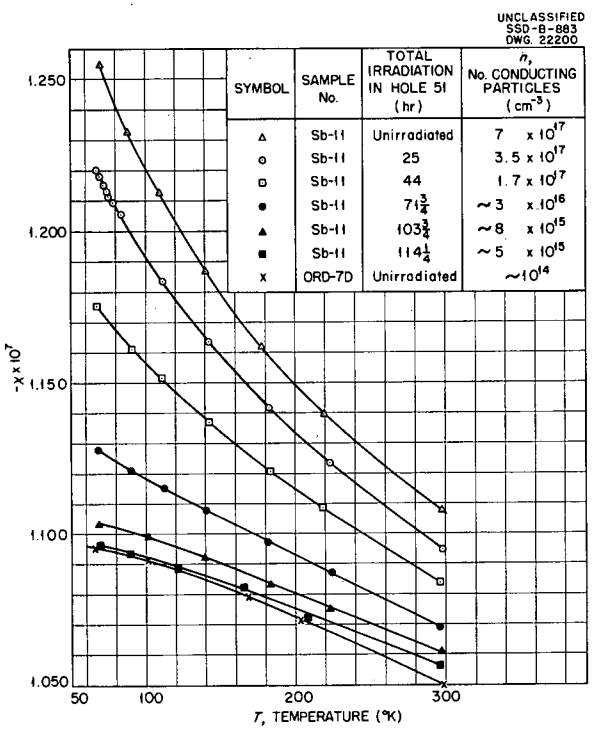

Fig. 32. Diamagnetic Susceptibility vs Temperature of Irradiated *n*-Type Germanium.

with the removal of the electrons from the conduction band by radiation-introduced traps. Although the electrical conductivity and Hall measurements indicate that the sample has not been irradiated a sufficient length of time to put it into the intrinsic region, the curves obtained after the last exposures show a lower temperature dependence near room temperature than do the unirradiated intrinsic samples. Perhaps this is a consequence of a radiation-induced disarrangement of the germanium lattice or of a change in the number of carriers in the conduction band caused by thermal excitation of trapped electrons. As yet there are insufficient data to attempt a quantitative evaluation of these and other possibilities relative to the nature of the radiation-introduced traps.[11]

In a manner previously described,[12] the susceptibility of an *n*-type impurity semiconductor may be written as the sum of the contribution of the host lattice χ_A, the contribution of un-ionized group III and group V impurities χ_I, and the spin and Landau orbital contributions of the current carriers χ_S and χ_O, respectively:

$$\chi = \chi_A + \chi_I + \chi_S + \chi_O \ .$$

Because of the low effective mass of the conduction electrons while they are in the conduction band, it can be assumed that in the initial stages of irradiation the principal change in the susceptibility is the result of removal of conduction electrons into traps. If, according to the James–Lark-Horovitz model, the electrons are trapped as pairs, the change in susceptibility in the classical range may be written

$$\Delta\chi = \Delta\chi_S + \Delta\chi_O = \frac{\Delta n \beta^2}{3\rho k T}(3 - f_e^2) \ ,$$

where Δn is the change in the number of conduction electrons, ρ the density, β the Bohr magniton, and f_e the ratio of rest mass to effective mass for orbital motion of conduction electrons in a magnetic field. Upon differentiation with respect to $1/T$:

$$\frac{d(\Delta\chi)}{d\left(\frac{1}{T}\right)} = \frac{\beta^2(3 - f_e^2)}{3\rho k}\left[\Delta n + \frac{1}{T}\frac{d(\Delta n)}{d\left(\frac{1}{T}\right)}\right] .$$

The equation may be further simplified to

$$\frac{d(\Delta\chi)}{d\left(\frac{1}{T}\right)} = \Delta n \frac{\beta^2(3 - f_e^2)}{3\rho k}$$

if the thermal excitation of trapped carriers is small and if Δn is very large.

The mass ratios f_e, calculated by using the simplified equation above, are listed in Table 3. The apparent trend toward increasing f_e with exposure is to be treated with suspicion since the

$$\frac{1}{T}\frac{d(\Delta n)}{d\left(\frac{1}{T}\right)}$$

term, which has been neglected in this tabulation, becomes increasingly important as the period of irradiation or the amount of irradiation already incurred increases. The inclusion of this term in the calculations tends to reduce the f_e values for

[11] H. M. James and K. Lark-Horovitz, Z. *Physik. Chem.* 198, 107 (1951).

[12] D. K. Stevens, J. H. Crawford, Jr., and J. W. Cleland, *Solid State Semiann. Prog. Rep. Aug. 31, 1953*, ORNL-1606, p 71.

that portion of the conduction electrons subsequently trapped (the first three groups in Table 3); the opposite effect would occur for conduction electrons. A precise accounting of this term cannot be given in this report because of increasing incongruity, as irradiation proceeded, between the Hall data and the electrical-conductivity data obtained from the companion plate. Further, the correspondence between the condition of the plate and the condition of the cube is open to question because after each of the first three irradiations the cube was given a hot HCl wash to remove surface contamination. No doubt some annealing occurred in the cube which did not take place in the plate. Thus, values of carrier concentration obtained from Hall measurements on the plate should be lower than those existing in the cube. Correction of this condition would tend to raise the f_e values in the first group in Table 3 and to lower the last three of the last group.

Since the precise determination of the room-temperature susceptibility of a given sample is important for effective analysis of the data, the susceptibility apparatus is being overhauled. The cubes and plates have been given high-temperature anneals in an attempt to increase homogeneity and thereby possibly avoid the divergences in the Hall and conductivity data observed in this work.

TABLE 3. DATA USED FOR CALCULATING MASS RATIOS

CURVE 1*	CURVE 2*	$\Delta n \times 10^{16}$	$\frac{d(\Delta\chi)}{d\left(\frac{1}{T}\right)} \times 10^{-7}$	MASS RATIO, f_e	EXPOSURE DIFFERENCE (hr)
Unirradiated Sb-11	First irradiation of Sb-11	35	3.0	5.0	25
	Second irradiation of Sb-11	53	7	6.0	44
	Third irradiation of Sb-11	67	11.2	6.8	71¾
	Fourth irradiation of Sb-11	69	13.4	7.3	103¾
	Fifth irradiation of Sb-11	69.5	13.9	7.4	114¼
First irradiation of Sb-11	Second irradiation of Sb-11	18	4.3	8	19
	Third irradiation of Sb-11	32	9.11	8.7	47
	Fourth irradiotion of Sb-11	34	11.6	9.4	79
	Fifth irradiation of Sb-11	34.5	11.4	9.3	90
Second irradiation of Sb-11	Third irradiation of Sb-11	14	4.78	9.5	28
	Fourth irradiation of Sb-11	16.2	7.50	11	60
	Fifth irradiation of Sb-11	16.5	7.67	11	70
Unirradiated Sb-11	ORD-7D	70	12.5	7	0
First irradiation of Sb-11	ORD-7D	35	9.6	8.6	25
Second irradiation of Sb-11	ORD-7D	17	5.4	9.1	44
Third irradiation of Sb-11	ORD-7D	3	1.25	10.5	72

*The column headed curve 2 designates the χ vs T curve which was subtracted from the χ vs T curve designated in the column headed Curve 1. The slope of the high-temperature portion of the resultant $\Delta\chi$ vs $1/T$ curve is listed in Column 4. Column 3 represents the difference in carrier concentration at room temperature between the two principal curves.

MAGNETIC SUSCEPTIBILITY OF SILICON AND DIAMOND

D. K. Stevens

The magnetic susceptibility of one *n*-type polycrystalline cube of silicon[13] has been measured as a function of temperature. The material is of fairly high purity, with an estimated carrier concentration of 10^{16} cm^{-3}. From reported values of the mass ratio of electrons in silicon,[14] estimates show that this concentration of electrons is not expected to make a measurable contribution to the susceptibility of the silicon sample. Figure 33 shows the data obtained for this sample and, for comparison purposes, similar data for a high-purity germanium cube (No. ORD-7D).

The magnetic susceptibility of a flawless, No. 1 color (colorless), emerald-cut diamond[15] weighing 639.7 mg has been measured from 88 to 294°K. The susceptibility at room temperature was found to be 4.56 (±0.03) × 10^{-7} cgs units and was independent of temperature ±0.1% in the same temperature range.

[13]The sample was supplied by M. Becker of Hughes Aircraft Company, Culver City, California.

[14]A. M. Portis, A. F. Kip, and C. Kittel, *Phys. Rev.* 90, 988 (1953).

[15]R. G. Chapman, manager of Kimball's Inc., Knoxville, loaned the diamond used for this measurement.

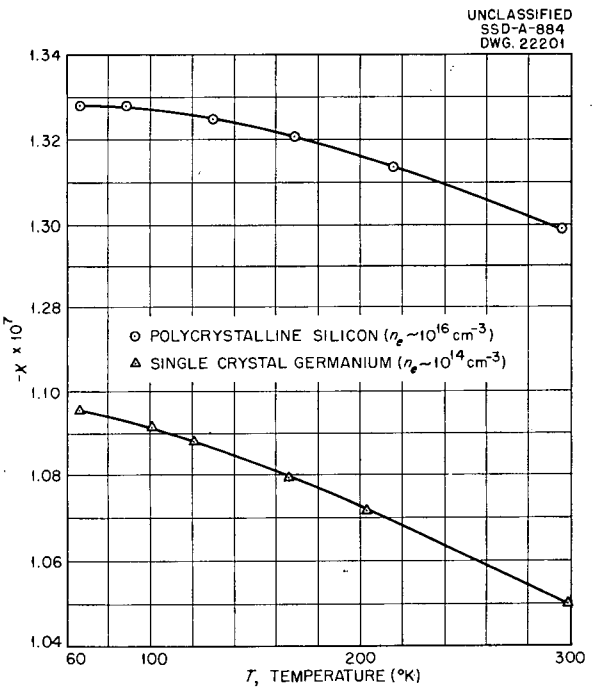

Fig. 33. Diamagnetic Susceptibility vs Temperature for Silicon and Germanium.

RECTIFIER BOMBARDMENT

J. C. Pigg

The behavior of two germanium rectifiers has been studied as a function of temperature and reactor irradiation.

When a rectifier is biased in such a direction as to exhibit low resistance, it is said to be biased in the forward direction. When it is biased so as to exhibit a high resistance, it is said to be biased in the reverse or back direction. A typical characteristic curve for a germanium diode illustrating the terms used is shown in Fig. 34.

Since the characteristic curve is symmetric about the origin for small voltages, the slope of the curve through the origin can be obtained from the slope of the reverse characteristic as the curve goes through zero and is called the zero slope. For voltages above 0.5 volt, the reverse characteristic is essentially linear. The slope of this section is called the reverse-saturation intercept.

The behavior of the rectifier depends upon the properties of the bulk material and the nature of the rectifying mechanism. Since the behavior of the bulk material is well known in the case of

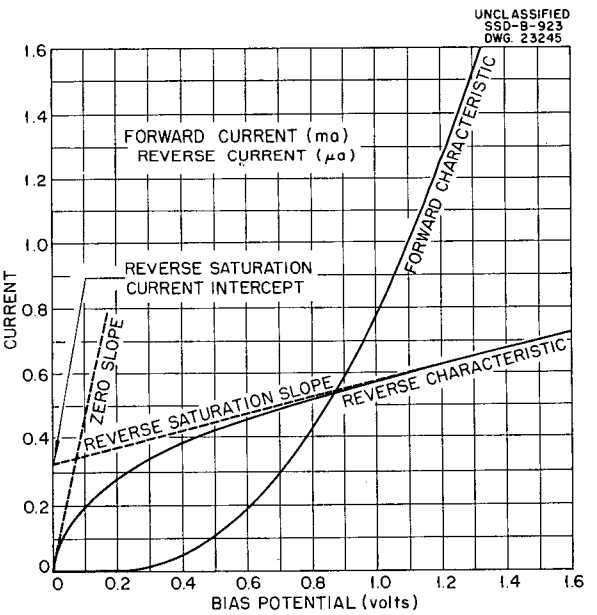

Fig. 34. Typical Rectifier-Characteristic Curve.

germanium for temperature variations and neutron bombardment, it may be possible to study the nature of the rectifying mechanism by means of temperature and radiation effects on the rectifier.

Figure 35 shows the relationship between the zero-voltage slope and the temperature for a 1N-38-A rectifier. The zero slope increases with an activation energy of 0.57 ev as the absolute temperature increases.

Figure 36 shows the variation of the reverse-saturation slope as a function of temperature. The mechanism involved here has an activation energy of 0.47 ev.

Figure 37 shows the variation of the reverse-saturation intercept as a function of temperature. The activation energy for this process is 0.745 ev,

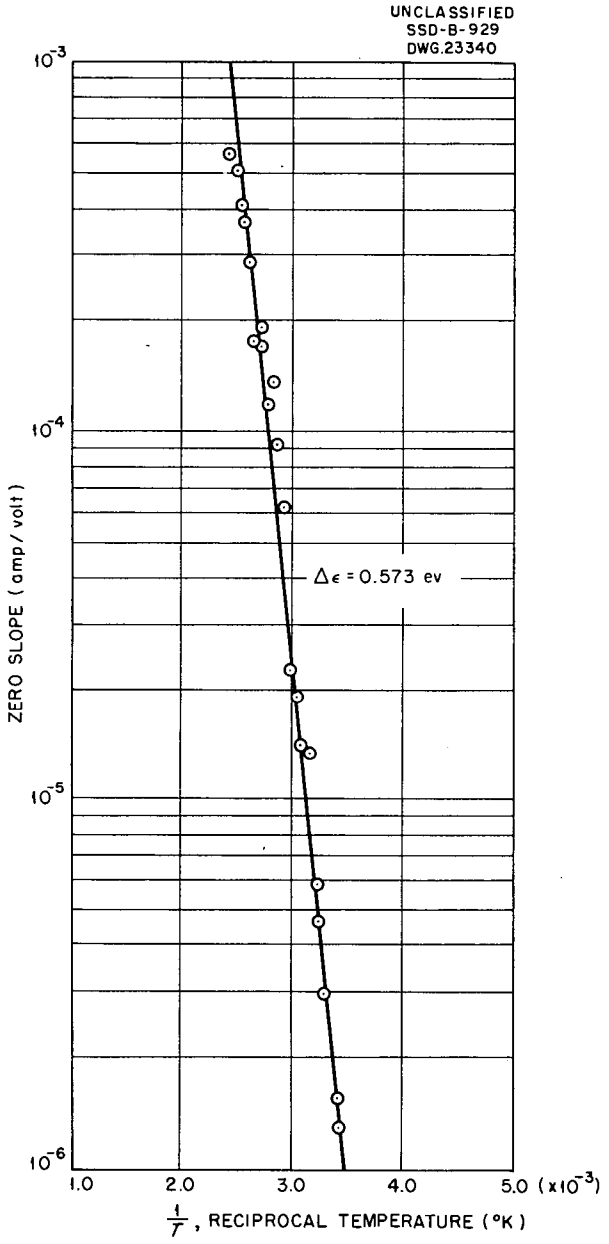

Fig. 35. Zero Slope vs Reciprocal Temperature Before Bombardment for Sample 1N38-A-2.

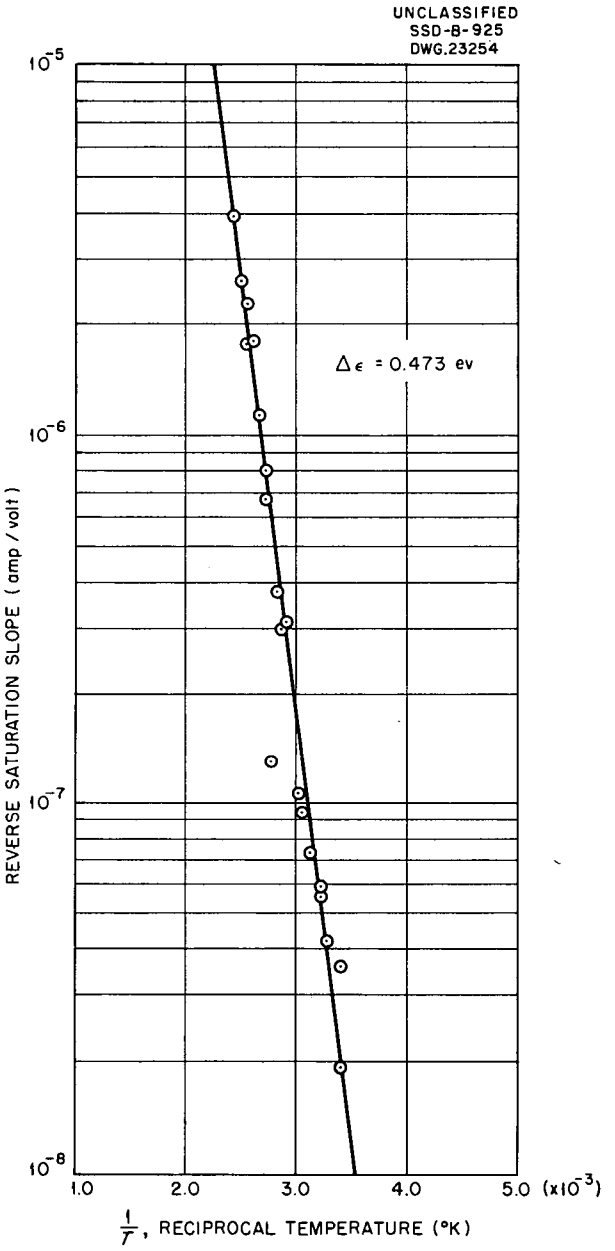

Fig. 36. Reverse-Saturation Slope vs Reciprocal Temperature Before Bombardment for Sample 1N38-A-2.

or essentially the forbidden-energy gap in germanium.

Figure 38 shows the reverse current for 1-volt bias as a function of temperature. The activation energy for this process is 0.672 ev.

Figures 39 and 40 show the forward current as a function of different biases. There seem to be different mechanisms operating above and below 290°K. Above 290°K, log I seems to be a linear function of $1/T$. The activation energy for the current is strongly dependent upon the bias.

A second rectifier, 1N38-A-4, was irradiated in the enhanced flux in hole 51N. Figure 41 shows the behavior of the conductance as a function of irradiation. These data check previous data but are

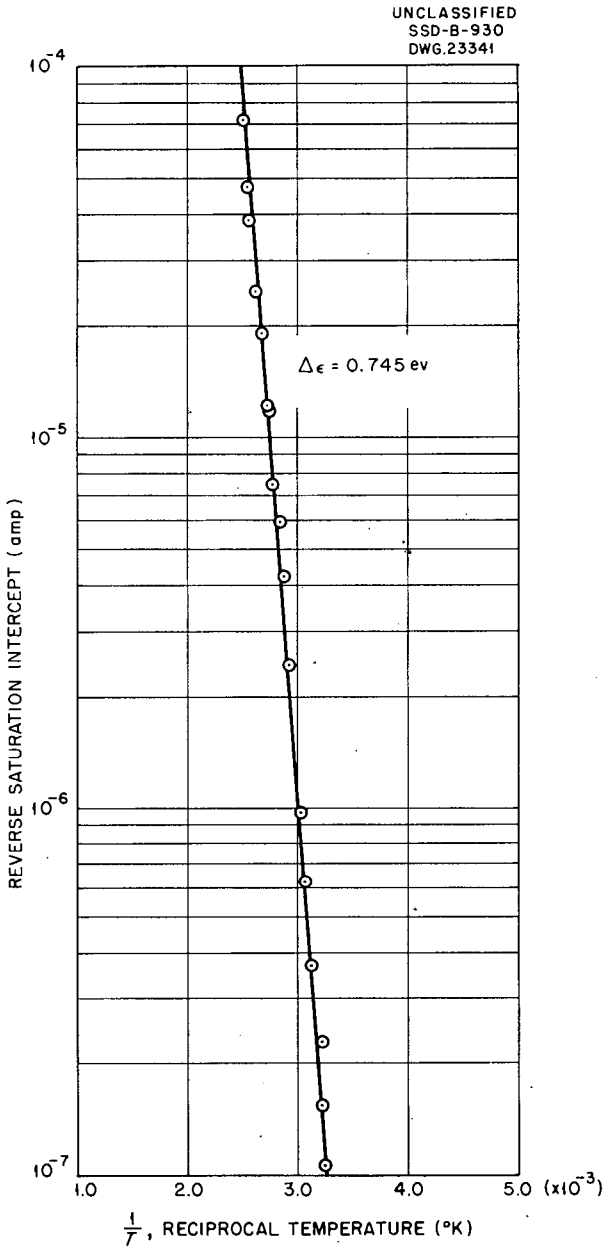

Fig. 37. Reverse-Saturation Intercept vs Reciprocal Temperature Before Bombardment for Sample 1N38-A-2.

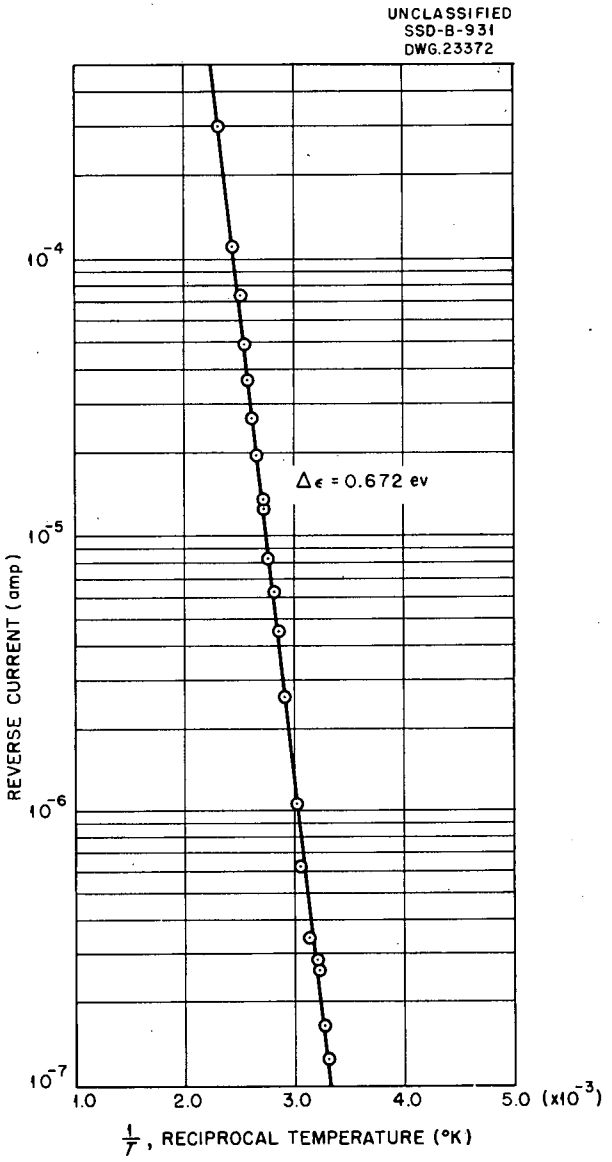

Fig. 38. Reverse Current at 1 volt vs Reciprocal Temperature Before Bombardment for Sample 1N38-A-2.

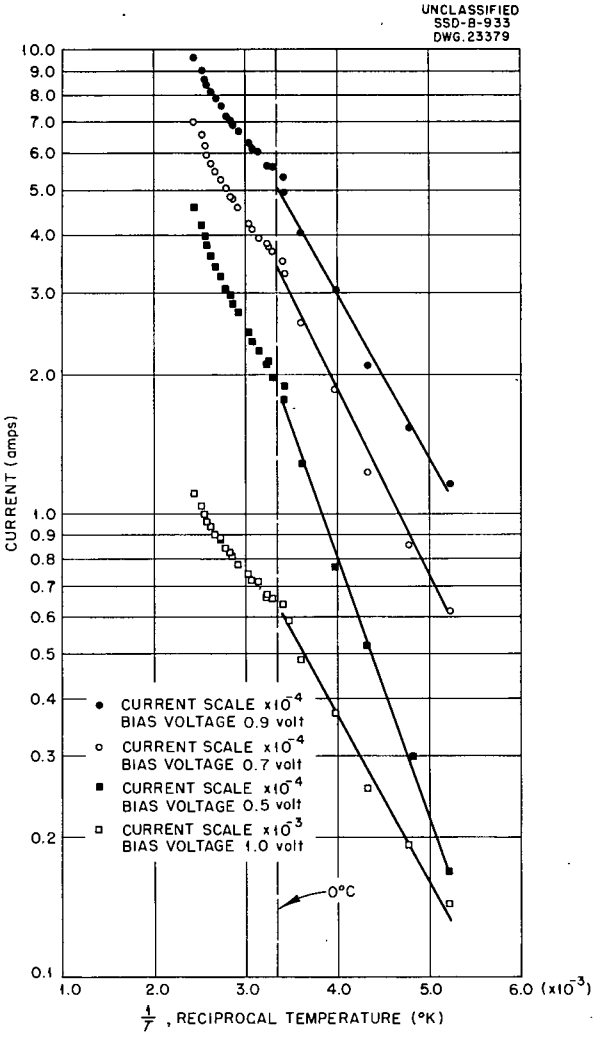

Fig. 39. Current vs Reciprocal Temperature as a Function of Bias Voltage for Sample 1N38-A-2 Before Bombardment.

more complete than previous observations have permitted.[16,17]

The forward conductance at various biases as a function of irradiation is shown in Fig. 41. The scattering of points in the initial part of the curve (small exposure) may be due to uncertainty in reactor power level. The operating power at larger irradiation was more certain. The slopes of the initial, or linear, part of these curves plotted as a function of bias are shown in Fig. 42.

For forward biases above a certain critical value, $dI/d(nvt)$ is negative; for reverse biases and forward biases below a certain critical value, $dI/d(nvt)$ is positive. In Fig. 42 the critical value is 0.18 volt; this value may vary from sample to sample and may be a function of sample temperature. Subsequent exposures at different temperatures will clear up this question.

The curve of the log of the reverse conductance at 1 volt vs the total neutron flux shown in Fig. 43 is very similar to that of the log of the reverse-saturation slope vs the total flux shown in Fig. 44. The curve of the zero slope vs integrated flux shown in Fig. 45 seems to be similar to the curves shown in Figs. 43 and 44.

Figure 46 shows the reverse-saturation intercept vs the total flux. Because of the difficulty in obtaining these values, the points are scattered; therefore the linearity of the line may be fictitious. Further experimentation will be required to determine the behavior of the saturation intercept.

The properties which should be studied and the techniques for conducting an intensive set of experiments on the properties of rectifiers are indicated in this report and in ORNL-1606.

ELECTRICAL EFFECTS IN IRRADIATED BARRIERS

J. C. Pigg

Several Ge-10-A germanium, diffused-*pn*-junction rectifiers have been exposed in holes 50N and 51N in the ORNL Graphite Reactor. The open-circuit output voltage was measured as a function of bombardment. On startup, the voltage was 125 mv and it decayed to zero after a few hours. The output voltage was strongly temperature dependent, decreasing as the temperature was raised.

Some of the rectifiers were removed from the reactor before the voltage output had decayed to zero and were allowed to sit for several hours. When they were placed in the reactor again, a partial recovery of the output voltage had occurred. Those units which were bombarded to zero output showed no recovery.

Experiments have been conducted by using a simulated barrier consisting of a gas between two dissimilar metals. A lead-brass unit with a surface area of 234 cm^2 and plates separated in air by 0.32 cm was tested in hole 50N. The output voltage increased from 0.20 to 0.27 volt upon

[16] J. C. Pigg, *Solid State Semiann. Prog. Rep. Aug. 31, 1953*, ORNL-1606, p 79.

[17] J. H. Crawford, K. Lark-Horovitz, and J. C. Pigg, *Phys. Quar. Prog. Rep. March 15, 1950*, ORNL-694, p 64.

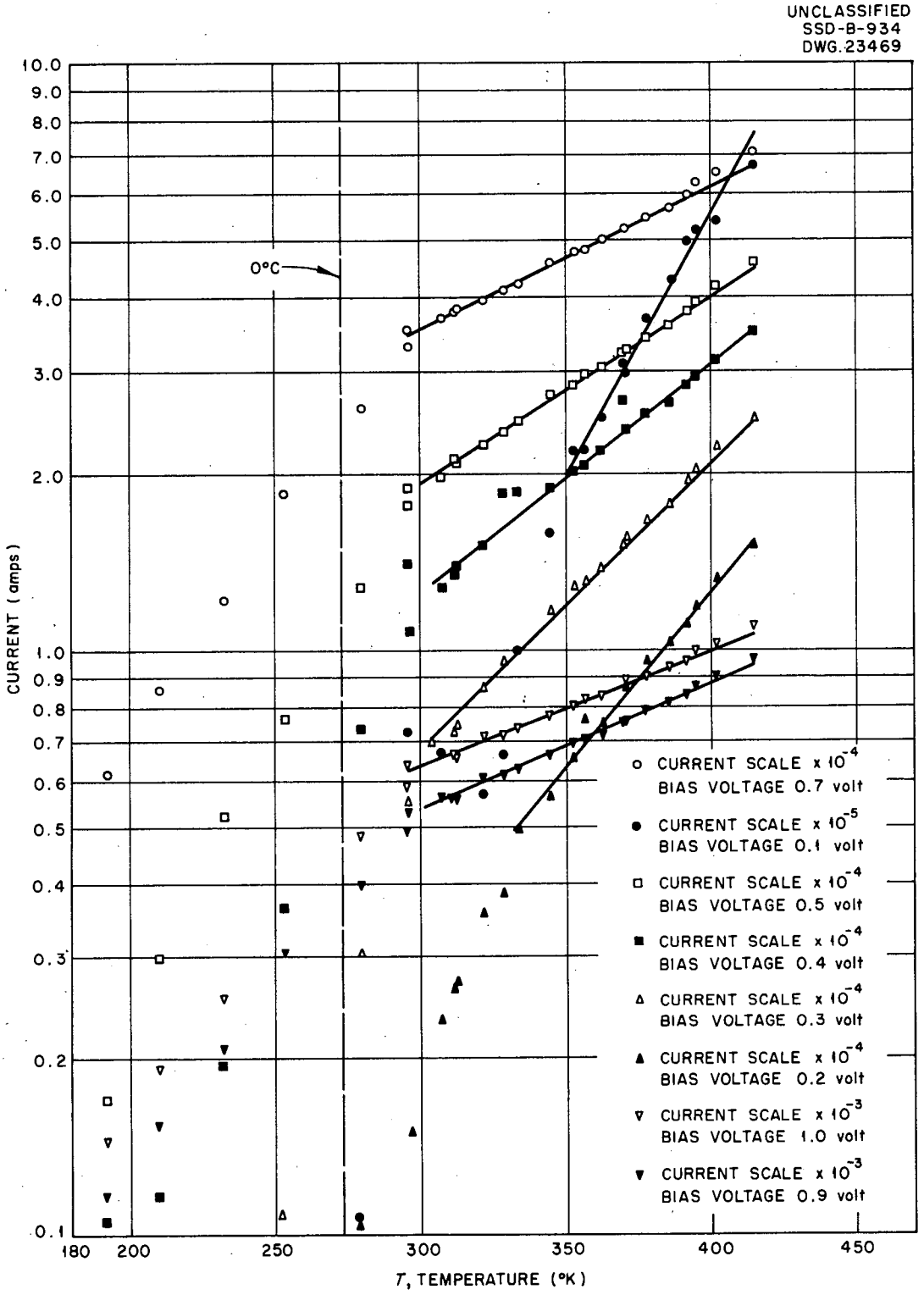

Fig. 40. Current vs Temperature as a Function of Bias Voltage of Sample 1N38-A-2 Before Bombardment.

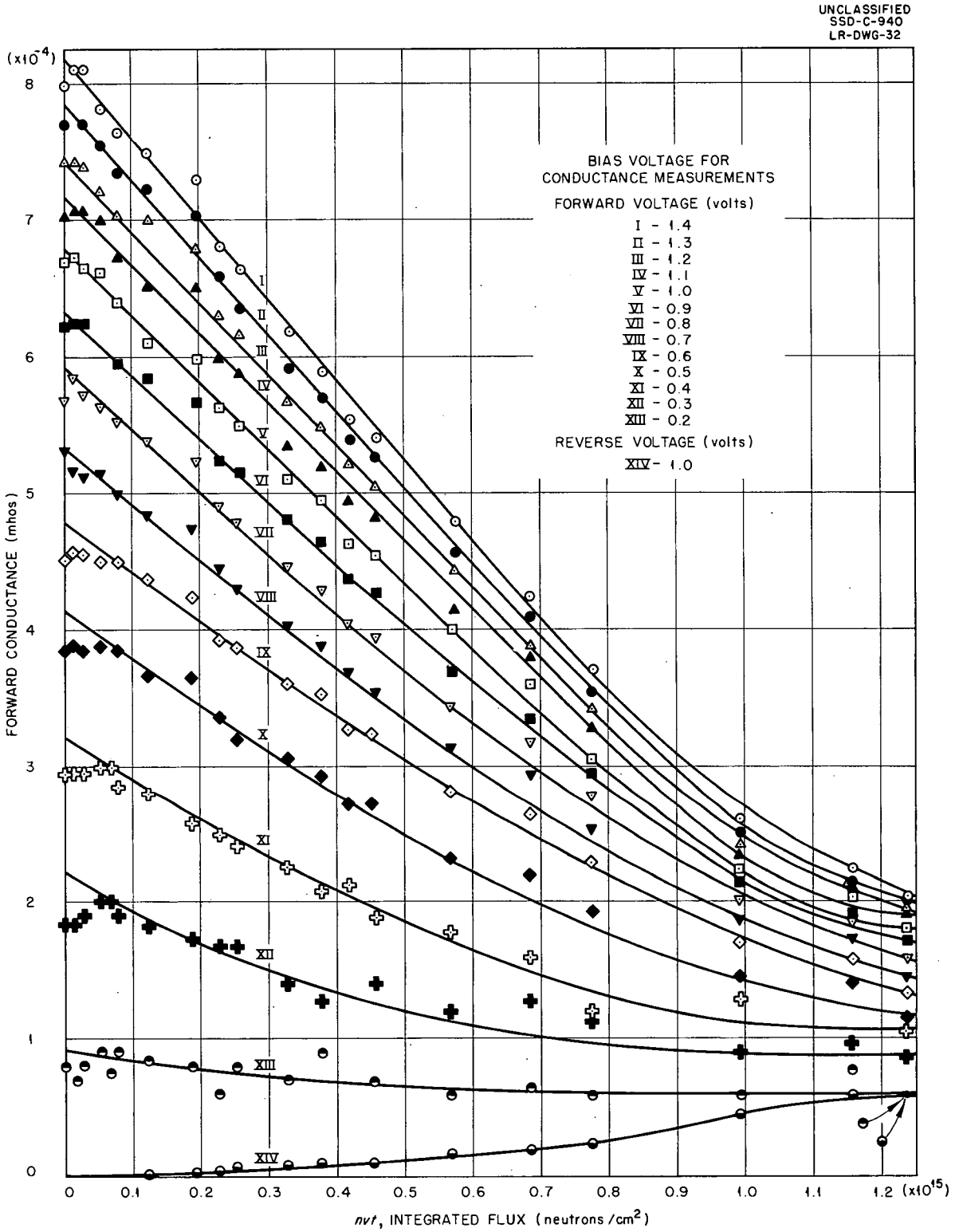

Fig. 41. Conductance vs Integrated Flux for Sample 1N38-A-4 Bombarded in Hole 51N of the ORNL Graphite Reactor.

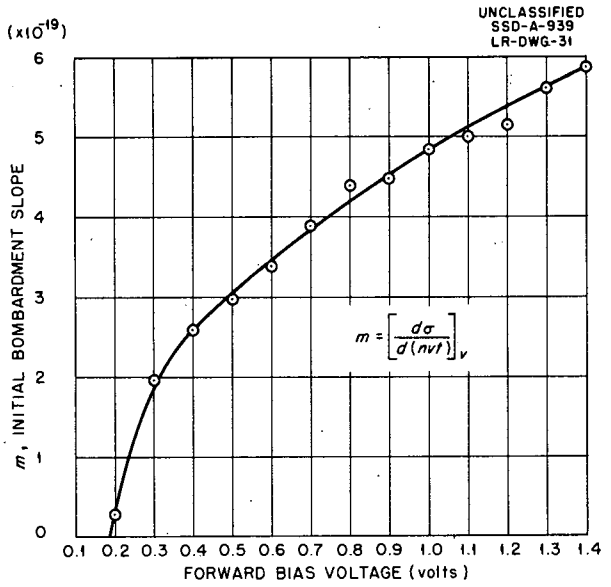

Fig. 42. Initial Bombardment Slope vs Bias Voltage for Sample 1N38-A-4.

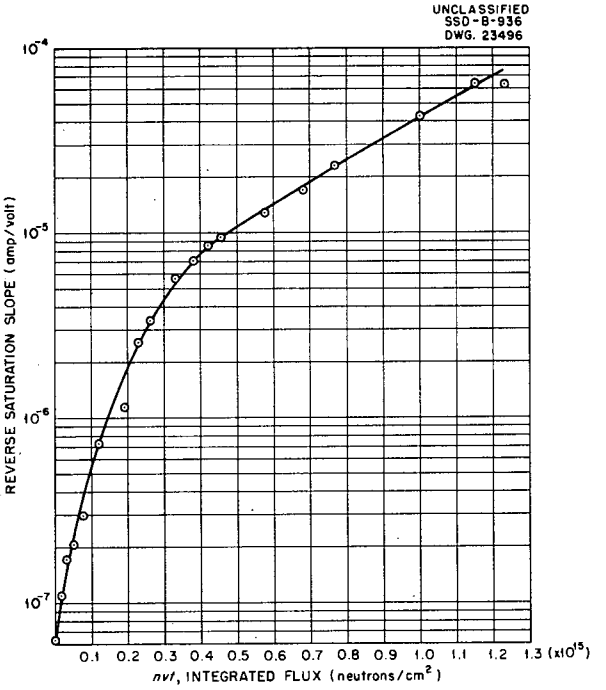

Fig. 44. Reverse-Saturation Slope vs Integrated Flux for Sample 1N38-A-4 Bombarded in Hole 51N of the ORNL Graphite Reactor.

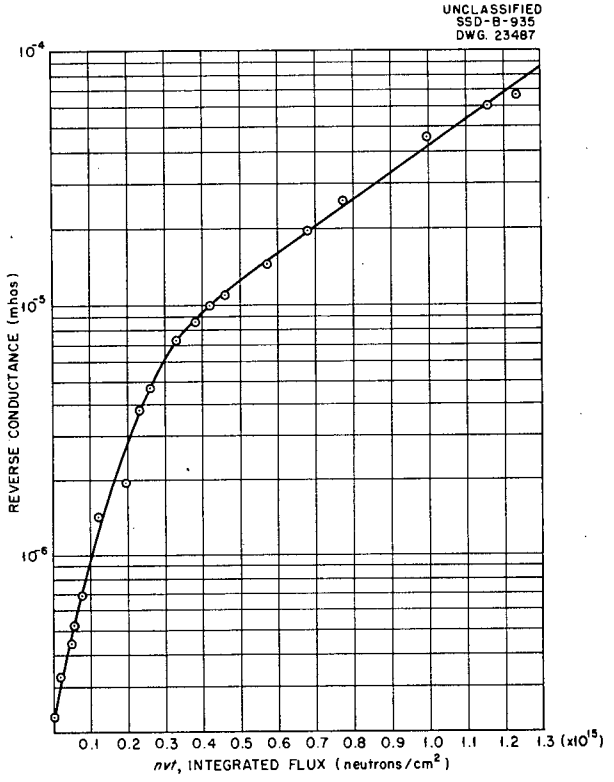

Fig. 43. Reverse Conductance at 1 volt vs Integrated Flux for Sample 1N38-A-4 Bombarded in Hole 51N of the ORNL Graphite Reactor.

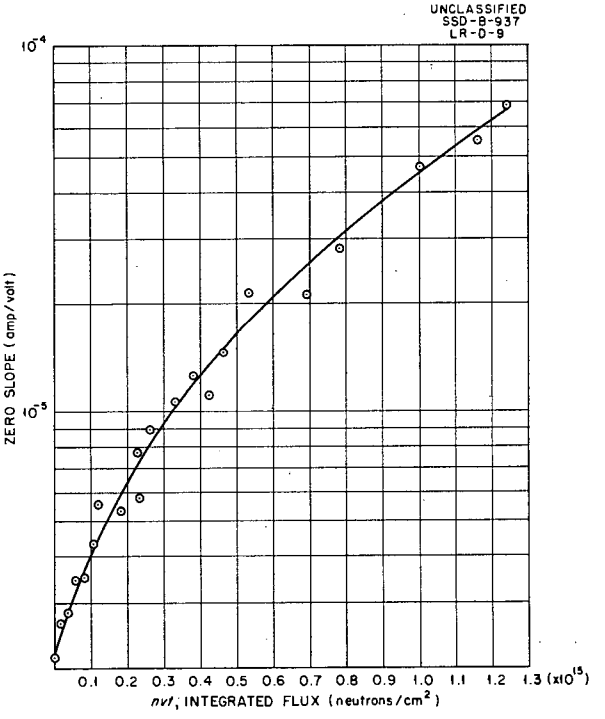

Fig. 45. Zero Slope vs Integrated Flux for Sample 1N38-A-4 Bombarded in Hole 51N of the ORNL Graphite Reactor.

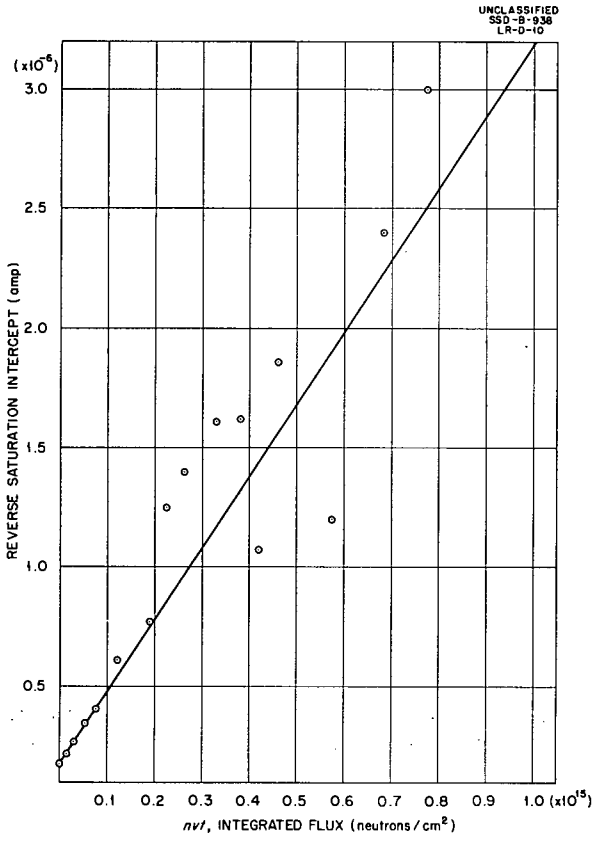

Fig. 46. Reverse-Saturation Intercept vs Integrated Flux for Sample 1N38-A-4 Bombarded in Hole 51N of the ORNL Graphite Reactor.

irradiation. No attempt was made to maximize the power output. The internal impedance of the unit was 1.06 megohms when the reactor power was 3700 kw.

RADIATION DAMAGE IN SiO_2 STRUCTURES

M. C. Wittels F. A. Sherrill

Heavy dosages of fast-neutron flux reduce four phases of the silicon-oxygen system to a common phase:[18] quartz, low cristobalite, low tridymite, and glass. This highly disordered material has the x-ray diffraction of a glass, is optically isotropic, and has a density of 2.26. This material was recrystallized by annealing at 930°C for 16 hr and resulted in the formation of polycrystalline alpha quartz. Debye-Scherrer diffraction patterns taken by using monochromatic radiation from a copper target gave x-ray reflections at angles up to $2\theta = 90$ deg. The fact that x-ray reflections were not observed at larger Bragg angles may be due to incomplete recrystallization, particle-size broadening, or strain. The contributions of each of these factors are being determined.

It appears that the bombardment of any of the above-mentioned phases produces a silica glass, with a density and an average refractive index near those of normal low tridymite, which can be transformed into alpha quartz in a solid-state reaction. Further annealing studies are necessary to confirm this view. This behavior is of major interest since investigators[19] have been unsuccessful in their attempts to transform any of the silica phases into alpha quartz by means of a solid-state transformation in the absence of chemical aids.

ANNEALING OF NEUTRON-IRRADIATED DIAMOND

M. C. Wittels F. A. Sherrill

Annealing phenomena in the diamond structure are complex.[20] Diamond powder bombarded[21] by 3×10^{20} neutrons/cm^2 was step-annealed for approximately 30 min at 100°C intervals up to 1025°C. This material, which has a reduced x-ray density of 3.46% prior to annealing, was heated and

[18] M. C. Wittels and F. A. Sherrill, *Solid State Semi-ann. Prog. Rep. Aug. 31, 1953*, ORNL-1606, p 98.

[19] R. B. Sosman, *The Properties of Silica*, The Chemical Catalog Co., New York, 1927.

[20] W. Primak, L. H. Fuchs, and P. Day, *Phys. Rev.* 92, 1064 (1953).

[21] M. C. Wittels and F. A. Sherrill, *Solid State Semi-ann. Prog. Rep. Aug. 31, 1953*, ORNL-1606, p 98.

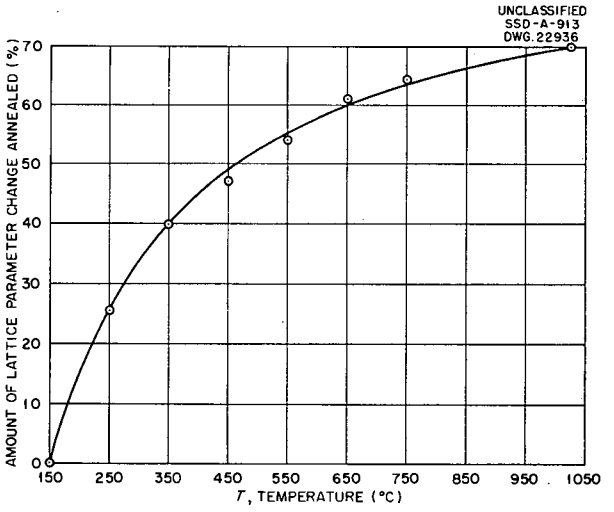

Fig. 47. Lattice-Expansion Annealing in Diamond.

x rayed following each anneal. The results shown in Fig. 47 indicate that defects begin to anneal at temperatures slightly higher than irradiation temperatures and that the annealing rate falls off rapidly above 450°C. Only 70% of the lattice-parameter change was annealed at 1025°C, which indicates that the thermal stability of some of the defects is extremely high. A more complete annealing study of neutron-irradiated diamonds is now in progress.

ENGINEERING PROPERTIES

DYNAMIC PROPERTIES OF IRRADIATED ELASTOMERS

C. D. Bopp R. L. Towns
O. Sisman W. K. Kirkland

Certain physical properties have been described[1,2] for a number of elastomer formulations which had been exposed to high-energy radiation. The hardening which occurs for most of these elastomers is believed to result from cross-linking between linear polymer chains. In order to measure hysteresis losses and in order to measure more sensitively the radiation-induced hardening, the dynamic properties of many of the formulations have been studied.

The resonant frequency and the band width were measured when specimens were vibrated as clamped-free bars. The two methods which were employed are depicted in Fig. 48. In method *A* the clamped end of the specimen is driven by a phonograph-record cutting head. This method is satisfactory only for soft specimens because coupling occurs between the resonant frequencies of the specimen and the clamp for elastomer specimens that have been irradiated sufficiently to make them very hard. For this reason method *B* was developed to test severely hardened specimens.

In method *B* the clamped end of the specimen does not move; the specimen is induced to vibrate by an electromagnetic driver that is placed in contact with the specimen near the clamped end. Method *B* can be used for both soft and hardened elastomers and is also suitable for ceramic and plastic materials. No coupling interaction was detected with this method. Since the equation of motion proves to be simpler for method *B* (as is noted below), this method is preferred even for soft elastomers. For soft specimens it is important that the driver be quite near the clamp. Method *A* was used only because much data were accumulated before trouble was encountered with the coupling interaction.

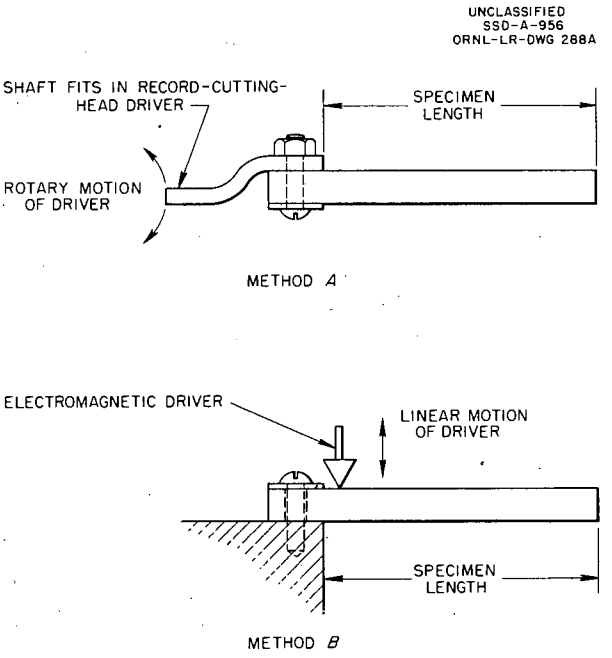

Fig. 48. Vibrating Apparatus.

In both methods the resonant frequency and the band width are determined from the frequency-amplitude relation. The amplitude is measured by observing the free end of the specimen with a microscope; the frequency is adjusted with an audio oscillator. A piezoelectric pickup was tried in place of the microscope but was found to be less satisfactory. It is believed that much of the force exerted by the driver is used in distorting the pressure-sensitive crystal, and for this reason the increase in amplitude at resonance is less when

[1] O. Sisman *et al.*, *Phys. of Solids Inst. Quar. Prog. Rep. July 31, 1951*, ORNL-1128, p 41.

[2] C. D. Bopp *et al.*, *Solid State Semiann. Prog. Rep. Aug. 31, 1953*, ORNL-1606, Table 18, p 92.

the pickup is used as part of the apparatus. A variable-reluctance pickup was also tried. The reluctance pickup proved to be unsuccessful for measuring the amplitude because of magnetic coupling which occurred between the pickup and the driver.

Linear motion was assumed in deriving the equations of motion.[3] Stroboscopic observation shows that this assumption is only approximately correct for the driver used in method *A*. Rotary motion is superimposed upon the linear motion as is shown in Fig. 48. The motion is more nearly linear for method *B* owing to the methods of clamping and driving. Evidence as to the applicability of the equations of motion is given by measuring the frequencies and band widths of a number of specimens of different lengths. If the data are plotted as shown in Fig. 49, the extrapolation of the plot should intersect the origin. Such is the case for method *B*; however, for method *A*, although the plot is linear (for soft specimens), the extrapolation deviates a little from the origin. The slope of the plots determined by method *A* proved to be proportional to those determined by method *B* and for this reason the slope of the plot was used in comparing the data or, alternatively, an empirical correction was applied to data determined by method *A*.

Amplitude dependence of resonant frequencies was observed only for high amplitudes or high frequencies and is therefore believed to be associated with heating. Correction for amplitude dependence was made by extrapolation to zero amplitude. High magnification (500X) made it possible to use very small amplitudes.

Irradiations were conducted in hole 19 of the ORNL Graphite Reactor which is water cooled to between 25 and 40°C. Since both fast-neutron and gamma radiation produce roughly equivalent changes in elastomers per unit of energy absorbed,[4] the exposure is expressed in rep units for both of them. The energy absorbed from fast-neutron radiation is roughly proportional to the hydrogen content since, for hydrogen, about 90% of the total energy absorbed is from fast-neutron radiation, but for carbon and heavier elements less than 30% of the total is from fast-neutron radiation. For materials composed entirely of hydrogen and carbon the energy absorbed[5] is given approximately by

$$(1) \qquad R = (4.8c + 0.31)N \times 10^{-9} ,$$

where

R = energy absorbed, rep,
c = wt % of hydrogen,
N = total thermal-neutron exposure, neutrons/cm^2.

If elements in addition to carbon and hydrogen are present, the applicability of the above relation is determined largely by the thermal-neutron absorption cross sections of the additional elements. The thermal-neutron absorption cross sections of hydrogen and carbon are small enough to produce negligible energy absorption. For elements (such as chlorine) with higher cross sections, additional energy will be absorbed from the gammas and betas emitted in the absorption process and from the recoil of the atoms upon emitting radiation.

Compositions of the formulations in Table 4 have been given.[6] For all the elastomers listed in Table 4 except Hypalon, neoprene, and Thiokol, Eq. 1 gives roughly 8×10^{-10} rep/nvt. For Thiokol (which contains sulfur) the figure is 4×10^{-10} rep/nvt. Equation 1 is inapplicable for neoprene and Hypalon (both contain chlorine), but comparison of irradiations made both in the reactor and in a gamma source[4] gives roughly about 2×10^{-9} rep/nvt

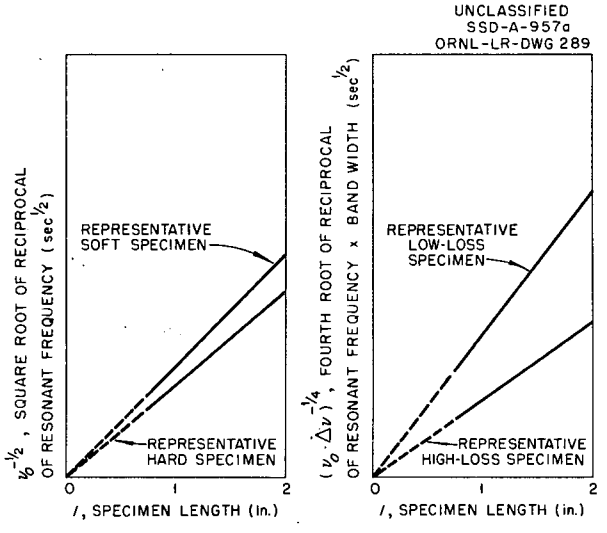

Fig. 49. Schematic Plot of Experimental Data.

[3] *Ibid.*, p 88.

[4] C. D. Bopp *et al.*, *Solid State Semiann. Prog. Rep. Aug. 31, 1953*, ORNL-1606, Table 14, p 87.

[5] D. M. Richardson, *Calorimetric Measurement of Radiation Energy Dissipated by Various Materials Placed in the Oak Ridge Pile*, ORNL-129 (Oct. 1, 1948).

[6] C. D. Bopp *et al.*, *op. cit.*, Tables 16 and 17, pp 90 and 91; O. Sisman *et al.*, *Phys. of Solids Inst. Quar. Prog. Rep. April 30, 1951*, ORNL-1095, Table 5.1, p 76.

TABLE 4. INITIAL VALUES OF THE DYNAMIC YOUNG'S MODULUS AND THE VISCOUS MODULUS

ELASTOMER FORMULATION*	POLYMER	THICKNESS (in.)	DENSITY (g/cm^3)	DYNAMIC YOUNG'S MODULUS (10^8 dynes/cm^2)	VISCOUS MODULUS (10^8 dynes/cm^2)
P1S1C1	Polybutadiene	0.082	1.04	0.9	0.2
P1S1C2	Hycar OR-15	0.082	1.12	1.2	0.3
P1S1C3	Hycar OS-10	0.082	1.12	1.2	0.3
P1S1C4	Neoprene GN	0.086	1.36	1.2	0.08
P1S1C7	Thiokol	0.088	1.46	4.0	0.4
P1S1C8	Silastic 250	0.078	1.21	0.3	0.04
P1S1C9	Natural rubber	0.068	1.05	0.6	0.04
P1S1C10	Hycar PA-21	0.075	1.22	0.7	0.4
P1S1C11	Hypalon S2	0.078	1.49	3.0	0.4
32A43	Natural rubber	0.075	1.19	2.3	0.15
32A47	GR-S	0.075	1.21	1.8	0.12
P1S2C1	Notural rubber with various plasticizers	0.080	1.04	0.33	0.03
P1S2C2	Natural rubber with various plasticizers	0.080	1.05	0.25	0.02
P1S2C3	Natural rubber with various plasticizers	0.080	1.05	0.30	0.03
P1S2C4	Natural rubber with various plasticizers	0.080	1.09	0.47	0.04

*C. D. Bopp *et al.*, *Solid State Semiann. Prog. Rep. Aug. 31, 1953*, ORNL-1606, Tables 16 and 17, pp 90 and 91; O. Sisman *et al.*, *Phys. of Solids Inst. Quar. Prog. Rep. April 30, 1951*, ORNL-1095, Table 5.1, p 76.

for neoprene. Since a better figure is lacking, the same value is used for Hypalon.

In Figs. 50 through 53 the increase produced in the dynamic Young's modulus is plotted against radiation exposure. The slope of the log plots indicates proportionality to the first power of exposure for all the formulations based on natural rubber; for formulations based on other polymers the slope of the plots indicates proportionality to higher powers of the exposure. The two GR-S formulations of Fig. 50 have nearly the same slope, although higher exposures are required to produce the same increase for the formulation containing more carbon black; a similar relation is shown in Fig. 50 for the two formulations of natural rubber with different proportions of carbon black. Insufficient data have been obtained to determine the relations for very short or long exposures, although in Fig. 53 it appears that completion of the process has been approached for the polymers with high rates of increase.

Butyl rubber was not included in these irradiations because it is much more sensitive to exposure than are the other elastomers. The sensitivity of butyl rubber to chain cleavage, which is believed to be related to the presence of quaternary carbon atoms, results in softening. In Fig. 53 only one point is plotted for Thiokol since the modulus re-

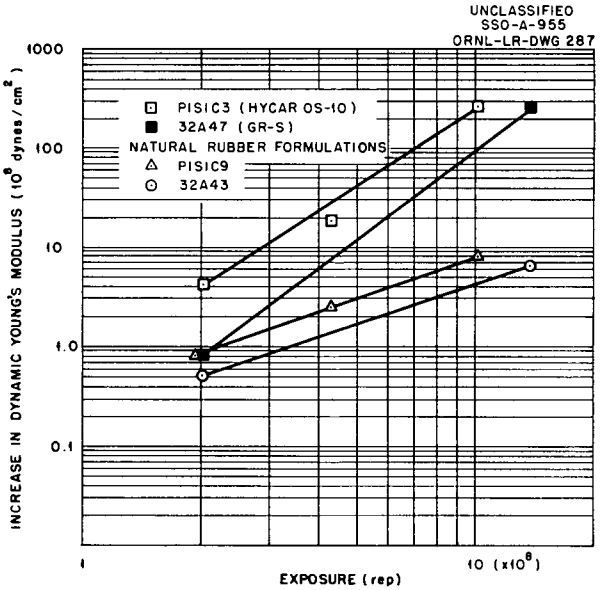

Fig. 50. Effect of Radiation on Dynamic Young's Modulus of GR-S and Natural-Rubber Formulations.

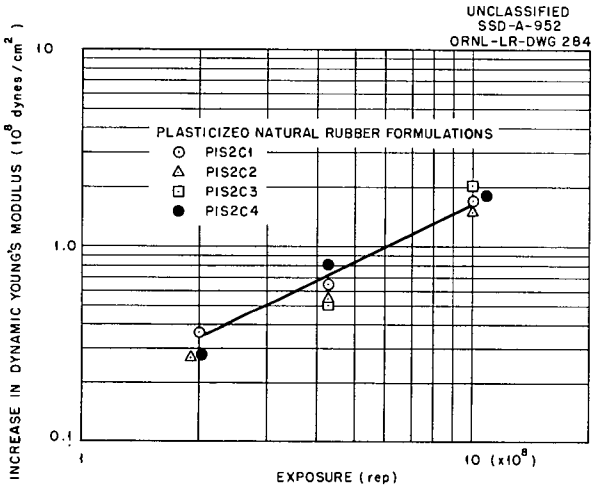

Fig. 51. Effect of Radiation on Dynamic Young's Modulus of Plasticized, Natural-Rubber Formulations.

mained constant for all except the longest exposure. Thiokol is hardened only after longer exposures than are required to harden other polymers; the hardening is believed to result from an equalization of the cross-linking and the chain-cleavage processes. Thiokol is sensitive to chain cleavage because sulfur is present in the chain.

The change in viscous modulus shown in Table 5 is small for short periods of irradiation and is

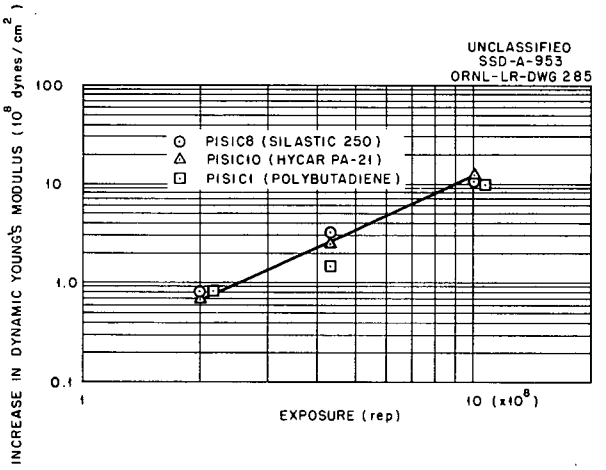

Fig. 52. Effect of Radiation on Dynamic Young's Modulus of Silastic, Hycar, and Polybutadiene.

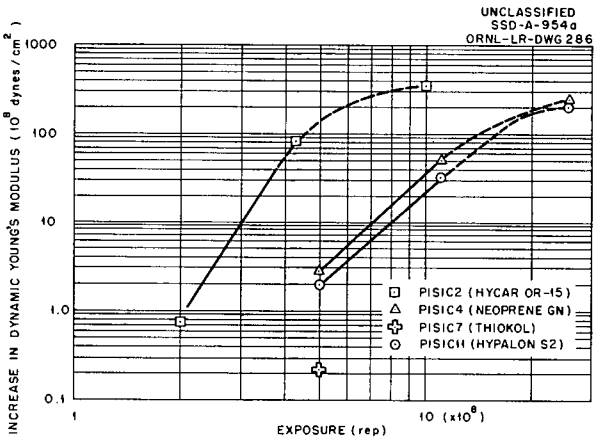

Fig. 53. Effect of Radiation on Dynamic Young's Modulus of Thiokol and of Polymers with High Rates of Increase.

usually less than the change in Young's modulus for all irradiations. Hysteresis losses for constant straining are proportional to the viscous modulus.[3]

The dynamic Young's modulus did not prove to be a good measure of radiation effects on Thiokol since no change was shown for periods in which the strength and the compression set[7] were affected. For the other elastomers tested, however, the dynamic Young's modulus provides a sensitive measure of radiation exposure over a large exposure range. An additional advantage of the dynamic test is the small statistical variation which makes it necessary to test only a few specimens.

[7] C. D. Bopp *et al.*, *Solid State Quar. Prog. Rep. Jan. 31, 1952*, ORNL-1261, Table 3, p 26.

TABLE 5. IRRADIATION-PRODUCED CHANGE IN THE VISCOUS MODULUS

ELASTOMER FORMULATION	POLYMER	EXPOSURE (rep)	VISCOUS MODULUS RATIO, IRRADIATED VALUE / UNIRRADIATED VALUE
P1S1C1	Polybutadiene	0.19	1.0
		0.43	1.7
		1.0	80
P1S1C2	Hycar OR-15	0.19	3
		0.43	70
		1.0	20
P1S1C3	Hycar OS-10	0.19	2
		0.43	5
		1.0	100
P1S1C4	Neoprene GN	0.5	5
		1.1	1000
		2.5	65
P1S1C7	Thiokol	0.10	1.0
		0.20	1.0
		0.50	1.7
P1S1C8	Silastic	0.19	1
		0.43	1
		1.0	5
P1S1C9	Natural rubber	0.19	1.0
		0.43	2.0
		1.0	20
P1S1C10	Hycar PA-21	0.19	2
		0.43	5
		1.0	20
P1S1C11	Hypalon S-2	0.5	3
		1.1	30
		2.5	30
32A43	Natural rubber	0.19	1
		1.4	9
32A47	GR-S	0.19	1.5
		1.4	150
P1S2C1	Natural rubber with various plasticizers	0.19	1
		0.43	1
		1.0	3
P1S2C2	Natural rubber with various plasticizers	0.19	1
		0.43	2
		1.0	

TABLE 5. (continued)

ELASTOMER FORMULATION	POLYMER	EXPOSURE (rep)	VISCOUS MODULUS RATIO, IRRADIATED VALUE / UNIRRADIATED VALUE
P1S2C3	Natural rubber with various plasticizers	0.19	1
		0.43	1
		1.0	5
P1S2C4	Natural rubber with various plasticizers	0.19	1
		0.43	2
		1.0	7

CRYSTAL PHYSICS

EFFECT OF DEFORMATION ON THE SUPERCONDUCTING PROPERTIES OF ALUMINUM

T. H. Blewitt R. E. Jamison
J. G. Daunt R. R. Coltman

Lasarew and Galkin[1] found that plastic deformation produced striking changes in the superconducting properties of tin. Their study of the influence of plastic deformation on superconductivity was a relatively crude one because of the manner in which deformation was introduced. Plastic deformation was more elegantly introduced to aluminum in the experiment described here.

The superconductivity of five aluminum samples was studied; three were single-crystal specimens and two were relatively coarse-grained polycrystalline specimens. Each sample was prepared from high-purity aluminum in the shape of a ¼-in. ASTM tensile specimen.

One of the single-crystal specimens, Al(III), was unstrained; the other two single crystals were deformed by tensile elongation in a bath of boiling nitrogen (77°K). The crystal orientation of the Al(II) sample was such that only one slip system was operative; this sample was elongated by 18%. The shear strain was 0.37 and the sample had work-hardened so that shear stress had increased from a value of 0.079 to 3.44 kg/mm^2. The remaining single crystal was deformed in a similar manner. Its orientation was such that two slip systems were operative during a substantial portion of the elongation. It was elongated 17.5%, which is equivalent to a shear strain of 0.37. Work-hardening had increased the shear stress from 0.085 to 3.02 kg/mm^2.

The polycrystalline samples Al-P-1 and Al-P-2 were also deformed at 77°K by tensile elongation of about 20%. In polycrystalline samples, according to an analysis by G. J. Taylor, five slip systems may be expected to be operative.

In order that the distortion of the magnetic field could be reduced, the shoulders of all the samples were cut off prior to the conductivity measurements. The strained specimens were maintained in liquid nitrogen during the period between the time of straining and the time of the magnetic measurements at liquid-helium temperature (4.2°K). The specimens were inserted into the liquid-helium cryostat from the liquid-nitrogen storage vessel in a matter of a few seconds and so suffered no appreciable warming during the transfer. Since the straining process was also carried out at various temperatures in liquid nitrogen, there was essentially no time for annealing of the specimens to occur, unless annealing could take place at 77°K.

The transition temperature, T_c, at which these specimens became superconducting and the slope of the superconducting magnetic-threshold curve, $(\partial H/\partial T)_{T=T_c}$, were measured at various tempera-

[1] B. Lasarew and A. Galkin, *J. Phys.* (U. S. S. R.) 8, 371 (1944).

tures in liquid helium by observing the magnetic moment of the specimens in small magnetic fields applied parallel to the axis of the specimens and by using a technique that has been described in detail by Daunt and Smith.[2] This technique was previously used successfully by Mendelssohn.[3]

The results obtained are shown in Fig. 54 in which it may be seen that there is no difference, within experimental error of about 2 to 3%, in the values for T_c and for $(\partial H/\partial T)_{T=T_c}$ obtained with the strained and with the unstrained specimens. Moreover, the values obtained for T_c and for $(\partial H/\partial T)_{T=T_c}$ were in good agreement with those previously reported by Shoenberg,[4] by Daunt and Heer,[5] and by Goodman and Mendoza.[6]

It is concluded that the process of deformation of aluminum single crystals and polycrystals by drawing at 77°K does not affect the superconducting transition temperature or the magnetic-threshold curve, as measured magnetically, to an extent greater than approximately 2 or 3%. This conclusion is in agreement with the results of work on polycrystals of tin and other metals by Khotkevich and Golik.[7] However, these results are in strong disagreement with the results of resistance measurements on the superconducting state in inhomogeneously strained tin obtained by Lasarew and Galkin.[1] It is possible that by carrying out the deformation of aluminum at temperatures lower than 77°K some changes in the superconducting properties may be observable. Care must be taken in such work to ensure that the substances chosen for investigation do not suffer phase changes as a result of physical strain at low temperatures.

[2] J. G. Daunt and T. S. Smith, *Phys. Rev.* 88, 309 (1952).

[3] K. Mendelssohn, *Proc. Roy. Soc. (London) A* 155, 558 (1936).

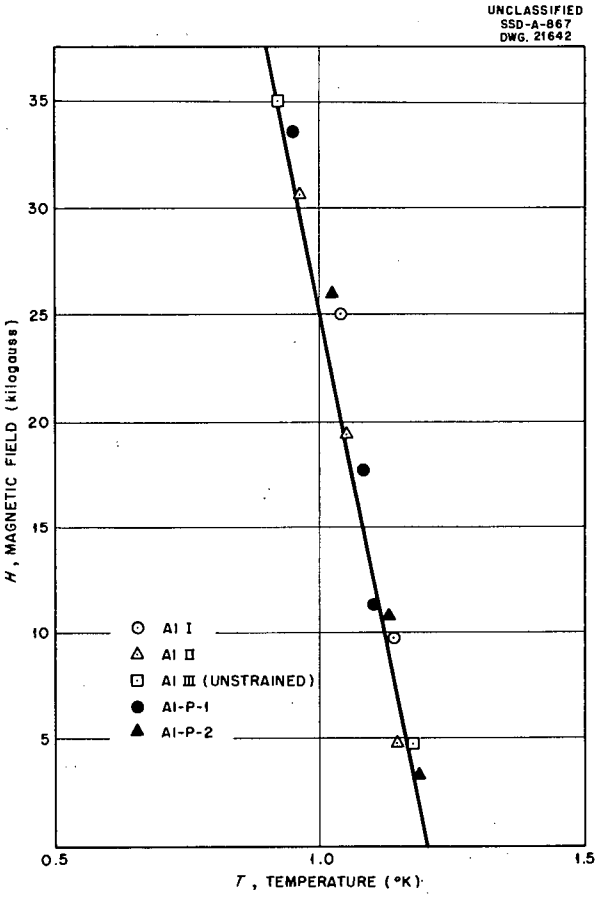

Fig. 54. Superconductivity Transition Temperature for Aluminum Specimens as a Function of Magnetic Field Strength.

RADIATION ORDERING IN Cu_3Au

T. H. Blewitt R. R. Coltman

Recently, Cook and Cushing[8,9] described the results of their investigation of the effect of reactor irradiation on the order-disorder transformation of Cu_3Au and CuAu. They studied the ordering kinetics in both the order and disordered alloys and their results substantiated the belief of earlier investigators[10,11] that the reactor irradiation was found in some cases to cause a disordering effect while in other cases the irradiation seemed to increase the rate of ordering.

There seems to be general agreement that the disordering phenomenon is a result of local regions called "thermal spikes" being rapidly heated to a high temperature with a subsequent rapid quench.

[4] D. Shoenberg, *Proc. Cambridge Phil. Soc.* 36, 84 (1940).

[5] J. G. Daunt and C. V. Heer, *Phys. Rev.* 76, 1324 (1949).

[6] B. B. Goodman and E. Mendoza, *Phil. Mag.* 42, 594 (1951).

[7] V. I. Khotkevich and V. R. Golik, *Zhur. Eksptl. i Teort. Fiz.* 20, 427 (1950).

[8] L. G. Cook and R. L. Cushing, *Acta Metallurgica* 1, 539 (1953).

[9] *Ibid.*, p 549.

[10] S. Siegel, *Phys. Rev.* 75, 1823 (1949).

[11] J. Adam and R. A. Dugdale, *Nature* 168, 583 (references) (1951).

The time duration of this spike has been estimated to be of the order of 10^{-10} sec.[12] On the other hand, there appears to be a rather basic disagreement in both the conditions under which the phenomenon of the increased ordering rate results and the mechanism by which it occurs. It has been suggested[13] that this phenomenon was intimately connected with the production of Frenkel defects during the bombardment, and evidence was cited for the increase of the diffusion rate by interstitial atoms or vacant lattice sites. Cook and Cushing,[8] however, interpreted their experiments to indicate that the radiation ordering was dependent on the slow-neutron flux. They consequently ruled out the influence of structural defects and attributed radiation ordering to the presence of mercury and in some cases to zinc and nickel impurities created by a transmutation process resulting from the capture of slow neutrons by the nucleus. The mechanism by which these impurity atoms increase the diffusion rate is not clear, but Cook and Cushing presumably assumed that these atoms play the role which is customarily attributed to vacant lattice sites or interstitial atoms in the diffusion process. The implications of this viewpoint are serious enough, in regard to the theory of atomic diffusion, to warrant further considerations as to the mechanism of radiation ordering. In this connection, experiments utilizing electron bombardment should probably be considered, as well as some of the more recent data obtained from reactor radiation.

It would seem that the relative influence on radiation ordering of structural defects produced by the elastic collisions of fast particles as compared with the chemical defects produced by nuclear reactions could be estimated by consideration of the effects of fast electrons as compared with reactor neutrons. In the former case, with electrons having energies of the order of a few Mev, the number of transmutations produced will be extremely small compared with the latter case. Recently,[14] the experimenters at Harwell studied the effect of 3-Mev electrons on the ordering rate of Cu_3Au. They found a pronounced increase in the rate of ordering as a result of a relatively small bombardment. If these data are representative of radiation ordering, it would appear that structural defects must play a role in the increased ordering rate.

The recent results[15] obtained at ORNL indicate that substantial radiation ordering can occur during reactor bombardment even when the number of chemical defects formed by nuclear reactions is very small. On Cu_3Au samples prepared by heat treatment to reduce to a minimum the contribution of domain walls to the electrical resistivity (the samples had a domain size in excess of 10^{-3} mm with the order within a domain equal to the equilibrium order at 375°C), the resistance was observed to decrease before appreciable mercury was formed. The data are plotted in Fig. 55. It should be noted that a resistance decrease, well beyond experimental error, is detected after the first hour of reactor radiation. The fraction of gold atoms transmuted to mercury in this period, computed on the basis of a capture cross section of 100 barns, a flux of 10^{12} neutrons/cm^2·sec, and a half life of 3 days, is less than 1×10^{-8}. Even after 20 hr the amount of mercury is only of the order of 1 ppm. It would be somewhat surprising if these trace amounts of mercury could change the diffusion rate so substantially. The original resistivity was 7.92 μohm-cm. The resistivity of Cu_3Au at equilibrium at 150°C is 5.50 μohm-cm. After 500 hr at a flux of 2.5×10^{11} fast neutrons/cm^2·sec and

[12] H. Brooks, personal communication.

[13] T. H. Blewitt and R. R. Coltman, *Phys. Rev.* 85, 384 (1952).

[14] J. Adam, A. Green, and R. A. Dugdale, *Phil. Mag.* 43, 1216 (1952).

[15] To be published.

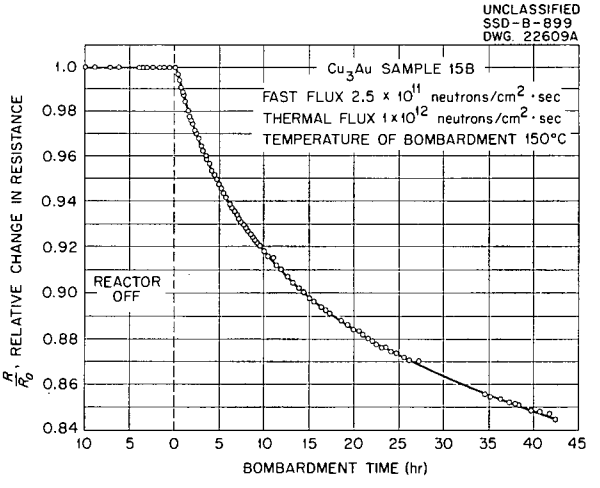

Fig. 55. Effect of Fast-Neutron Irradiation on the Rate of Radiation Ordering.

1×10^{12} thermal neutrons/cm^2·sec, the resistivity dropped to 5.94 μohm-cm.

The principal substantiation of the important role attributed to transmutations is that the radiation ordering is decreased when the sample is bombarded in a neutron converter (a thimble of fissionable material which converts thermal neutrons to fast neutrons). It was assumed that the predominate factor introduced by the converter was a reduction of slow-neutron flux, and the effects of a corresponding increase in the fast-neutron flux were ignored. While it would appear at first that an increase in the fast-neutron flux would increase the magnitude of the radiation ordering if it were associated with structural defects formed by fast-neutron interactions, a reasonable and more sophisticated approach seems to be that the increased fast flux in Cook and Cushing's experiment could be responsible for the suppression of radiation ordering. This apparent anomaly can be rationalized by considering a localized region of Frenkel defects. One of the components of the Frenkel defect, say the vacancy, will have a high jump frequency in comparison with the other component, say the interstitial atom.[16] At an appropriate temperature, the vacancy will be free to move while the interstitial atom will remain relatively fixed. While many vacancies will combine with interstitials and the defect pair will be annihilated, some of the vacancies will escape from the damaged region and will increase the ordering rate as they wander throughout the crystal. The number of jumps the defect can make, if it is assumed that the number of other types of defects (such as dislocations) capable of trapping vacancies is small, will depend on the probability that the defect will encounter a damaged region and be annihilated by the residual interstitial atoms.

If the above picture is applicable, then the damaged regions will affect the diffusion rate in two competitive ways. Increasing the number of damaged regions will increase the number of defects available for diffusion but at the same time will decrease the efficiency of the defect by decreasing the number of jumps. In the case of samples 15B and 18A of Fig. 56 it is apparent that the latter factor is the more important, since increasing the fast flux reduces the magnitude of the radiation ordering. It would be expected that the magnitude of the observed effects in the case of the sample exposed to the higher fast flux would increase to that of the sample exposed to the lower fast flux if the temperature of bombardment is raised sufficiently to increase the mobility of the defects by a factor corresponding to the increase in the fast flux.

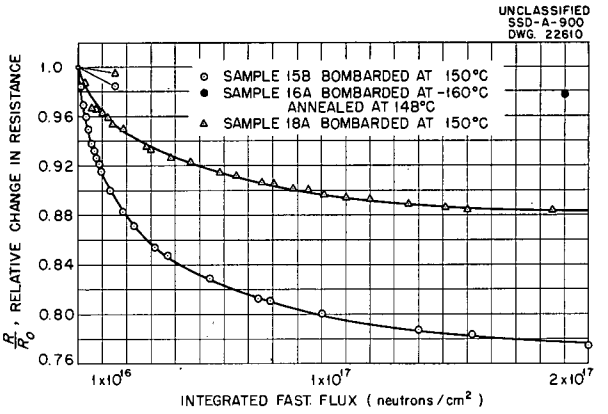

Fig. 56. Effect of Neutron Irradiation on the Resistance of Partially Ordered Cu_3Au.

The effectiveness of the damaged regions as a sink for vacant lattice sites can be determined experimentally. By bombarding the samples at temperatures where the jump frequency of the vacancies is negligibly small, a concentration of damaged regions can be created before the defects are allowed to move. In this way a study of the efficiency of the defect as a function of the number of damaged regions can be made. The result of one measurement of this type is shown in Fig. 56. Sample 16A, which was bombarded at −160°C in a flux of 2.5×10^{11} fast neutrons/cm^2·sec and 1×10^{12} thermal neutrons/cm^2·sec and which was then annealed to equilibrium at 148°C, is ordered only slightly in comparison with samples bombarded for equivalent integrated fast fluxes at high temperatures where the vacancies were permitted to migrate at low concentrations of damaged regions. Sample 15B was bombarded at 150°C in a flux of 2.5×10^{11} fast neutrons/cm^2·sec and 1×10^{12} thermal neutrons/cm^2·sec, and sample 18A was bombarded at 150°C in a flux of 1×10^{12} fast neutrons/cm^2·sec and 1×10^{12} thermal neutrons/cm^2·sec. It is perhaps noteworthy that samples 15B and 16A were exposed to very nearly the same integrated slow-

[16] It is not clear which component of the Frenkel defect is the most mobile. It has been arbitrarily assumed that the vacancy is the more mobile defect.

neutron flux. These data offer experimental evidence that the diffusion-producing defects are annihilated in the localized neutron-damaged region. It should also be noted that the proposed mechanism of radiation ordering is probably somewhat oversimplified in that combinations of effects probably move rather than the individual defects. There is evidence[15] which shows that there is a continuous spectrum rather than a single activation energy associated with radiation ordering. It may be, however, that the concept introduced here as a simple picture will be an aid in the basic understanding of radiation effects.

RADIATION EFFECTS IN COPPER SINGLE CRYSTALS

T. H. Blewitt R. R. Coltman
J. K. Redman R. E. Jamison

The resistivity of neutron-irradiated copper single crystals was measured at 4.2°K as a function of integrated flux. Measurements at this temperature are rather important since the value is that of the residual resistance and only the residual resistance is increased by bombardment. The resistance at 4.2°K is only a fraction of a per cent of the room-temperature measurement; therefore the analysis of radiation effects is quite enhanced by measurements at this temperature. It was found that the resistivity increases at a rate proportional to approximately the $\frac{2}{3}$ power of the integrated flux.

Stress-strain measurements of irradiated copper single crystals were extended to 4.2°K; it was found that the critical shear stress was greatly increased over that at 78°K for all irradiations.

STRUCTURAL DEFECTS IN COPPER AND THE ELECTRICAL RESISTIVITY MINIMUM

T. H. Blewitt R. R. Coltman
J. K. Redman

The observation of de Haas, de Boer, and van den Berg[17] that a minimum in the electrical resistivity of polycrystalline gold wires occurred in the vicinity of liquid-helium temperatures resulted in considerable interest since it raised some doubt as to the validity of Matthiessen's rule. Since that experiment, many others have been performed, with the result that the minimum in electrical resistivity has not only been verified in gold but has also been found in many other metals. Several explanations and suggestions to account for this anomalous behavior have been advanced. While many of these comments have attributed the anomalous behavior to the presence of chemical defects, particularly ferromagnetic impurities, Lane[18] on the basis of Meissner's[19] data suggested that grain boundaries might play a predominate role in the phenomena.

While it was possible in earlier experiments[20] to measure the resistivity change associated with the motion of defects (presumably similar to those caused by neutron irradiation), it was not feasible to measure the total change in resistivity because only a small fraction of the total at 78°K was changed by deformation. The resistivity of samples deformed at 4.2°K increased with the shear stress at a rate which was proportional to approximately the square of the stress. None of this increased resistivity annealed out at 78°K, but at 300°K approximately half the resistivity change was recovered. In addition, it was found that the change in resistivity was dependent on the stress rather than on the elongation; it seemed to be independent of the onset of duplex slip. Measurements have also been made of the resistivity of samples worked at 78, 200, and 300°K. It was found that the resistivity of all these samples, after an anneal at 300°K which, to a first approximation, did not affect the stress-strain curve, had the same relationship with the shear stress despite the fact that stress-strain curves were considerably different.

In the course of investigating the effect of plastic deformation[21] on the residual resistivity of high-purity copper single crystals, several factors arose which seemed to suggest that a substantial fraction of the residual resistivity observed during the investigation of the resistance minimum came from the interaction of conduction electrons with structural defects (especially grain boundaries). It has generally been assumed that the residual resistivity was determined by the scattering of conduction electrons by chemical defects. The

[17] W. J. de Haas, J. de Boer, and G. J. van den Berg, *Physica* 1, 1115 (1934).

[18] C. T. Lane, *Phys. Rev.* 76, 304 (1949).

[19] W. Meissner, *Z. Physik* 38, 647 (1926).

[20] T. H. Blewitt, *Phys. Rev.* 91, 1115 (1953); T. H. Blewitt *et al.*, *Solid State Quar. Prog. Rep. Feb. 10, 1953*, ORNL-1506, p 57.

[21] To be published.

suggestion of the importance of structural defects arose from the observation that the annealed single crystals exhibited a residual resistivity many times lower than the usual values reported for polycrystalline materials, that severe deformation could increase the resistivity to the order of that usually observed in polycrystalline materials, and that recrystallization of the worked crystals by annealing in high vacuums (10^{-5} mm or better) at 1000°C only slightly reduced the resistivity. It thus appears that the dislocations created by the deformation have merely polygonized to form grain boundaries. This situation, which was observed in many crystals, is typified by the data for crystal 304C in Table 6.

If a substantial fraction of the residual resistivity is associated with grain boundaries, as these observations suggest, it would seem that the minimum in the resistivity may arise as a result of the scattering or trapping properties of the grain boundaries. A survey-type experiment was made to examine this hypothesis. The effect of temperature in the region from 1.6 to 4.2°K on the electrical resistivity was determined on single crystals of copper as well as on polycrystalline copper. The results are shown in Table 6. The results for crystal 305D are of particular interest in that the resistance minimum was not found until recrystallization had occurred. The data of Table 6, while of only a survey nature, would seem to indicate that grain boundaries are one type of defect which can result in a negative temperature coefficient of resistance in metals. It would seem to be especially significant that the defects introduced by the deformation, presumably dislocations (apparently the vacant lattice sites have been annealed out), scatter in a normal fashion until they have been polygonized to form grain boundaries. Whether impurity atoms, especially those which are ferromagnetic, can cause similar effects, as measurements on polycrystalline metals seem to show, is open to question. However, the apparent influence of impurity atoms on the resistance minima should probably be re-examined in terms of grain-boundary scattering, especially with regard to the effect of the impurities on the grain size. In the case of the results described here, however, to definitely ascribe the negative tempera-

TABLE 6. RESISTIVITY OF COPPER AT VARIOUS TEMPERATURES

	RESISTIVITY (ohm-cm × 10^8)				
	At 4.2°K	At 3.4°K	At 2.7°K	At 1.67°K	At 1.60°K
Sample 305D					
Annealed single crystal	0.080				
Worked single crystal	1.308	1.310	1.308		1.306
After recrystallization	0.908				0.933
Sample 305C					
Annealed single crystal	0.036	0.035	0.035		0.035
Worked single crystal	1.099				1.101
Sample 304C					
Annealed single crystal	0.080				
Worked single crystal	1.140				
After recrystallization	0.830			0.846	0.847
Sample 305F					
Annealed single crystal	0.090				
Worked single crystal	0.720				
After recrystallization	0.636			0.648	0.650

ture gradient in any way to the presence of chemical defects would be difficult, as the magnitude of the effect is in excess of the residual resitivity of the annealed single crystals.

It may be pertient to mention that the magnitude of the residual resistivity of single copper crystals is in good accord with the data of Meissner's values for gold and zinc single crystals. Meissner, however, found polycrystalline wires of these metals to have a residual resistivity of the same magnitude. In neither of his samples was a resistance minimum found. It may be that the grain size of Meissner's samples was large compared with the wire diameter and therefore that the contribution of grain-boundary scattering to the total residual resistivity was small.

The manner in which the conduction electrons and the grain boundaries interact is not clear. It would appear that suitable experiments, possibly Hall-constant measurements, should be made to distinguish between the scattering and trapping properties of the grain boundary.

Studies of the slip-line phenomena have also been made. The length of slip lines was found to decrease with the elongation and was possibly due to the formation of barriers to the motion of dislocations. It would thus appear possible to measure the distance that the dislocations can move before they are trapped. It was found that the reciprocal of the length of the slip-line segment on samples deformed at 4.2 and at 300°K is directly proportional to the change in resistivity. These data should be a stringent test to various models of work-hardening in metals.

SPECIAL PROJECTS

NEUTRON IRRADIATION OF LiF CRYSTALS

D. Binder W. J. Sturm

The investigation of the equivalence of density and x-ray measurements in neutron-irradiated LiF crystals[1] has been extended in two directions. First, more exact calculations of the neutron attenuation establishes the equivalence to within 10%. Second, the nature of the defects has been considered and Schottky defects have been ruled out as the cause of the lattice expansion.

The earlier calculation of neutron attenuation was only an estimate based on the average neutron path. The present calculation assumes a spacially isotropic distribution of thermal neutrons. It is then possible, with an infinite slab approximation, to calculate the ratio of the surface-to-volume reaction yield of the (n,α) reaction in the "thin" crystals used. The plot of the x-ray lattice-parameter change $(\Delta a/a)_x$ vs the density-parameter change $(\Delta a/a)_\rho$ is a straight line.[1] The slope is then a valid comparison of the two measurements. Also, the straight line indicates a constant ratio for the effect on the surface, measured by x rays, and the volume effect, measured by density. Since both measurements are of the same phenomenon (lattice expansion), this slope or ratio is equal to the ratio of the numbers of particles causing the expansion. This ratio, in turn, is equal to the ratio of surface-to-volume yields of the (n,α) reaction, providing there is an equivalence between the two measurements for the resultant distorted lattice. Given below are data on the experimental and calculated slopes:

Crystal	Experimental	Calculated
Thin	1.38	1.35
Thick	2.41	2.24

When the experimental error and the errors of calculation are considered, the agreement between these values for the thin crystals means that the x-ray and density lattice-parameter changes are equivalent to within 10%.

The thin crystals were about 0.2 cm thick by 2.6 cm square, and the thick crystals were 0.8 cm thick by 2.6 cm square; thus the thick crystals do not approximate an infinite slab. The surface yield can be calculated easily but not the volume yield. The ratio of the volume yields for thin and thick crystals was determined by an "inhour" measurement that measured the relative numbers of neutrons absorbed by thin and thick crystals and was used to determine the calculated value of 2.24 in the preceding tabu-

[1] D. Binder and W. J. Sturm, *Solid State Semiann. Prog. Rep. Aug. 31, 1953*, ORNL-1606, p 101.

lation. The agreement with experiment is consistent with the equivalence of 10%.

When an atom is displaced, it may go to an interstitial position or to a regular lattice site. The former leads to a vacancy-interstitial pair or Frenkel defect. The latter, if the vacancy remains and an atoms comes to the surface, gives rise to a Schottky defect. Numerous Schottky defects cause extra regular layers of atoms and an equivalent number of vacancies inside. Around these vacancies will be distortion which can be detected by x-ray measurements, but the extra layers will show up only as an increase in volume or only in the density measurements. This idea was used by Seitz[2] to estimate an upper limit on the concentration of Schottky defects in crystals used in Avogadro's number measurements. It can similarly be used here to estimate the upper limit on Schottky defects caused by the irradiation.

The maximum lattice-parameter increase measured[1] was 1.6×10^{-3}, or a volume expansion of 5×10^{-3}. The maximum concentration of Schottky defects is 5×10^{-4}, as obtained from the simple theorem derived by Seitz.[2] Adding an atom to the surface would roughly expand the lattice by an atomic volume; so the maximum lattice expansion due to Schottky defects is 5×10^{-4}, or 10% of the observed expansion. Schottky defects are then ruled out as the major cause of the expansion.

THERMAL AND ELECTRICAL CONDUCTIVITIES OF DUCTILE IRONS AND GRAY CAST IRONS

A. Foner Cohen L. C. Templeton

Interest in whether the thermal conductivity of ductile cast iron differs from that of gray cast iron prompted the measurements reported herein. The samples were provided by the International Nickel Company and the compositions were as follows:

	Gray Iron	Ductile Iron
Total carbon	3.56	3.56
Silicon	2.33	2.38
Manganese	0.38	0.38
Nickel	0.58	0.52
Copper	0.45	0.29
Magnesium		0.043

From electrical resistivity measurements alone, it might be deduced that since the electrical conductivity (reciprocal of resistivity) of gray cast iron is about half that of ductile cast iron (Fig. 57) the thermal conductivity of gray cast iron would also be correspondingly lower. This deduction would be based upon use of the Wiedemann-Franz-Lorenz law. Only when the electrical conductivity and the thermal conductivity are entirely due to electrons can use of the Lorenz function serve as a guide to deduce thermal conductivity from electrical resistivity measurements.

The measured thermal conductivities of two ductile iron specimens (one as-cast and one annealed) and of one gray cast iron are shown in Fig. 58. Armco iron and Inconel are plotted on the same graph for comparison. The thermal conductivity of the gray cast iron is greater than the thermal conductivity of ductile cast iron in the temperature region 95 to 240°C (Fig. 58) and is roughly parallel to that of Armco iron, whereas the thermal conductivity of the ductile iron in this temperature range does not appear to be strongly temperature dependent.

The principal difference between the gray cast iron and the ductile iron is structural rather than chemical; the iron is made ductile by virtue of a small amount of magnesium that causes the graphite phase to form in the shape of spherules, whereas the graphite in the gray cast iron is in the form of flakes. The measured differences in thermal conductivity and electrical resistivity of the gray cast iron and the ductile iron are thus to be related to

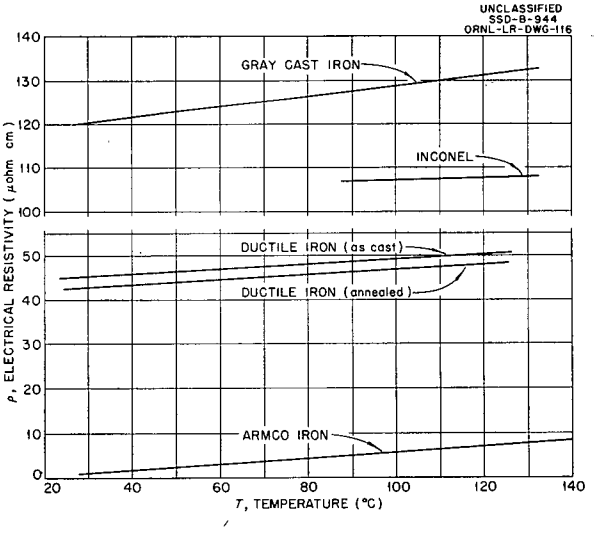

Fig. 57. Electrical Resistivity vs Temperature for Iron and Inconel.

[2]F. Seitz, *Revs. Mod. Phys.* 18, 384 (1946).

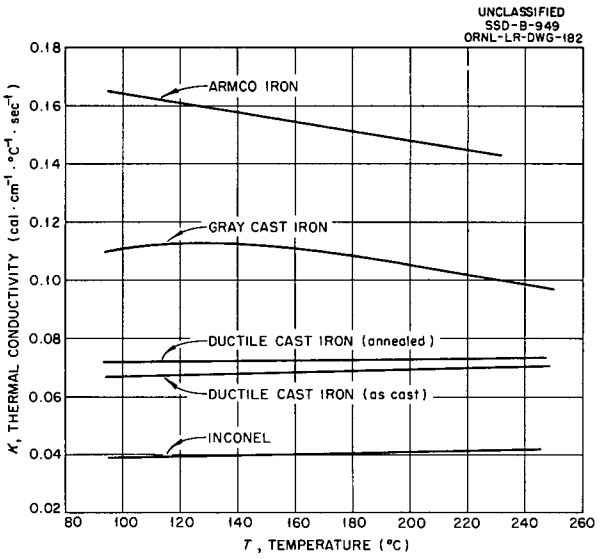

Fig. 58. Thermal Conductivity vs Temperature of Ductile and Gray Cast Iron.

the difference in graphite particle shape and distribution.

THERMAL CONDUCTIVITY OF DIELECTRICS AT LOW TEMPERATURES

A. Foner Cohen W. J. Sturm L. C. Templeton

The cryostat and associated equipment for measuring thermal conductivity of dielectrics at low temperatures have been tested at liquid-helium temperatures as low as 1.7°K. Satisfactory testing of equipment at liquid-nitrogen temperatures was reported earlier.[3] Figure 59 shows the assembled apparatus and its associated vacuum system during an experiment.

When the low-temperature part of the cryostat, the specimen, etc. are cooled to approximately 4.2°K, the evaporation rate of liquid helium is about 24 cc/hr. With a 1-liter volume for the cryostating liquid, it is possible with a single filling of liquid helium to carry out a complete series of thermal-conductivity measurements at several temperatures over the temperature range 1.7 to 5°K even in cases of the poorest conductors where time to achieve thermal equilibrium at a given temperature is of the order of 1 hr or more.

As an initial test of the equipment, measurements of the thermal conductivity of a single crystal of quartz have been made in the temperature region 45 to 80°K when the cryostating liquid was liquid nitrogen. Figure 60 shows a plot of relative thermal conductivity vs temperature. The qualitative behavior is in fair agreement with Berman's results.[4]

Since results depend critically upon the accuracy of calibration of the carbon resistors used for temperature determination, an attempt was made to evaluate the calibration data in constant-temperature baths (liquid helium, nitrogen, etc.) outside the vacuum system of the apparatus. However, it was found that the surfaces of these resistors are extremely sensitive to atmospheric and other contaminants and possibly somewhat sensitive, as well, to previous electrical history. Under these circumstances it was decided to effect the calibration during the course of the actual thermal-conductivity measurements by using the pressure over the pumped liquefied gases to determine the temperatures required.

This method of calibration was used in a second series of tests of thermal-conductivity measurements on quartz in the helium temperature range (1.9 to 5.3°K). The system was precooled with liquid nitrogen, liquid helium was introduced, and thermal equilibrium was obtained in the inner Dewar within 2 hr after the introduction of helium. The relative conductivity measurements in the helium temperature range (Fig. 61) are a composite of the results of five runs; varying uncertainties are involved because the composite graph shown includes data from preliminary measurements. The measurements discussed here extend to temperatures lower than those reported by Berman.[4] Several conductivity measurements over this temperature range (2.5 to 4.5°K) were also made by de Haas and Biermasz[5] and other measurements in this range have recently been made by Berman;[6] the results of these measurements are in good qualitative agreement with the value reported here. Quantitative differences may arise because of the difference in size or other properties of the crystals used for thermal-conductivity determinations.

[3] A. Foner Cohen, *Solid State Semiann. Prog. Rep. Aug. 31, 1953*, ORNL-1606, p 53.

[4] R. Berman, *Proc. Roy. Soc. (London)*, *A*, **208**, 90 (1951).

[5] W. J. de Haas and T. Biermasz, *Physica* **5**, 619 (1938).

[6] R. Berman, private communication.

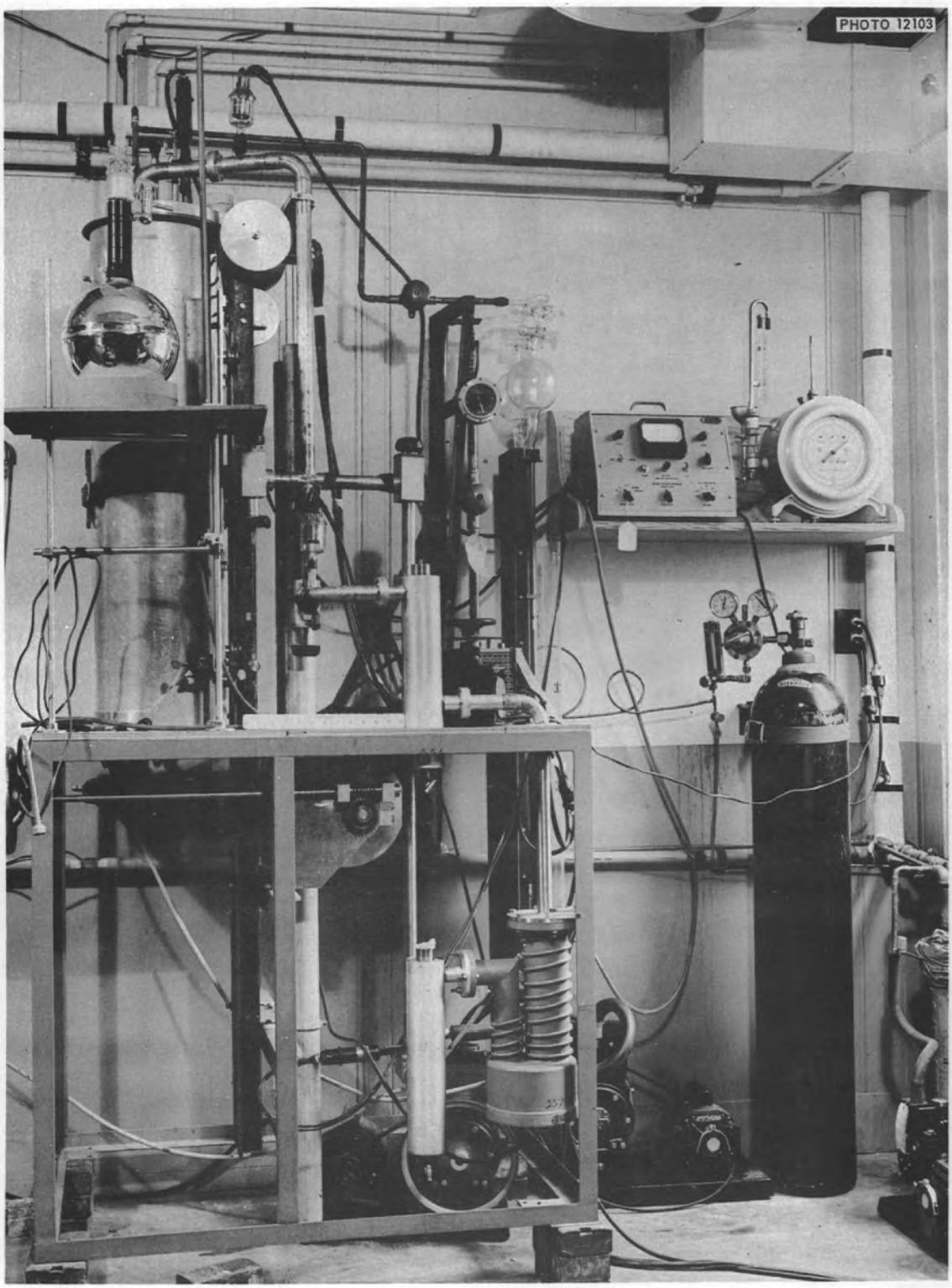

Fig. 59. Thermal-Conductivity Apparatus.

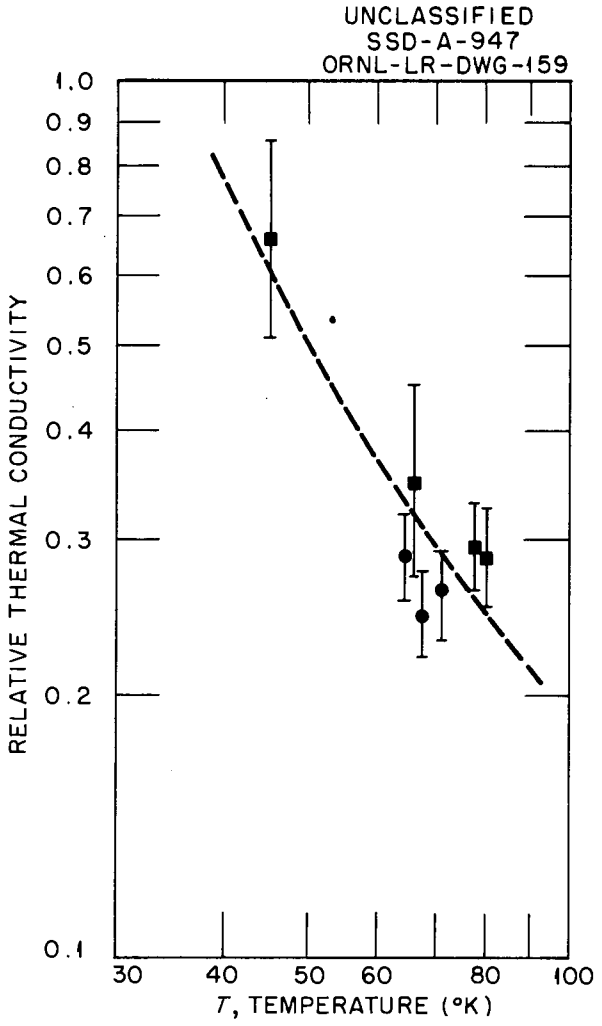

Fig. 60. Relative Thermal Conductivity vs Temperature of Single-Crystal Quartz.

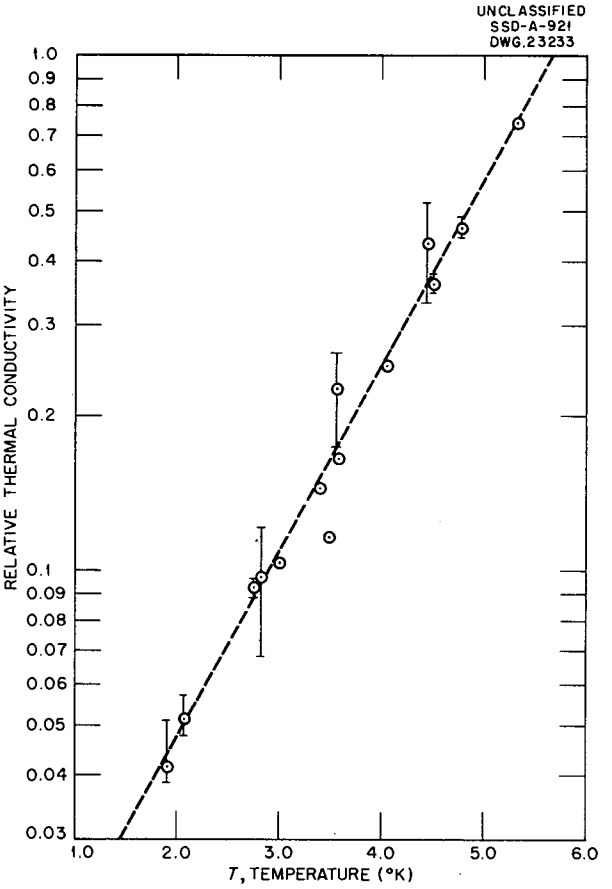

Fig. 61. Relative Thermal Conductivity of Single-Crystal Quartz in the Helium-Temperature Range.

THERMAL AND ELECTRICAL CONDUCTIVITIES OF ALUMINUM BRONZES

A. Foner Cohen L. C. Templeton

The thermal conductivity and the electrical resistivity of the alloys 94% Cu, 6% Al and 92% Cu, 8% Al have been measured by using a relative method for the thermal measurements. The results are shown in Figs. 62 and 63. The thermal conductivity of these two alloys is higher than that of pure nickel at temperatures of 130 to 200°C, as is shown in Fig. 62. At higher temperatures it would be expected that the thermal conductivity would continue to increase. Measurements at higher temperatures are anticipated.

SMALL-ANGLE X-RAY SCATTERING

R. E. Jamison

A small-angle x-ray scattering camera has been constructed for use in qualitative studies of cluster formation and growth phenomena in various materials as a function of fast-neutron irradiation and temperature history, with particular interest in the work started by Murray and Taylor.[7] More recently published work by Walker and Guinier[8] and others will also be used as a guide. The first purpose is to follow cluster size change in a precipitate alloy as a function of irradiation; the second purpose is to obtain knowledge of the precipitation mechanism as it occurs during the ordinary quenching and annealing process.

[7] G. T. Murray and W. E. Taylor, *Solid State Quar. Prog. Rep. May 10, 1952*, ORNL-1301, p 50.

[8] C. B. Walker and A. Guinier, *Acta Metallurgica* 1, 568 (1953).

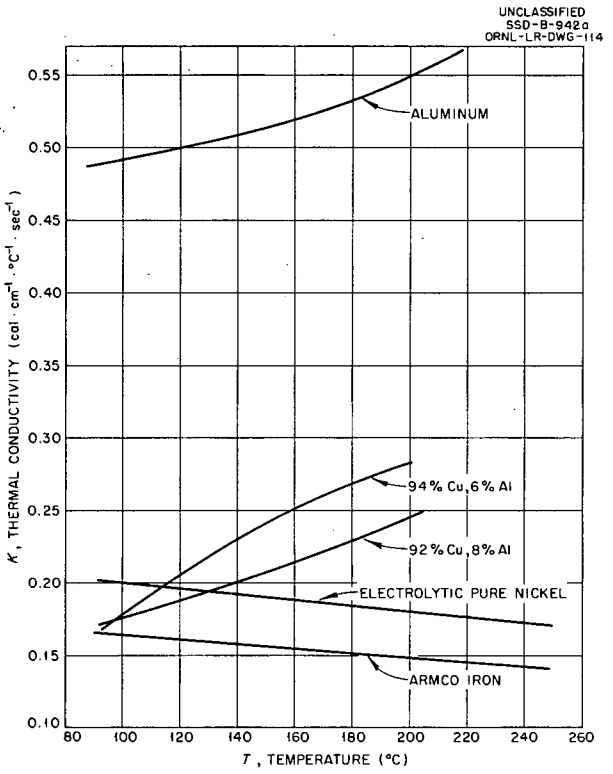

Fig. 62. Thermal Conductivity of Aluminum Bronze vs Temperature.

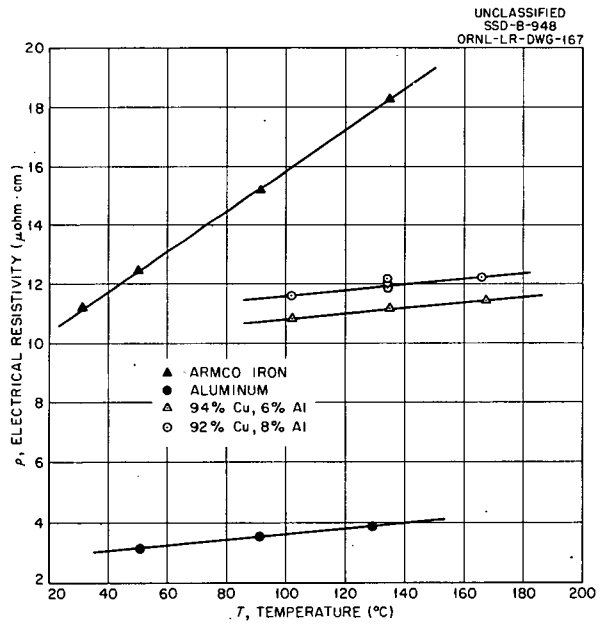

Fig. 63. Electrical Resistivity vs Temperature for Various Metals and Alloys.

The camera as it is now constructed will not be capable of giving quantitative results with any degree of accuracy. However, if it becomes evident that quantitative results would be desirable, the camera will be converted by refining the slit construction and by using crystal-monochromated irradiation. These possible changes have been anticipated and consequently would not be difficult to make, but (considering alignment problems, necessary intensity measurements, various corrections for slit dimensions, spurious scattering, etc.) actual accumulation of good quantitative data would be difficult. In either case, the qualitative results already obtained by other workers in ordinary precipitate-hardening experiments[8] should be reproduced before an attempt is made to measure irradiation effects.

The camera is much like that described by Yudowitch.[9] The Ross method of monochromatization[10] eliminates alignment difficulties, and a simple two-aperture collimating system is used; the distance between apertures is about 30 cm and the distance from the second aperture and the sample mount to the film is about 30 cm. These dimensions will make it possible to measure scattering at angles lower than $2\theta = 0° 20'$ but will probably necessitate exposure times up to 100 hr with a 45-kv, 45-ma, copper K_α source.

EFFECT OF RADIATION ON THE DIELECTRIC CONSTANT AND ATTENUATION OF TWO COAXIAL CABLES AT RADIO FREQUENCIES[11,12,13]

R. A. Weeks D. Binder

Plastic dielectrics in the form of coaxial cables are often used in and around radiation sources. Many of the physical properties of such plastics have been studied[14] as a function of irradiation in neutron and gamma-ray sources. It is of interest to extend these studies to the effect of radiation on

[9] K. L. Yudowitch, *Rev. Sci. Instr.* 23, 83 (1952).

[10] P. A. Ross, *J. Opt. Soc. Amer.* 16, 433 (1928).

[11] D. Binder and R. A. Weeks, *Solid State Quar. Prog. Rep. Nov. 10, 1952*, ORNL-1429, p 21.

[12] D. Binder, W. J. Sturm, and R. A. Weeks, *Solid State Quar. Prog. Rep. Feb. 10, 1953*, ORNL-1506, p 27.

[13] The method used in these experiments was suggested by B. R. Gossick, Purdue University.

[14] O. Sisman and C. D. Bopp, *Physical Properties of Irradiated Plastics*, ORNL-928 (June 29, 1951); see list at end of this section for other reports.

certain electrical properties, dielectric constant and attenuation, of importance in high-frequency applications.

An accurate technique of measuring relative changes in the dielectric constant and attenuation in coaxial cables during irradiation has been devised. With this technique and the theory developed, it was possible to determine changes in the relative value of the attenuation and the specific dielectric constant, e', with an error less than 2 and 0.2%, respectively. Two types of coaxial cable have been inserted in the ORNL Graphite Reactor and measurements of attenuation and e' have been made during irradiation. One of the cables was type RG-11/U with a polyethylene dielectric. The other cable was a high-voltage type with a Teflon dielectric, and its characteristic impedance Z_0 was approximately 50 ohms. The latter cable was irradiated for approximately 700 hr (Fig. 64) and the RG-11/U was irradiated for approximately 900 hr (Fig. 65). The observed e' increased about 1% for both cables. The observed attenuation of the Teflon cable showed little change during the period of irradiation. The observed change in attenuation of the RG-11/U cable was approximately 9%. The measurements were made in the region of 4 megacycles.

The advantages of this method of measuring relative changes in e' and attenuation are: with one measurement the relative magnitudes of e' and attenuation can be determined with an accuracy not achievable by other methods; instruments and personnel can be shielded from the radiation source during irradiation of cable; measurements can be made during irradiation; and standard instruments can be used. The major disadvantages are: the

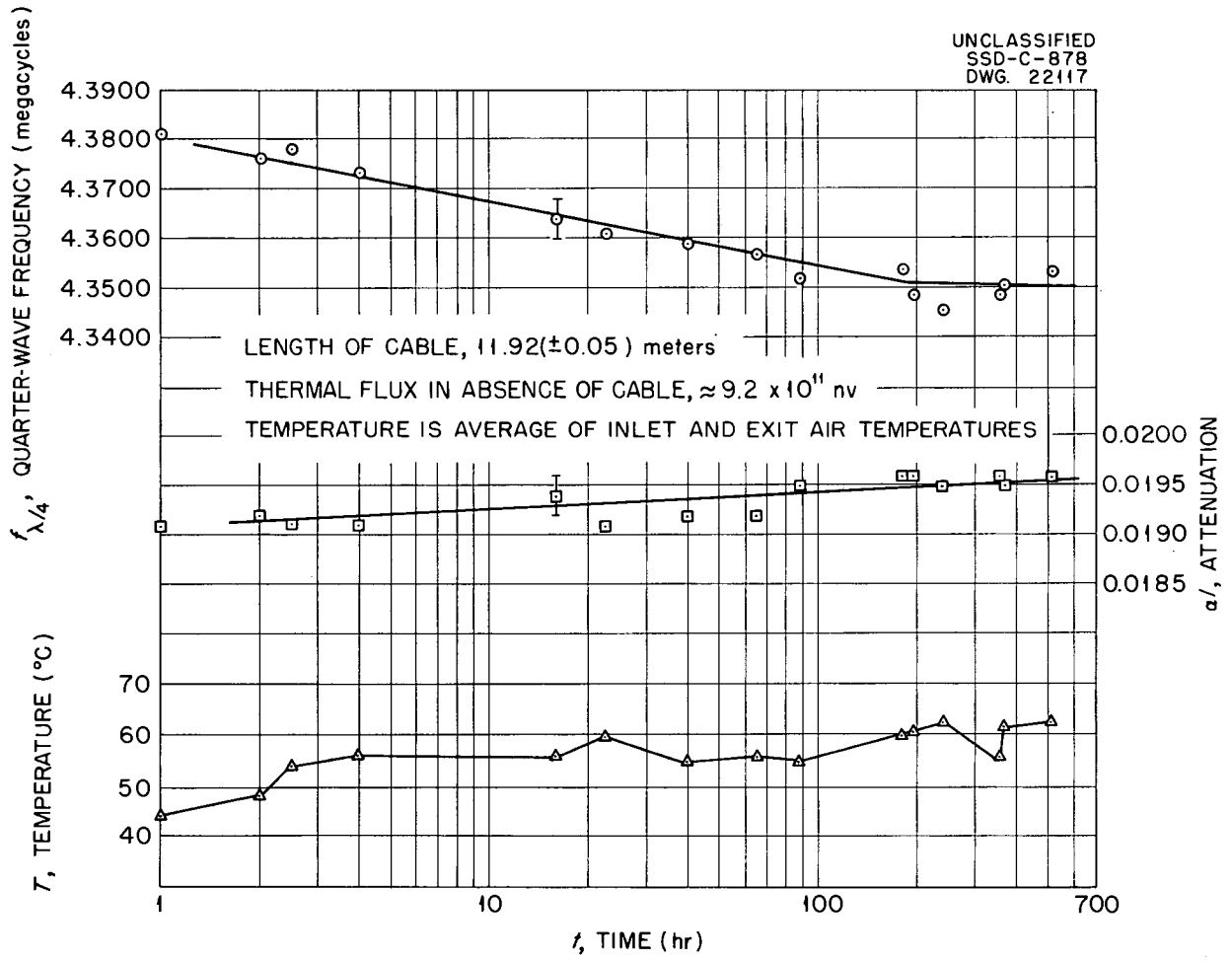

Fig. 64. $f_{\lambda/4}$ and αl of a Teflon Cable Irradiated in Hole B of the ORNL Graphite Reactor.

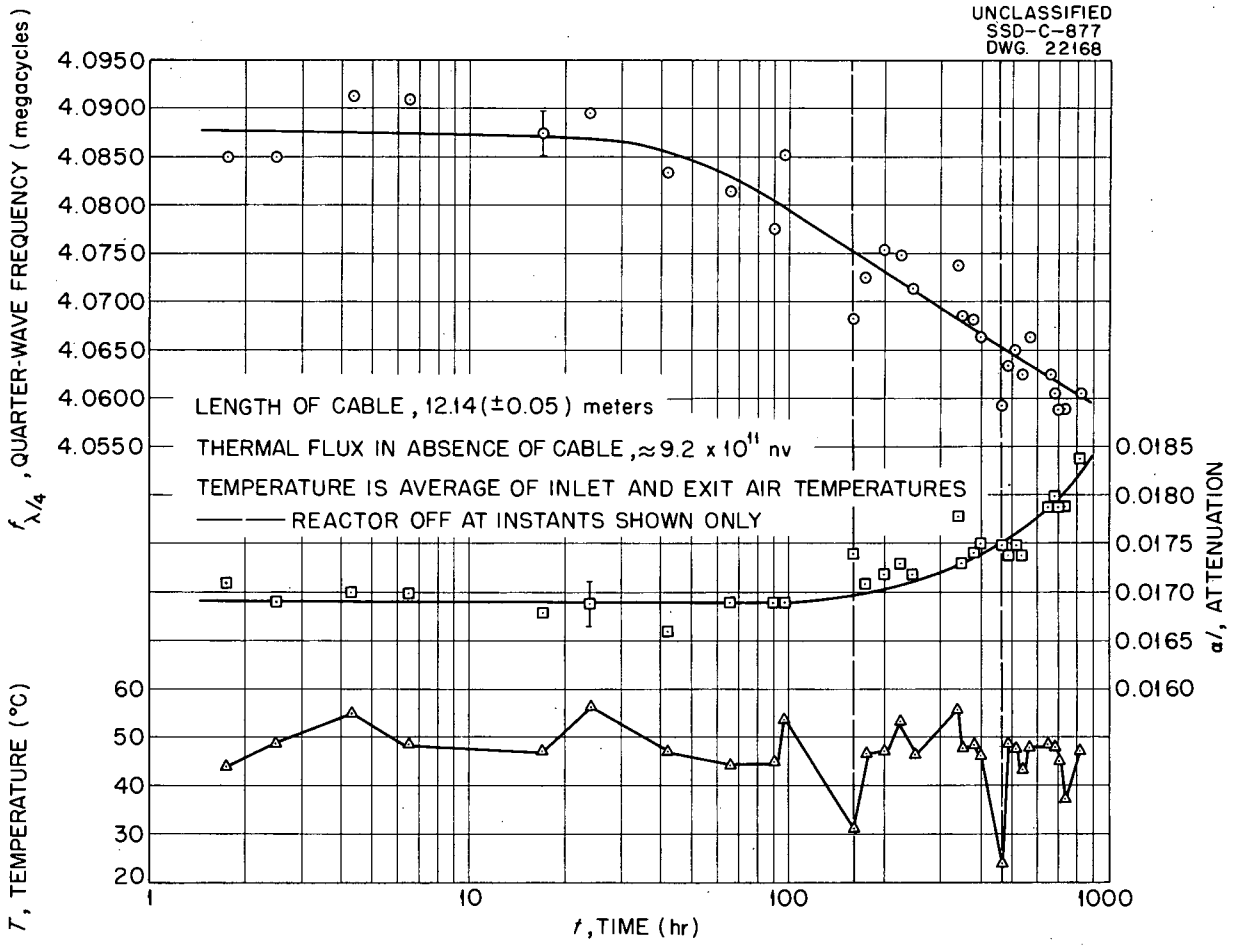

Fig. 65. $f_{\lambda/4}$ and αl of Polyethylene Cable RG-11/U Irradiated in Hole B of the ORNL Graphite Reactor.

cable is not uniformly irradiated and there is a temperature gradient along the length of the cable. However, the conditions of irradiation are similar to those that would exist if the cables were used in and around a radiation source.

The equations pertinent to the technique are developed below. The input impedance of a transmission line[15,16] of length l is

$$(1) \quad Z_{in} = Z_0 \frac{Z(l) \cosh \gamma l + Z_0 \sinh \gamma l}{Z(l) \sinh \gamma l + Z_0 \cosh \gamma l} ,$$

where

Z_{in} = input impedance,
$Z(l)$ = impedance of load,
Z_0 = characteristic impedance,
γ = propagation constant.

For low-loss lines,

$$\gamma = \alpha + j\beta ,$$

where

α = attenuation per unit length,
$\beta = \omega\sqrt{\mu e}$,

in which

ω = frequency in radians per second,
μ = permeability = 1 for dielectrics of interest in this case,
e = dielectric constant.

[15] G. C. Southworth, *Principles and Applications of Wave-Guide Transmission*, p 39-72, Van Nostrand, New York, 1950.

[16] C. G. Montgomery, R. H. Dicke, and E. M. Purcell (ed.), *Principles of Microwave Circuits*, p 67, McGraw-Hill, New York, 1948.

For an open-end line, $Z(l) \gg Z_0$, Eq. 1 becomes

(2) $$Z_{in} = Z_0 \coth \gamma l \ .$$

Then, if

$$\beta l = \frac{\pi(2n-1)}{2} \ , \quad n = 1, 2, 3, \ldots ,$$

Eq. 2 becomes

(3) $$Z_{in} = Z_0 \tanh \alpha l \ .$$

At the quarter-wave frequency, $n = 1$,

(4) $$\beta l = \frac{\pi}{2}$$

and

(5) $$e' = \frac{e}{e_0} = \left(\frac{c\pi}{2\omega_{\lambda/4} l}\right)^2 ,$$

where

c = the velocity of light,
$\omega_{\lambda/4}$ = the angular quarter-wave frequency,
l = the length of the line,
e_0 = the dielectric constant of free space,
e' = the specific dielectric constant.

Equation 2 can be written

(6) $$\frac{Z_{in}}{Z_0} = \frac{1 + e^{-2\alpha l}(+\cos 2\beta l - j \sin 2\beta l)}{1 - e^{-2\alpha l}(+\cos 2\beta l - j \sin 2\beta l)}$$

when

(7) $$2\beta l = \pi \pm \Delta\theta \ , \qquad \Delta\theta \ll \pi$$

and then, retaining only first-order terms, Eq. 6 becomes

(8) $$\frac{Z_{in}}{Z_0} = \alpha l \pm \frac{j\Delta\theta}{2} \ .$$

The absolute magnitude is

(9) $$\left|\frac{Z_{in}}{Z_0}\right| = \sqrt{(\alpha l)^2 + \left(\frac{\Delta\theta}{2}\right)^2} \ ,$$

and when $\Delta\theta = 0$,

(10) $$\frac{Z_{in}}{Z_0} = \alpha l \ .$$

At the quarter-wave frequency the magnitude of Z_{in}/Z_0 goes through a minimum. By plotting $|Z_{in}/Z_0|$ vs frequency, both the attenuation and the quarter-wave frequency can be determined. A curve drawn from Eq. 9 is compared with observed values of $|Z_{in}/Z_0|$ in Fig. 66; the agreement between observed and calculated values is quite good. The value of αl used in the equation was that found from the minimum in the experimental data, $\alpha l = 0.0169$.

A block diagram of the circuit used to measure $|Z_{in}/Z_0|$ is shown in Fig. 67a. The procedure of the experiment was set up so that $|Z_{in}/Z_0|$ could be found from two voltages that were easily measured. In Fig. 67b the signal generator is treated as a Thevenin voltage source.[17] With the terminals open the potential across them is

(11) $$V = V_1 \ ,$$

where V_1 = the Thevenin voltage. With the cable attached to the generator terminals the Thevenin voltage is increased until the potential across the terminals is the same as that in Eq. 11. Then

(12) $$V = iZ_{in} \ ,$$

where i = the current, and the new Thevenin voltage

[17] G. C. Southworth, *Principles and Applications of Wave-Guide Transmission*, p 26, Van Nostrand, New York, 1950.

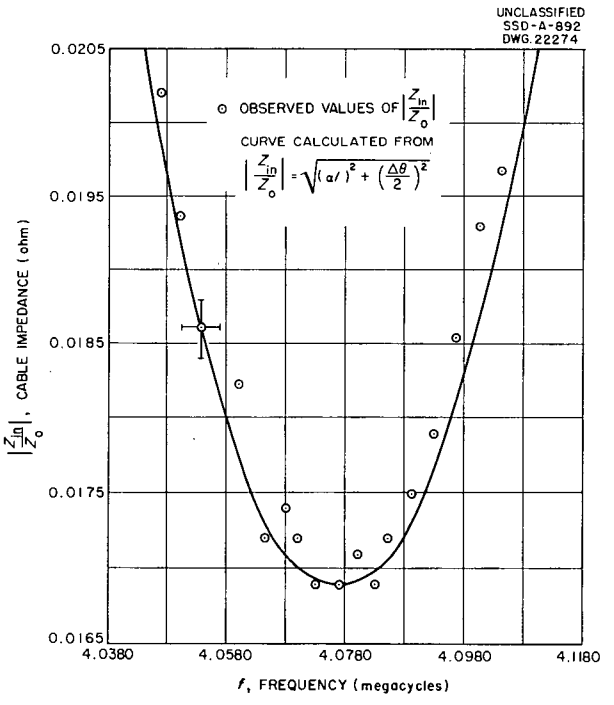

Fig. 66. Cable Input Impedance vs Frequency About $f_{\lambda/4}$.

is

$$V_2 = i(Z_g + Z_{in}) , \tag{13}$$

where Z_g is the generator impedance. By substituting $i = V_1/Z_{in}$ in Eq. 13, the input impedance is

$$Z_{in} = \frac{V_1 Z_g}{V_2 - V_1} . \tag{14}$$

At the quarter-wave frequency Eq. 14 becomes

$$Z_0 \tanh \alpha l = \frac{V_1 Z_g}{V_2 - V_1} . \tag{15}$$

If the generator impedance is matched to the characteristic impedance of the cable, $Z_0 = Z_g$, $\tanh \alpha l \approx \alpha l$, then

$$\alpha l = \frac{V_1}{V_2 - V_1} \tag{16}$$

and all that is necessary to find αl and e' is to measure V_1 and V_2 in the region of $\omega_{\lambda/4}$. In the signal generator used in these measurements (a General Radio 605-B) a calibrated attenuator preceding the output terminal was used to measure the relative magnitudes of V_1 and V_2. The signal-generator impedance was matched to the cable by a series resistor of appropriate value. The incidental shunting capacitance was negligible at the frequencies used. The value of the series-impedance matching resistor was found by measuring the impedance of the generator and of the cable. Since the cable impedance was larger than the generator impedance for both cables, the matching resistance was in series with the generator impedance. The cathode follower, receiver, and VTVM shown in Fig. 67*a* were used to set the voltage V at a constant value. This was done by modulating the output of the signal generator; a small fraction of the r-f signal was passed by the cathode follower to the receiver (a National HRO-60) and the modulation component then went to the VTVM. A cathode follower was used because of its high input impedance, approximately 100 megohms. The deflection of the VTVM was kept constant by varying the calibrated attenuator of the signal generator for the conditions of cable connected and cable disconnected. The frequency was measured by means of the receiver tuning condenser of the HRO-60 which had been calibrated.

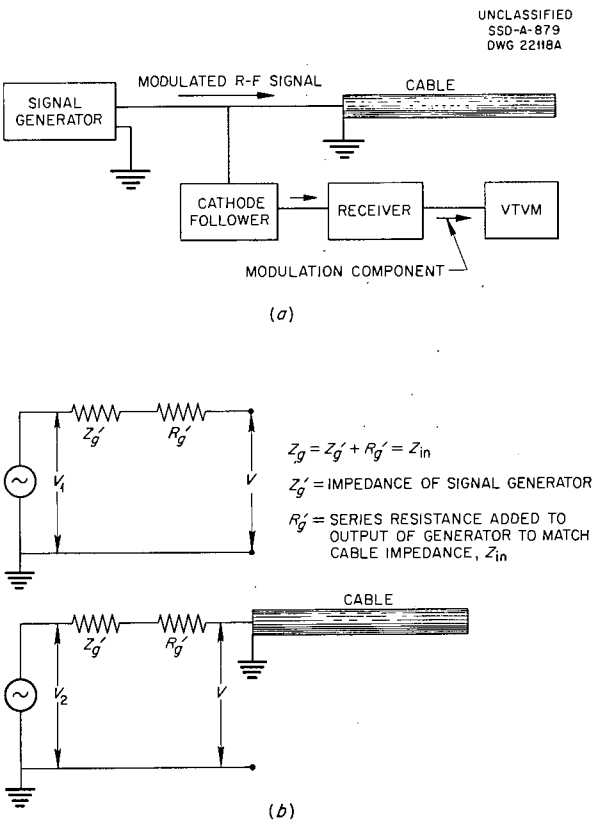

Fig. 67. Circuit Diagram for Measuring $f_{\lambda/4}$ and αl.

Changes in e' and αl in two coaxial cables have been measured by the above method during irradiation in the ORNL Graphite Reactor. The cables were inserted in hole B of the reactor, and the measurements were made over a period of approximately 700 hr ($\sim 1.6 \times 10^{18}$ neutrons/cm^2) for one cable and 900 hr ($\sim 2.1 \times 10^{18}$ neutrons/cm^2) for the other. The one irradiated for the 700-hr period had Teflon as the dielectric, and the other had polyethylene. The results for the two cables are shown in Figs. 64 and 65. It can be seen from these figures that the effect of radiation on the measured e' is small, the total observed change for both cables being approximately 1% of the initial value. The change in e' is proportional to twice the change in $\omega_{\lambda/4}$, that is,

$$\frac{\Delta e'}{e'} = \frac{2\Delta\omega_{\lambda/4}}{\omega_{\lambda/4}} . \tag{17}$$

The measured αl for the Teflon cable exhibited changes that were not outside the range of error for the period of irradiation. The total change in the measured αl for polyethylene cable was approximately 9%.

In order to determine whether there were transient effects resulting from variations in the flux around the cable, measurements were made during the weekly shutdowns of the reactor. These measurements were then compared with those made just prior to shutdown and just after startup. In the Teflon cable no significant change in e' and αl could be detected between the reactor-on and the reactor-off conditions. In the RG-11/U cable there were observable differences in the value of e' but none in αl between the two conditions. These differences were much smaller than the total change in e' for the period of irradiation. The change in e' for the two conditions seems to be correlated with the change in the temperature of the irradiated section of the cable. This temperature effect can be seen by comparing adjacent points on the $f_{\lambda/4}$ graph, Fig. 65, for which there was a change in the average temperature of the irradiated section of the cable. The changes in e' are of the same sign as the changes in average temperature; the average temperature is the average of the temperature of the reactor inlet air and outlet air. The air coolant flowed through the channel in which the cables lay; the air entered at one end of the cable and was removed from the other end. Hence the average of the inlet and outlet air temperature is an approximate measure of the average temperature of the cable. At full power of the reactor the difference between inlet and outlet air temperature was approximately 70°C.

The reason for speaking of "measured e'" and "measured αl" arises from the conditions of the experiment. The entire lengths of the cables were not irradiated. Approximately 60% of the cable length was in the active lattice of the reactor and the remaining 40% passed through the reflector and shield of the reactor and to the instruments. In addition, the flux distribution across the active lattice is not uniform; it has a maximum of 9.2×10^{11} thermal neutrons/cm^2 at the center and falls off to zero at the reflector. As a result of these conditions the cables should be considered as having, to a first approximation, two dielectrics after the irradiation began. Hence the measured e' and the measured αl are not those of the irradiated section but of the combination of the unirradiated and the irradiated section. The measured αl is simply the arithmetic sum of the αl's of the two sections. The measured e' is a somewhat involved combination of the e's of the two sections. In view of the small change in the measured e' it seems reasonable to assume that the observed change is approximately that of the irradiated section. Since 60% of the cable was irradiated, the measured αl is approximately 60% of the αl of the irradiated section. Hence the change of 9% in the measured αl of the polyethylene cable would be approximately 15% for the irradiated section.

Teflon[18] exhibits quite radical changes in its mechanical properties for an integrated flux of 10^{16} neutrons/cm^2, whereas the effects of radiation damage begin to show up in polyethylene[19] between 10^{17} and 10^{18} neutrons/cm^2. In the above measurements of e' and αl the cables were inserted in a horizontal hole in the reactor and were not moved until the end of the tests. Thus they were subjected to no mechanical strains. In view of the small changes observed in e' and αl (in the region of 4 megacycles) in these two materials as a result of irradiation, the criterion of their usefulness in a radiation field would be the effect of this radiation on their mechanical properties.

Some of the other publications relating to studies of radiation damage in plastics are given below:

O. Sisman and C. D. Bopp, *Physical Properties of Irradiated Plastics*, ORNL-928 (June 29, 1951).

J. G. Burr and W. M. Garrison, *The Effect of Radiation on the Physical Properties of Plastics*, AECD-2078 (decl. June 25, 1948).

A. O. Allen and D. M. Richardson, *Effect of Clinton Reactor Radiation on Plastics: A Compilation of Existing Observations*, CNL-16 (Jan. 30, 1948).

M. Burton, "Effects of High-Energy Radiation on Organic Compounds," *J. Phys. Chem.* **51**, 786 (1947).

J. W. Ryan, *Effects of Radiation on Organic Materials – II*, GEL-57 (Dec. 5, 1952); J. W. Ryan, "Effects of Gamma Radiation on Certain Rubbers and Plastics," *Nucleonics* **11**, No. 8, 13-15 (1953).

S. Gordon *et al.*, *Gamma Irradiation of Insulating Material*, ANL-OCS-75 (1947).

J. C. Horsman, *Summary of NRX Pile Irradiations*, NP-1922 (Dec. 8, 1950).

F. E. Faris, *A Compendium of Radiation Effects on Solids*, Vol II, NAA-SR-241 (Nov. 2, 1953).

[18] O. Sisman and C. D. Bopp, *Physical Properties of Irradiated Plastics*, ORNL-928, p 88-92.

[19] *Ibid.*, p 78-82.

DIELECTRIC CONSTANT AND LOSS TANGENT OF IRRADIATED PLASTICS AT MICROWAVE FREQUENCIES

R. A. Weeks

In extending the study of irradiation-induced changes of e' and αl in plastics, dielectric measurements before and after irradiation have been made on Teflon (D), polyethylene (A), polystyrene (B), and bakelite (E) at 1000, 3000, and 8700 megacycles. Measurements were made of e' and of the loss tangent, tan δ, for these materials by using a microwave dielectrometer made by Central Research Laboratories. A schematic diagram of the instrument is shown in Fig. 68. These materials were taken from laboratory supplies and were machined to appropriate size. After measurements were made of e' and tan δ for each sample, the samples were sealed in an identified aluminum capsule and irradiated in hole 19 of the ORNL Graphite Reactor. The cooling water of this facility flowed over the capsules. The temperature of the water, 26 ± 3°C, was approximately the same as that of the sample when it was measured. After the capsules were removed, a sufficient period of time was allowed for the induced activity to decrease to a safe level before measurements were made.

Eight samples of each material have been irradiated thus far. Four samples of each material received a dose of 0.5×10^{18} fast neutrons/cm^2 and four samples[20] received 0.9×10^{18} fast neutrons/cm^2. Of the four samples in each group, two were measured at 1 and 3 kmc (cavity oscillating in the coaxial TEM mode[21]) and the other two were measured at 8.7 kmc (cavity oscillating in the

[20] C. D. Bopp and O. Sisman, *The Neutron Flux Spectrum and Fast and Epithermal Flux in Hole 19 of the ORNL Reactor*, ORNL-525 (July 28, 1950); the values given are the total integrated flux from epithermal up.

[21] G. C. Southworth, *Principles and Applications of Wave-Guide Transmission*, p 87, Van Nostrand, New York, 1950.

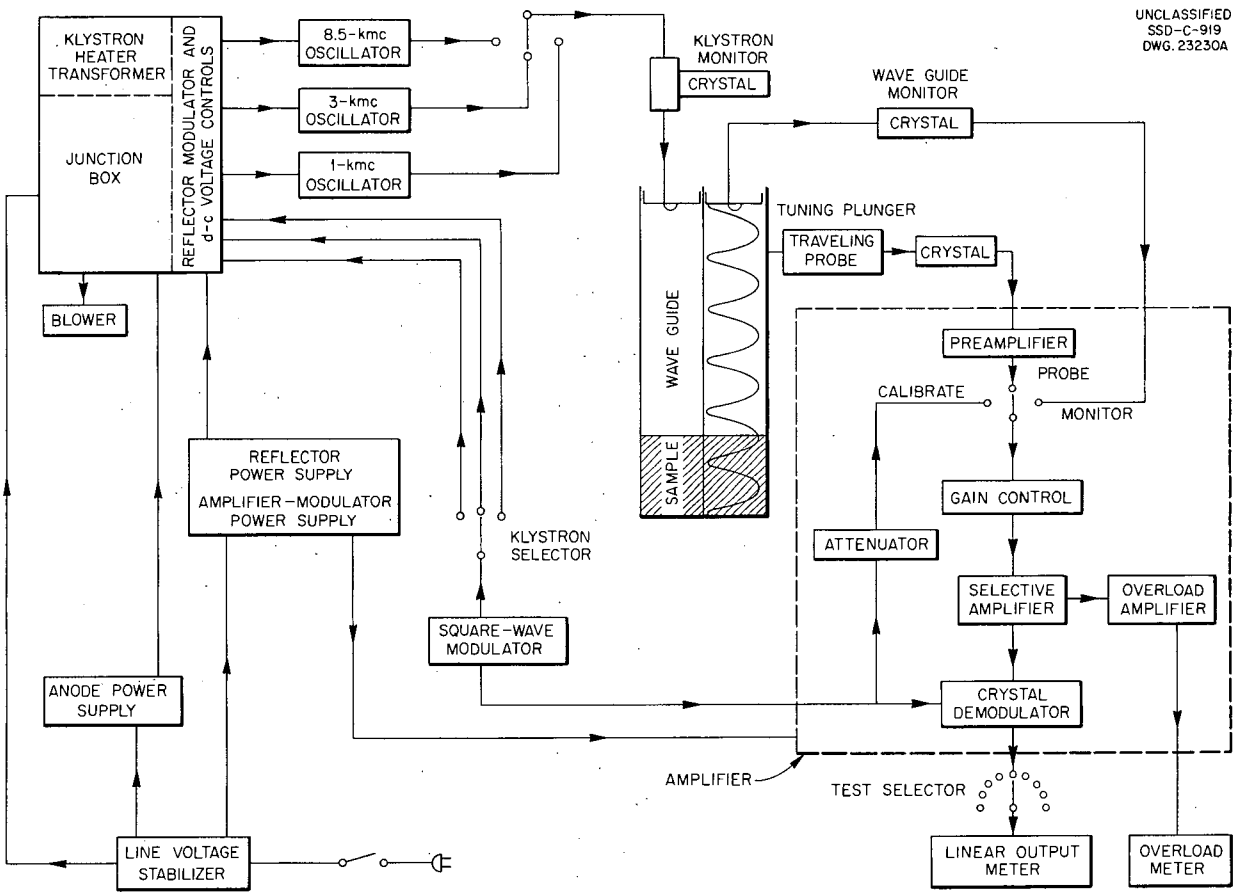

Fig. 68. Microwave Dielectrometer Block Diagram.

TE_{11} mode[22]). The cavity is coaxial in the first case and cylindrical in the second case. All samples were maintained at 26 ± 3°C before, during, and after irradiation. In Table 7 the before-and-after irradiation values of e' and tan δ are each the average of two measurements. The sample was removed from the cavity and turned over for the second measurement. The values of tan δ and e' for samples A-1, A-2, B-1, and B-2 for all frequencies and B-3 and B-4 for 8.7 kmc were inconsistent and therefore are not included. The sources of the inconsistency are being investigated.

The ratios of the before-and-after irradiation values for all the samples in Table 7 are found in Table 8. It can be seen that e' changed very little for all samples; the maximum change was an increase of 3% in the D-3 sample at 3 kmc. The D-2 sample shows a decrease of 6% in e', but there is reason to believe that this value is spurious since D-2 is the only sample that showed a decrease in the nine recorded values. The decrease in tan δ of approximately 30% at 8.7 kmc in samples A-3 and A-4 is not consistent with the increases

[22] *Ibid.*, p 120.

TABLE 7. LOSS TANGENT AND DIELECTRIC CONSTANT OF IRRADIATED PLASTICS

SAMPLE		FREQUENCY (kmc)	BEFORE IRRADIATION		AFTER IRRADIATION*	
			tan $\delta \times 10^4$	e'	tan $\delta \times 10^4$	e'
Polyethylene,	A-3	1	3.3 ± 1.5	2.238 ± 0.01	7.6 ± 1.5	2.016 ± 0.01
	A-4	1	3.6 ± 1.5	2.235	8.3 ± 1.5	2.226 ± 0.01
	A-3	3	4.6	2.177	7.0	2.190
	A-4	3	4.5	2.189	8.3	2.204
	A-3	8.7	6.4	2.258	4.5	2.262
	A-4	8.7	5.7	2.270	4.2	2.231
Polystyrene,	B-3	1	2.9	2.488	3.4	2.496
	B-4	1	2.6	2.485	3.1	2.493
	B-3	3	2.2	2.480	4.0	2.490
	B-4	3	2.6	2.480	3.7	2.487
Teflon,	D-3	1	4.5		35.6	2.06 ± 0.02
	D-4	1	Sample cracked			
	D-3	3	2.9	2.01	42.7	2.06
	D-4	3	Sample cracked			
	D-3	8.7	3.5	2.04	15.1	2.06
	D-4	8.7	8.6	2.04	28.8	2.06
					AFTER IRRADIATION**	
	D-1	1	5.8 ± 2.0	1.99 ± 0.02	15.8 ± 2.0	2.04 ± 0.02
	D-2	1	5.0	1.99	8.6	2.01
	D-1	3	3.7	1.99	17.7	2.04
	D-2	3	3.8	1.99	8.5	2.03
	D-1	8.7	6.1	2.11	23.0	2.12
	D-2	8.7	5.0	2.05	17.2	1.92
Bakelite,	E-1	8.7	75.3 ± 1.0	3.73 ± 0.01	72.9 ± 1.0	3.677 ± 0.01
	E-2	8.7	74.7	3.734	74.0	3.705

*0.9×10^{18} fast neutrons/cm^2.
**0.5×10^{18} fast neutrons/cm^2.

at the other two frequencies. Both samples decreased by almost the same amount. A careful check of this anomaly is to be made. Teflon shows the largest changes in tan δ; polyethylene, polystyrene, and bakelite in that order follow Teflon. For the bakelite, e' and tan δ decreased.

The lengths of the samples, recorded in Table 9, show small decreases after irradiation for the Teflon and polyethylene samples and for one polystyrene sample (B-4) for 8.7 kmc. There were no appreciable changes in the other samples. These lengths were used in the calculation of the before-and-after values of e' and tan δ. These measurements indicate that, for these plastics at microwave frequencies, irradiation in a reactor at constant temperature gives rise to small changes in e' (of the order of 2%) and large changes in the loss tangent (from 15% to several hundred per cent). Since the changes in e' are small and the changes in the loss tangent are large, energy losses in the dielectrics are increased at these frequencies by irradiation. The values of integrated flux given above are for neutron flux and do not include gamma-ray-flux effects on the materials. In an accurate evaluation of the integrated flux this additional factor should be considered. In view of the rather considerable changes in tan δ this preliminary investigation will be extended to larger radiation doses and to other dielectric materials.

TABLE 8. RATIO OF POSTIRRADIATION TO PREIRRADIATION VALUES OF DIELECTRIC CONSTANT AND LOSS TANGENT

SAMPLE	FREQUENCY (kmc)	$\frac{\text{Tan } \delta_{\text{after}}}{\text{Tan } \delta_{\text{before}}}$	$\frac{e'_{\text{after}}}{e'_{\text{before}}}$
A-3	1	2.3	1.00
	3	1.5	1.01
	8.7	0.70	1.00
A-4	1	2.3	1.00
	3	2.0	1.01
	8.7	0.74	0.98
B-3	1	1.17	1.00
	3	1.82	1.00
B-4	1	1.19	1.00
	3	1.42	1.00
D-1	1	2.72	1.02
	3	4.8	1.02
	8.7	3.8	1.00
D-2	1	1.72	1.00
	3	2.24	1.02
	8.7	3.44	0.94
D-3	1	7.9	1.02
	3	14.7	1.03
	8.7	4.31	1.01
D-4	8.7	2.77	1.01
E-1	8.7	0.97	0.97
E-2	8.7	0.99	0.99

The method used in measuring e' and tan δ at microwave frequencies was developed by Roberts and von Hippel.[23] As applied in the microwave dielectrometer, it consists in measuring the phase shift of the standing wave in a resonant cavity when a dielectric sample is placed in one end of the cavity. The shift in node position from empty cavity to cavity with dielectric is a function of the dielectric constant e'. These relationships are illustrated in Fig. 69. Tan δ is found from the

[23] S. Roberts and A. von Hippel, *J. Appl. Phys.* **17**, 610 (1946).

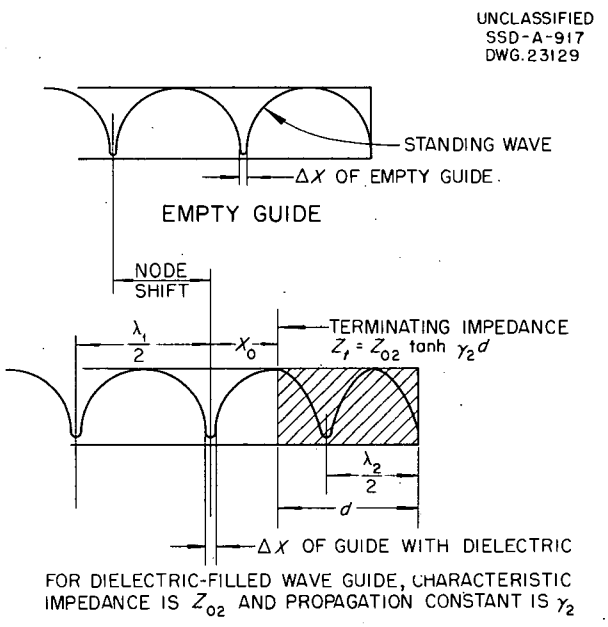

Fig. 69. Node Shift and Voltage Standing-Wave Ratio in a Wave Guide.

TABLE 9. LENGTH OF SAMPLES BEFORE AND AFTER IRRADIATION*

SAMPLE	LENGTH (mm)				PERCENTAGE CHANGE	
	At 1 and 3 kmc		At 8.7 kmc			
	Before	After	Before	After	At 1 and 3 kmc	At 8.7 kmc
A-3	49.86	49.78	11.20	11.11	−0.2	−0.8
A-4	49.89	49.78			−0.2	
B-3	49.99	49.97			−0.04	
B-4	49.96	49.96	11.23	11.20	0.0	−0.2
D-1	49.89	49.53	11.20	11.12	−0.7	−0.7
D-2	49.91	49.60	11.20	11.15	−0.6	−0.4
D-3	49.99	49.86	11.20	11.15	−0.3	−0.4
D-4			11.20	11.15		−0.4
E-1			11.21	11.20		0.0
E-2			11.20	11.21		0.0

*Error, ±0.02 mm.

standing-wave ratio R, that is, the ratio of amplitude of the wave incident on the dielectric to the amplitude of the wave transmitted through the sample, reflected from the end of the cavity and back through the sample. The ratio of the amplitude of the incident wave and the reflected wave then determines the amount of energy absorbed from the wave by the dielectric.

The derivation of the relationships between the measured quantities and e' and tan δ can be found elsewhere[23,24] and need not be fully developed here. Some of the important equations will be given, and the approximations that are made in practice will be indicated. The equations will be in terms of an impedance concept[25] and single-layer dielectric samples. In the notation of Fig. 69 the expression for the input impedance of a short-circuited transmission line[26] is

$$Z_t = Z_{02} \tanh \gamma_2 d \ . \tag{1}$$

This impedance, Z_t, can be regarded as the terminating impedance for the air-filled section of the line, and the impedance in the line a distance x from the termination is given by

$$\frac{Z_x}{Z_{01}} = \frac{Z_{01} \sinh \gamma_1 x + Z_t \cosh \gamma_1 x}{Z_{01} \cosh \gamma_1 x - Z_t \sinh \gamma_1 x} \ . \tag{2}$$

The normalized impedance $z_x = Z_x/Z_{01}$ has minima at the voltage nodes where

$$x = x_0 + \frac{n\lambda_1}{2}$$

and has maxima coinciding with the voltage maxima. The relationship between the voltage standing-wave ratio and the maximum and minimum impedance is

$$\frac{z_{max}}{z_{min}} = \frac{(z)_{x=x_0+\lambda_1/4}}{(z)_{x=x_0}} = R^2 \ . \tag{3}$$

If the attenuation in the air-filled line is neglected, then

$$\gamma_1 = j\frac{2\pi}{\lambda_1} \ .$$

If this relationship is used and the values $x = x_0$ and $x = x_0 + \lambda_1/4$ are substituted in Eq. 2 to obtained z_{max} and z_{min} and these values are

[24] T. W. Dakin and C. N. Works, *J. Appl. Phys.* 18, 789 (1947).

[25] G. L. Ragan, *Microwave Transmission Circuits*, p 13, McGraw-Hill, New York, 1948.

[26] G. C. Southworth, *Principles and Applications of Wave-Guide Transmission*, p 39, Van Nostrand, New York, 1950.

substituted in Eq. 3,

$$(4) \qquad R = \frac{1 - z_t \tanh j\dfrac{2\pi x_0}{\lambda_1}}{\tanh \dfrac{j2\pi x_0}{\lambda_1} + z_t},$$

where the normalized terminating impedance

$$(5) \qquad z_t = \frac{Z_t}{Z_{01}} = \frac{Z_{02}}{Z_{01}} \tanh \gamma_2 d \ .$$

To find z_t in terms of measured quantities,

$$(6) \qquad z_t = \frac{1 - R \tanh j\dfrac{2\pi x_0}{\lambda_1}}{R - \tanh j\dfrac{2\pi x_0}{\lambda_1}}$$

may be expressed in terms of known quantities

$$(7) \qquad z_t = \frac{1 + jR \tan U}{R + j \tan U} \ ,$$

where

$$U = \frac{\Delta + d}{\lambda_1} 2\pi \ ,$$

Δ = displacement of node toward the termination produced by the sample,

d = sample length,

λ_1 = measured wavelength in the empty guide.

If Eqs. 7 and 5 are equated and characteristic impedances are replaced by propagation functions[27] according to the relation $Z_0 = j\omega\mu/\gamma$,

$$(8) \qquad \frac{\tanh \gamma_2 d}{\gamma_2 d} = \frac{\lambda_1}{2\pi d} \frac{\tan U - j\dfrac{1}{R}}{1 + j\dfrac{\tan U}{R}} \ ,$$

where $\gamma_2 = \alpha_2 + j\beta_2$ for low-loss dielectrics. The desired quantity, γ_2, is obtained by evaluating Eq. 8. Values for e' and $\tan \delta$ are found from the relation

$$(9) \qquad \gamma_2^2 = \left(\frac{2\pi}{\lambda_c}\right)^2 - \omega^2 \mu_0 e_0 \cdot e'(1 - j \tan \delta) \ ,$$

where

λ_c = cutoff wavelength determined by guide dimensions and mode of propagation,

$$e_0 \mu_0 = \frac{1}{c^2} \ ,$$

c = velocity of light.

Equation 9 can be rewritten as

$$(10) \qquad e'(1 - j \tan \delta) = \left(\frac{\lambda_0}{\lambda_c}\right)^2 - \left(\frac{\gamma_2 \lambda_0}{2\pi}\right)^2 \ ,$$

and for the TEM mode in the coaxial line, $\lambda_c \to \infty$ and Eq. 10 becomes

$$e'(1 - j \tan \delta) = - \left(\frac{\gamma_2 \lambda_0}{2\pi}\right)^2 \ .$$

Certain approximations can be made to simplify the solution of Eq. 8 if

$\tanh \alpha_2 d \approx \alpha_2 d < 0.25$,

$\tan \delta < 0.1$,

$R > 10$, and

$R \tan U > 10 < \dfrac{R}{\tan U}$;

then Eqs. 8 and 10 simplify to give

$$(11) \qquad \frac{\tan \beta_2 d}{\beta_2 d} = \frac{\lambda_1}{2\pi d} \tan U$$

and Eq. 10 becomes

$$(12) \qquad e' = (\eta)^2 + \left(\frac{\lambda_0}{2\pi d}\right)^2 (X)^2 \ ,$$

where $X = \beta_2 d$ and $\eta = \lambda_0/\lambda_c$. If the small term α_2 is retained in the expansion of Eq. 8,

$$\tan \delta = \frac{2\alpha_2}{\beta_2} \left(1 - \frac{\eta^2}{e'}\right)$$

and

$$(13) \qquad \tan \delta = \frac{\Delta X'}{d} \left(\frac{1 + \tan^2 U}{1 + \tan X - \dfrac{\tan X}{X}}\right) \left(1 - \frac{\eta^2}{e'}\right),$$

where $\Delta X'$ is measured between the double-minimum power points and then corrected for the ΔX of the waveguide[28] for low-loss samples. The

[27] Valid, in general, only for the TE and TEM waves.

[28] The correction is necessary only if $R > 20$.

standing-wave ratio is related to $\Delta X'$ by

$$R = \frac{\lambda_1}{\pi \Delta X'} . \tag{14}$$

Equations 12 and 13 are the ones used in finding the values of e' and tan δ given in Table 7. It has been found[21] that for low-loss samples a sample of approximately $\frac{1}{4}$ or $\frac{3}{4}$ wavelength gives a maximum R and that the ratio of x_0/λ_1 has its highest value for these lengths.[23] Two lengths of each sample were prepared, one for the 1- and 3-kmc frequencies and the other for the 8.7-kmc frequency. The length of the sample for 1 and 3 kmc was $\frac{1}{4}$ wavelength at 1 kmc and $\frac{3}{4}$ wavelength at 3 kmc.

The microwave- and radio-frequency measurements on polyethylene and Teflon show small increases in e' of the same order of magnitude for approximately the same integrated flux. However, the accuracy of e' in the microwave-frequency range is not the same as in the radio-frequency range. The observed changes are within the range of error at the high frequencies, whereas they are well beyond the range of error in the low range. At best, within an order of magnitude, the irradiation-induced changes in e' are the same in both frequency ranges. This is not so with the attenuation and loss tangent. Since the attenuation is related to the loss tangent by the approximate relation

$$\alpha = \frac{\pi \tan \delta \sqrt{e'}}{\lambda_0}$$

which is valid for low-loss materials, and since e' can be considered constant at the long and short wavelengths and λ_0 is assumed to be a constant in both ranges, changes in α (or αl when l is assumed to be constant) are proportional to changes in tan δ. If this proportionality is assumed, the irradiation-induced changes in tan δ in the low range are smaller by a factor of several hundred than the changes in the high range. In the low range the irradiation-induced increase in tan δ was within the range of error: 2% of the measured value; the increase in the microwave region was several hundred per cent. The difference between the irradiation-induced radio-frequency increase in tan δ and the microwave-frequency increase in polyethylene, although not so large as for Teflon, is appreciable. The difference in this case is a factor of 10 to 15 if the anomalous value obtained at 8.7 kmc is not included. The irradiated materials show less change[29] in the loss tangent from 100 cps to 25 kmc than the irradiated ones in the range of 1 kmc to 8.7 kmc. At present there is no explanation for the frequency-sensitive loss tangent of these irradiated materials.

PARAMAGNETIC RESONANCE IN IRRADIATED SOLIDS

R. A. Weeks

Microwave apparatus has been set up to investigate radiation-induced paramagnetic resonances in various simple cubic crystals such as LiF and in semiconductors, particularly germanium. The apparatus is a transmission type[30] operating in the x band. Availability of microwave apparatus and stability of oscillators for this band were the reasons for making the preliminary investigation in the x band.

In a preliminary investigation of an irradiated LiF single crystal with approximately 10^{19} trapped electrons, the resonance reported by Hutchison[30] was obtained.

[29] *Tables of Dielectric Materials*, Vol. IV, NP-4665, Laboratory for Insulation Research, MIT (Jan. 1953).

[30] C. A. Hutchison, Jr., *Technical Report No. 1*, NP-3631, Contract N6ori-20, Office of Naval Research, 1951.